University of Calgary

PRISM Repository **https://prism.ucalgary.ca**

The Vault Open Theses and Dissertations

2018-06-11

In Search of Physical Explanation of Co-development of Plants and Landscape

Ding, Junyan

Ding, J. (2018). In Search of Physical Explanation of Co-development of Plants and Landscape (Doctoral thesis, University of Calgary, Calgary, Canada). Retrieved from https://prism.ucalgary.ca. doi:10.11575/PRISM/32227

http://hdl.handle.net/1880/107005

Downloaded from PRISM Repository, University of Calgary

UNIVERSITY OF CALGARY

In Search of Physical Explanation of Co-development of Plants and Landscape

by

Junyan Ding

A THESIS

SUBMITTED TO THE FACULTY OF GRADUATE STUDIES

IN PARTIAL FULFILMENT OF THE REQUIREMENTS FOR THE

DEGREE OF DOCTOR OF PHILOSOPHY

GRADUATE PROGRAM IN BIOLOGICAL SCIENCES

CALGARY, ALBERTA

JUNE, 2018

© Junyan Ding 2018

Abstract

The physical structure of the landscape is the subject of geology and geomorphology based on physical and chemical principles of material and energy movement under climatic and tectonic forces. The biological inhabitants of this physical landscape, area subject rooted in biological, ecological and evolutionary theories, but the primary focus has been on how the physical environment shaped life on land. It is only recently that we begin to recognize the evolution of the abiotic and biotic worlds are intimately intertwined via complex feedback loops of physical hydrological, and biological pathways, and at a range of spatial and temporal scales. In my thesis, I addressed a subset of these complex interactions: the coevolution of the landform organized as hills-valleys and the plants that occupy the different landscape positions. I used an integrated modeling approach that captures the first-order, well recognized, and mechanistic links to explore feedbacks and to shed new lights on the coupled evolution of the landform and the plants.

The landscape is a battleground of tectonics (mountain building) vs. denudation (weathering/erosion that destroy the mountains). The landscape structure, e.g. hillslope shape/size and stream density, depends on the relative dominance of diffusive type erosion (e.g., soil creep and shallow landslides) vs. the advective type (e.g., runoff erosion and channel incision). Climate exerts strong regulation on the dominance erosion processes with increasing rainfall intensity resulting in more advective type erosion landform. The result is a landscape evolution model, with three levels of diffusive vs. advective dominances. Diffusion dominated landscapes tend to have wider/longer hillslopes, more rounded hilltops, and fewer streams (i.e.,

less dissected). This will have consequences to water movement on land and the resulting soil hydrology.

These distinct landforms lead to distinct patterns of soil hydrology. A simple and powerful way to characterize soil hydrology is the Topographic Index (TI) a proxy of equilibrium of water table depth, defined for each point in a watershed as the ratio of drainage area above the point (proxy of rain caught upstream) and local slope at the point (proxy for outflow). Using TI, I translated the three landscape structures above into three hydrologic structures. Higher TI occurs in flat valley bottoms with a large slope above it, low TI on ridge tops, and intermediate TI on hillslopes. These patterns will influence the distribution of plants genetically adapted to different soil moisture conditions.

Plants have evolved genetic traits to survive and optimize their performance in given environmental niches. Soil hydrology is a powerful discriminator of plants according to their drought and waterlogging tolerance. To a first order watershed, I represented plants in three tolerance curves: hydric (waterlogging tolerant), xeric (drought tolerant), and mesic (moderate moisture tolerance), each with a preferred distribution along the TI index. This allows me to connect hydrology to plant distribution for each tolerance type. Each plant type occupies a distinct hydrologic position in all three landscapes, but more mesic plants are found in diffusive landscapes.

Water and nutrients move from soils to roots, stems, shoots, leaves, and to the atmosphere through a series of resistant flow paths. Plant hydraulic traits reflect evolutionary trade-offs between efficiency and safety. For leaves, denser veins, lower stomatal resistance, wider and

larger leaves all decrease leaf hydraulic resistance and increase net primary productivity (NPP), but the same traits also increase risks of embolism and leaf death. I developed a leaf NPP optimization model to explore the joint adjustment of several leaf traits to different levels of soil water stress. It offered a theoretical framework to explain leaf traits seen across hydrologic gradients; e.g., narrow-leaved species tend to occupy xeric habitats on hilltops, and species of large and wide leaves occupy hydric habitats in valleys.

In this thesis, by using aboveground traits, I provided a mechanistic connection between abundance and distribution of plant functional groups (PFG) on landscape and the geomorphic processes that created it. It sets the foundation for further investigating how landscape composition of PFGs can regulate topography and hillslope hydrology under the regulation of changing climate thus close the feedback cycle. A missing component here is a mechanistic expressing of soil water-root interaction that creates the dynamic rooting structure across landscape. This should be the focus of future study.

Acknowledgements

I thank my supervisor Edward A. Johnson for enlightening, guiding, and supporting me in forming this theory and Kiyoko Miyanishi for helping me with learning/improving my writing skills, and my co-supervisor Yvonne Martin for helping me on geomorphology. I also thank Dr. Ying Fan Reinfelder for helping me synthesize my thesis, discussing with and inspiring me on my future research direction. I thank my dad for being unconditionally supportive for my research. I also thank my friend Jean Willey for supporting and encouraging me during my difficult time.

Dedication

I want to dedicate this thesis to three most important people to me at different stages of my life, past, present, and future: my mother who gave life to me and taught me to be a decent person, my supervisor Edward Johnson who guided, taught, and fostered me like a father, and handed me the key to open the scientific door, and Dr. Ying Fan Reinfelder, who broadened my world view, shaped the direction of my future study, and with whom I will chase my scientific dream to the end!

Table of Contents

Abstract ii
Acknowledgements v
Dedication vi
Table of Contents vii
List of Tables ix
List of Figures and Illustrations x

List of Symbols, Abbreviations and Nomenclature xii
List of Symbols of Chapter 3 xiv

Chapter 1 Introduction 18

Chapter 2: Linking soil moisture variation and abundance of plants to geomorphic processes: a generalized model for erosional uplifting landscapes 22
1. **Introduction** 22
2. **2D analytical model connecting frequency distribution of soil moisture to geomorphic processes** 25
   - **2.1 Quantify landscape development and connection with soil moisture** 25
   - **2.2 The 2D analytical model of frequency distribution of contributing area A** 29
   - **2.3 The 2D analytical model of frequency distribution of soil moisture** 31
3. **Synthetic landscapes 3.1 Model setup** 39
   - **3.2 Results from CHILD model** 39
4. **The effect on abundance and spatial distribution of three plant groups** 44
5. **Suggestion on model testing** 52
6. **Conclusions** 53
7. **Acknowledgments** 54
8. **Supporting Material** 55
   - **Introduction** 55
   - **Text S1. Derivations of frequency distribution of contributing area (A) of channel** 55
   - **Text S2. Derivations of frequency distribution of TI** 59
   - **Text S3. Description of the Setting of CHILD** 60
9. **References** 64

Chapter 3: A Constrained Maximization Model for Optimization of Stoma and Leaf Size in Relation to Water Potential: A Theory 74
1. **Introduction** 74
2. **The leaf optimization model** 76
3. **Optimal leaf size, stomatal resistance, and maximum net leaf primary productivity** 82
4. **From Stoma to Plant to Landscape – Ways to upscale through plant vascular system** 92
   - **4.1 Implication on whole plant performance and impact on plant distribution along hillslope** 92

4.2 Connecting plant hydraulic system properties with other traits by the leaf shape 95
5. Conclusion 97
6. Supplement Material 101
S1. Derivation of Equation 2 and 8 101
S2. Solution of optimization model 105
7. References 109

Chapter 4 knowledge gaps and direction for future study 119
1. Introduction 119
2. Knowledge gaps and future study 119
3. Additional notions 122
4. References 123

Chapter 5: Conclusion 124

List of Tables

Table 1 Detailed setting of each parameter of three scenarios 62

Table 2 Parameters of the leaf model 107

List of Figures and Illustrations

Figure 1.0.1 Conceptual model of the components and mechanism of the feedback cycle. 20

Figure 2.1 Classified landscape components (redrawn from Hack and Goodlett, 1960 Figure 2) 23

Figure 2.2. Impact of D/K on frequency distribution of TI of hillslope 33

Figure 2.3 Change of the frequency distribution of TI of channel, the order of the basin and the total length of first order channel with D/K ratio..... 34

Figure 2.4 Impact of D/K on a) the total length of first order channel and b) basin order. 35

Figure 2.5 Hypothetical change of the shape of frequency distribution of TI of a basin with shifting of the relative magnitude of diffusive erosion to advective erosion. 38

Figure 2.6 Digital elevation model (top) of three synthetic landscapes 41

Figure 2.7 Frequency distribution of TI of three synthetic landscapes and the values of three critical TI values as well as the range of variation between them. TI_{max} is the maximum TI value, TI_{min} is the minimum TI value and TI_c is the TI value of the peak of the frequency distribution which is the TI value of the theoretical channel initiation point. 42

Figure 2.8 Tolerance curves of three hypothetical plants describing changes of performance along a TI gradient generated by Gaussian function..... 45

Figure 2.9 Effect of D/K on: a. the distribution of different plants on the landscape; b. spatial variation of the performance of hydric, mesic, and xeric plants on three synthetic landscapes; 46

Figure 2.10 The impact of the combined effect of differentiation of moisture preference of plants and the shape of the frequency distributions of TI determined by D/K ratio on the relative proportion of the three plant types on landscapes shown by different colors. 47

Figure 3.1 Schematic leaf model 77

Figure 3.2 Change of maximum net leaf primary productivity with petiole xylem water potential of leaves with different width to length (W/L) ratio 83

Figure 3.3 Impact of leaf shape on the relation between of optimal leaf size and xylem water potential at the petiole. 84

Figure 3.4 Impact of leaf shape on the relation between optimal stomatal resistance and petiole xylem water potential. 85

Figure 3.5 Impact of leaf width to length ratio (W/L) on the optimal marginal increase of net leaf primary productivity to petiole total xylem water potential ratio (λopt) at different petiole xylem water potential (Ψ_P)..... 86

Figure 3.6. Isoline of the constraint function g() at -10^6 Pa with a) r_{es} vs. r_{Xtotal}, b) r_{es} vs. LA.... 88

Figure 3.7 Change of total xylem resistance with leaf area……..……..89

Figure 3.8 Modelled the relation between total leaf NPP and average petiole xylem potential... 94

Figure 3.9 Schematic change of plants along hillslope as a result of safety-efficiency trade-off.95

List of Symbols, Abbreviations and Nomenclature

List of Symbols of Chapter 2

Symbol	Definition	Units
∇	divergence operator, representing the difference in incoming (both upslope and bedrock decay) and outgoing flux per unit length from two spatial dimensions	
∇^2	exponent '2' means second derivative	
ζ	relief of the basin	m m^{-1}
λ	basin order	
A	upslope contributing area per unit contour	m^2 m^{-1}
A_1	average area of first order basin	m^2 m^{-1}
A_c	contributing area of the transition point where channel starts	m^2 m^{-1}
A_k	average area of *k*th order basin	m^2 m^{-1}
A_{max}	Contributing area at the outlet of a watershed	m^2 m^{-1}
A_{min}	Contributing area of the pixel on the ridge	m^2 m^{-1}
$\overline{A_k}$	average contributing area of kth order channel	m^2 m^{-1}
C	shape parameter of basin	dimensionless
D	diffusive erosion coefficient	m^2 yr^{-1}
D_d	drainage density	m m^{-2}
ε	Tokunaga channel network parameter, defines the number of *n*th order channel drains into the side of a *n+1*th order channel	
$F()$	frequency distribution function	
K	advective erosion coefficient	m^{1-2m} yr^{-1}

K	Tokunaga channel network parameter	dimensionless
k_w	parameter of the hillslope flow pattern	dimensionless
L_1	the average length of first order channel	m
L_c	hillslope length	m
L_k	average length of *k*th order channel	m
L_{total}	total length of channels	m
m	empirical scale constant of contributing area A	dimensionless
n	empirical scale constant of local slope S	dimensionless
${}_{\lambda}N_k$	number of *k*th order channel in a basin	
${}_{\lambda}N_{k_total}$	total length of *k*th order channels in a λth order basin	m
S	local slope	m m^{-1}
t	time	yr
TI	topographic index	dimensionless
Tic	topographic index of transition point	dimensionless
TI_{max}	maximum topographic index of a watershed	dimensionless
TI_{min}	minimum topographic index of a watershed	dimensionless
U	uplifting rate	m yr^{-1}
w	width of the stream	m
W_0	total length of ridge	m
W_A	total hillslope width of a given contributing area A	m
z	elevation	m

List of Symbols of Chapter 3

Symbol	Definition	Units
a_1	plant biochemical parameter, in case of Rubisco limited photosynthesis, it is the maximum carboxylation capacity (Vc,max or Vm)	μmol m^{-2} s^{-1}
a_2	constant, for Rubisco limited case, a2=Kc(1+Coa/Ko),where Kc and Ko are the Michaelis constants for CO_2 fixation and oxygen inhibition and Coa is the oxygen concentration in air	μmol mol^{-1}
Ca	CO_2 concentration of air (ambient CO_2 concentration)	mol mol^{-1}
C_l	CO_2 concentration within space of leaf	mol mol^{-1}
Cons1	constant (1.4), gives the ratio of resistance of CO_2 to H_2O	dimensionless
Cons2	1/specific gas constant of water vapor R_wT	s^2 m^{-2}
Cons3	constant, mass per volume of water	mol m^{-3}
GPP	net carbon acclimation rate per unit leaf area	μmol m^{-2} s^{-1}
k_{Rm}	constant, dark respiration scaling rate	μmol m^{-2} s^{-1}
k_{SP}	leaf shape parameter W/L	
L	leaf length	m
L_*	dimensionless leaf length as L/(Z/2) (leaf length to minor length ratio)	
l_T	length of terminal vein	m
M_k	number of xylem conduits of kth level vein	
N_k	number of branches of k_{th} level vein, k=0...T	
NPP_{leaf}	net primary productivity of one leaf	μmol s^{-1}

r_0	radius of xylem conduit of major vein	
R_C	life span standardized construction cost (e.g., the total mass of the leaf divided by its lifespan)	$\mu mol\ m^{-2}\ s^{-2}$
r_{Cs}	stomatal resistance of CO_2	$s\ m^{-1}$
r_{em}	mesophyll resistance	$s\ m^{-1}$
r_{es}	stomatal resistance of water vapor	$s\ m^{-1}$
r_k	radius of xylem conduit of kth level vein	
R_R	respiration rate per unit leaf area	$\mu mol\ m^{-2}\ s^{-1}$
r_T	radius of xylem conduit of terminal minor vein	μm
r_{XT}	xylem resistance of a single minor vein	$s\ m^{-1}$
r_{Xtotal}	total xylem resistance of vein of a single flow pathway	$s\ m^{-1}$
T	terminal minor vein order, also as the total order of the vein	
W	average leaf width	m
Z	thickness of leaf	m
ρ_l	leaf density	$kg\ m^{-3}$
l_0	length of major vein	m
l_k	length of kth level vein	m
n	branching ratio of vein (N_{k+1}/N_k)	
m	branching ratio of conduits	
γ	vein network xylem length scaling parameter: l_{n+1}/l_n	

β	vein network xylem radius scaling parameter (r_{n+1}/r_n)	
m	xylem branching rate M_{k+1}/M_k	
J	water flux per unit area, the speed of flow	$m^3\ s^{-1}\ m^{-2}$
Ψ_0	water potential of xylem at petiole	Pa
Ψ_T	water potential of xylem of terminal vein, here we assume the variation of water potential along terminal vein is very small and can be ignored	Pa
Ψ_C	critical xylem water potential air bubble will form permanently in xylem	Pa
$\Delta\Psi_{Xtotal}$	total loss of xylem water potential from petiole to terminal minor vein	Pa
E_m	water flux from minor vein to inner leaf space through mesophyll	$kg\ m^{-2}\ s^{-1}$
E	flux of water vapor from inner leaf space to atmosphere through stoma and boundary layer of leaf per unit leaf area	$kg\ m^{-2}\ s^{-1}$
E_{leaf}	transpiration rate of a leaf	$kg\ s^{-1}$
L_T^*	minor vein density	$m\ m^{-2}$
μ	dynamic viscosity of water at 25°C	$kg\ m^{-1}\ s^{-1}$
g	acceleration of gravity	$m\ s^{-2}$
e_{sat}	saturated water vapor pressure/concentration, a constant, assume air temperature is 25°C	Pa

e_l	water vapor pressure/concentration within leaf space	Pa
e_a	partial pressure water vapor of air at 25 °C	Pa
w_0	saturated water concentration in mesophyll, a constant	kg m^{-3}
w_1	water concentration at the evaporative mesophyll surface	kg m^{-3}
D_m	diffusivity of water in mesophyll	m^2 s^{-1}
k_b	physical constant	$s^{0.5}$ m
d_T	distance between two adjacent terminal minor veins	m
λ	Lagrangian multiplier	
δ	distance between minor vein and leaf surface	m

Chapter 1 Introduction

Understanding the mechanisms of terrestrial environmental change, particularly changes in water, soil, and vegetation, is of paramount importance to understanding/predicting past/future trajectory of our planet and its inhabitants.

The biological inhabitants of this physical landscape, e.g., plant and animal life, is a subject rooted in biological, biochemical, ecological, and evolutionary theories. Ecohydrologists have developed knowledge on how vegetation components vary in relation with landscape position at catchment scale (e.g. Parker and Bendix, 1996;Bridge and Johnson, 2000; Stallins 2006). Plant physiologists gained understanding on how plant traits affect the net carbon gain in relation with soil moisture and nutrient content (e.g. Hacke and Sauter, 1995; Hodge, 2004; Hacke et al. 2006; Collins and Bras 2007; Sack et al. 2013; Liese, Alings, and Meier 2017). Through small scale studies, biologists have realized that plants not only respond to their physical environment but also directly modify the flow of energy, water, and nutrients, but the primary focus of these studies has been on how the physical environment shaped life on land, not the other way around (Amundson et al., 2015).

On the other hand, the physical structure of the landscape, e.g., the size and arrangement of its hills and valleys across the landscape, is the subject of an old discipline rooted in geology and geomorphology and based on physical and chemical principles of material and energy movement under climatic and tectonic forces. Geomorphologists have well established theory on how landscapes of catchments develop over time controlled by weathering and erosion processes. It is only recently that we have begun to recognize how the evolution of the abiotic and biotic worlds are not in parallel, but are intimately intertwined via complex feedback loops

of physical, geochemical, and biological pathways and at a range of spatial and temporal scales (Figure 1.1).

This thesis aims to provide a theoretical framework that can: 1) bridge the knowledge of two groups of disciplines – plant physiologic ecology and geomorphology through hydrologic processes; and 2) provide a means to understand the feedback mechanisms between plants and landscape using first order rules—the physical processes.

In the thesis, I focus on vascular plants, e.g trees and low order basins. The strategy is using hydrologic processes to connect topographic induced soil moisture variation to geomorphic processes that create the landscape. The plant vascular system is used to link the plants traits, their impact on plant net primary productivity to transpiration regarding to soil moisture. The adaption and evolution processes is captured by the optimization algorithm addressing the co-adjustment of several plants traits to maximize their fitness. Therefore, the thesis is broken into two related subject: landscape evolution and soil moisture variation (Chapter 2), and plant optimization to soil water availability (Chapter 3).

Chapter 2 provides a theoretical model connecting the erosion processes to soil moisture variation across the landscape and the resulting influence on plant distribution.

Chapter 3 describes an optimality-based leaf model that explains the joint adjustment of several leaf traits to different levels of soil water stress. It provides a means to upscale cell and leaf level processes to whole plants and ecosystem level. By this means, the leaf model offers a theoretical framework to explain leaf trait variation observed across hydrologic gradients.

Chapter 4 discusses the knowledge gaps and suggests future research to close the feedback cycle.

Chapter 5 gives the conclusion to the thesis.

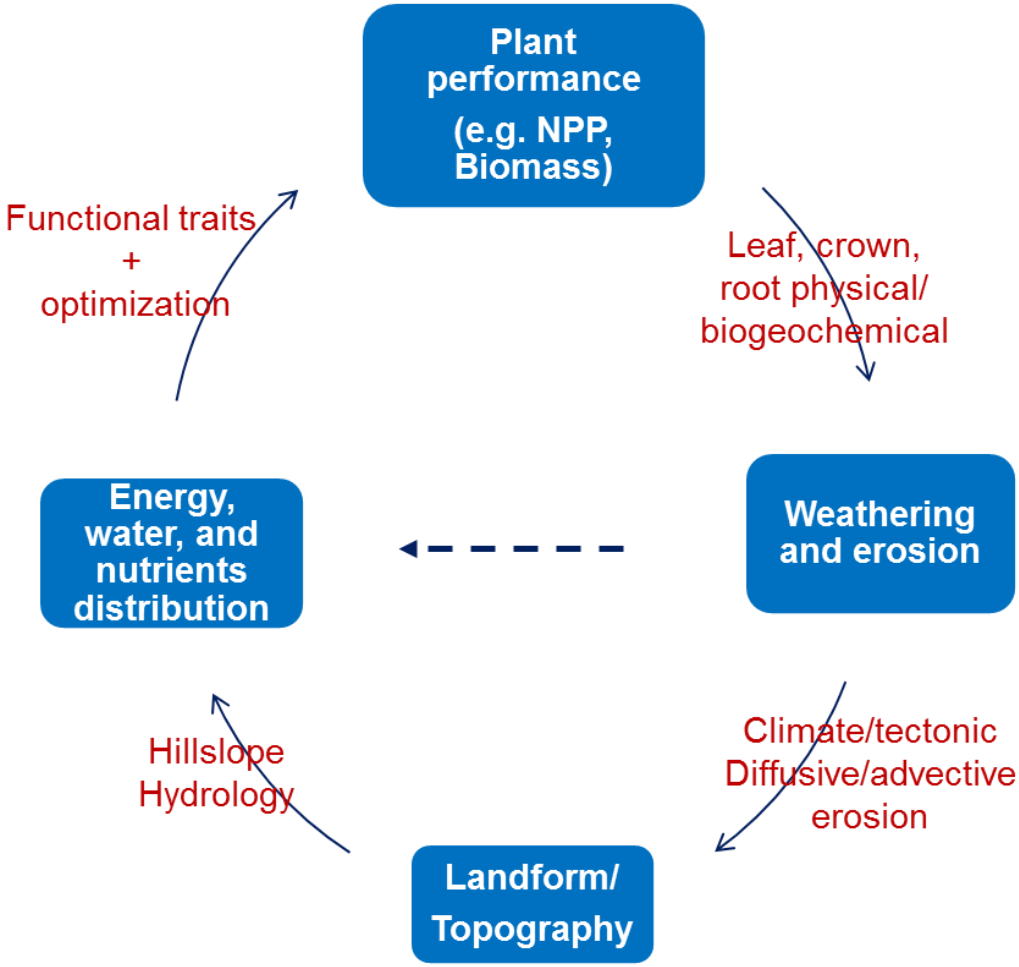

Figure 1.0.1 Conceptual model of the components and mechanism of the feedback cycle.

References

Amundson, Ronald et al. 2015. "Hillslope Soils and Vegetation." Geomorphology 234: 122–32. http://dx.doi.org/10.1016/j.geomorph.2014.12.031.

Bridge, S.R.J., and E.A. Johnson. 2000. "Geomorphic Principles of Terrain Organization and Vegetation Gradients." Journal of Vegetation Science 11: 57–70.

Collins, D. B G, and R. L. Bras. 2007. "Plant Rooting Strategies in Water-Limited Ecosystems." Water Resources Research 43(6): 1–10.

Hack, John T, and John C. Goodlett. 1960. Geomorphology and Forest Ecology of a Mountain Region in the Central Appalachians.

Hacke, U, and J J Sauter. 1995. “Vulnerability of Xylem To Embolism in Relation To Leaf Water Potential and Stomatal Conductance in Fagus-Sylvatica F Purpurea and Populus-Balsamifera.” Journal of Experimental Botany 46(290): 1177–83.

Hacke, U. G., J. S. Sperry, J. K. Wheeler, and L. Castro. 2006. “Scaling of Angiosperm Xylem Structure with Safety and Efficiency.” Tree Physiology 26(6): 689–701. https://academic.oup.com/treephys/article-lookup/doi/10.1093/treephys/26.6.689.

Hodge, Angela. 2004. “The Plastic Plant: Root Responses to Heterogeneous Supplies of Nutrients.” New Phytologist 162(1): 9–24.

Liese, Rebecca, Katrin Alings, and Ina C. Meier. 2017. “Root Branching Is a Leading Root Trait of the Plant Economics Spectrum in Temperate Trees.” Frontiers in Plant Science 8(March): 1–12. http://journal.frontiersin.org/article/10.3389/fpls.2017.00315/full.

Parker, Kathleen C, and Jacob Bendix. 1996. “Landscape-Scale Geomorphic Influences on Vegetation Patterns in Four Environments.” Physical Geography 17(2): 113–41.

Sack, Lawren et al. 2013. “How Do Leaf Veins Influence the Worldwide Leaf Economic Spectrum? Review and Synthesis.” Journal of Experimental Botany 64(13): 4053–80.

Stallins, J. Anthony. 2006. “Geomorphology and Ecology: Unifying Themes for Complex Systems in Biogeomorphology.” Geomorphology 77(3-4): 207–16.

Chapter 2: Linking soil moisture variation and abundance of plants to geomorphic processes: a generalized model for erosional uplifting landscapes

1. Introduction

Empirical studies of soil mantled watersheds have found that soil moisture is correlated to plant abundance and distribution and that plant species have different (soil moisture) tolerance curves, i.e., their abundance varies according to different soil moistures (e.g. Whittaker 1956, Curtis 1959 and many more). The shape of the landscape has an important effect on the distribution of soil moisture and vegetation. Hack and Goodlett (1960) put a firmer foundation on the connection with geomorphology by showing how in watersheds the geomorphic processes shape the landscape and that vegetation composition varied according to these processes. This early study connected vegetation and soil moisture to geomorphic processes. The study produced a famous diagram (Figure 2.1) that classified low order watersheds by the geomorphic processes of erosion and sediment transport. There have been major advances in geomorphology and hydrology since Hack and Goodlett showed that geomorphic *processes* are one of the basic drivers of plant abundance and distribution.

Hydrologists have linked soil moisture variation on hillslopes to topographic regulated lateral flow paths and steepness of local slope (Barling et al., 1994; Beven and Kirkby, 1979; Iorgulescu and Musy, 1997; O'Loughlin, 1986). By combining these lateral flow processes and simplifying assumptions, a Topographic Index (TI) was developed by Beven and Kirkby (1979) which estimates the water table (saturated zone of soil) height above bedrock of every location in a basin from the digital elevation model (DEM). Each pixel of the DEM is characterized by its upslope contributing area, A, and local slope, S, from which TI is expressed as $TI = ln(A/S)$.

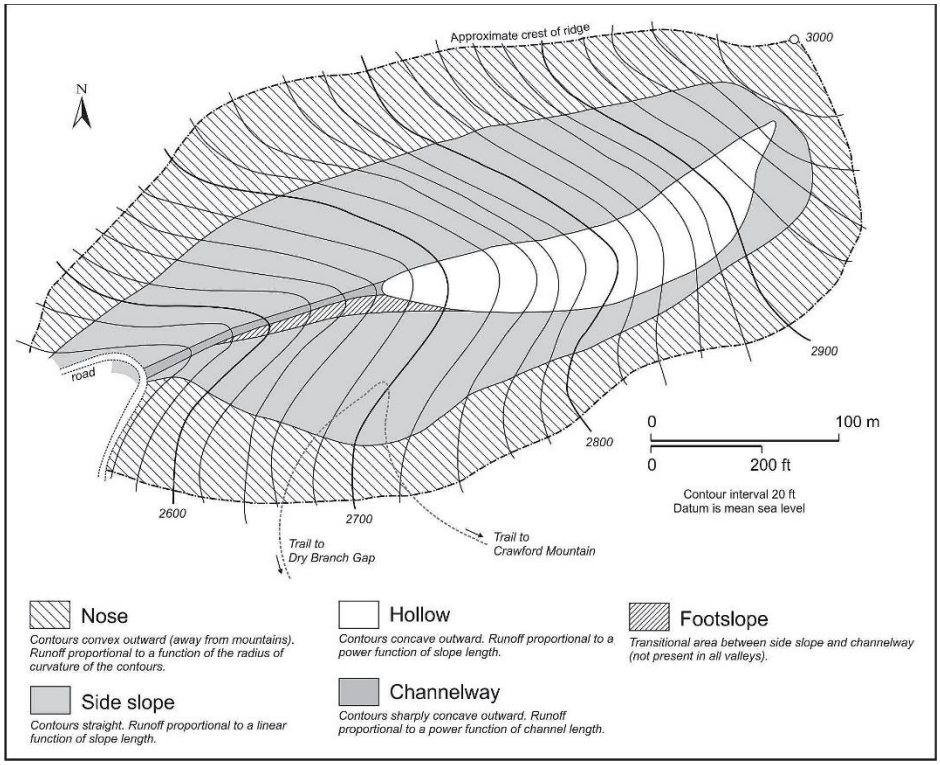

Figure 2.1 Classified landscape components (redrawn from Hack and Goodlett, 1960 Figure 2)

Field studies have shown that this index gives a reasonable estimation of annual mean soil moisture (Western et al., 1999; Sørensen et al., 2006) and is correlated to plant distribution (e.g., Bridge and Johnson, 2000; Dirnbock et al., 2002; Dymond and Johnson, 2002; Zinko et al., 2005; Brolsma and Bierkens, 2007; Oddershede et al., 2015).

Geomorphologists using landscape development models have shown how soil mantled landscapes of low order basins are controlled by the relative magnitude of geomorphic processes which determine properties such as average basin relief (Tucker and Bras, 1998; Perron et al., 2008), slope-area relation (Willgoose et al., 1991; Willgoose, 1994), cumulative area distribution (Perera and Willgoose, 1998), hillslope length and shape (Kirkby, 1971; Smith and Bretherton, 1972; Tucker and Bras, 1998; Hancock and Willgoose, 2001), drainage density (Howard, 1990; Willgoose et al., 1991; Tucker and Bras, 1998), and first order valley width (Perron et al., 2008). Studies using a numerical model of landscape development (Perron et al., 2008) and laboratory experiments (Sweeney et al., 2015) show that the ratio of diffusive erosion to advective erosion is the major control of these landscape properties.

Hack and Goodlett (1960) was one of the earliest studies that quantified the processes that shaped low-order, soil mantled watersheds. However, despite the pioneering use of geomorphology, the vegetation composition was simply correlated to the processes of sediment erosion and transport through the landscape position. The soil moisture relationship to the landscape processes was inferred from the soil texture and to some extent from the vegetation composition. There was no connection of the erosion and transport processes to the hydrology of soil moisture processes. This study continues the Hack and Goodlett approach by using geomorphic and hydrological processes to explain plant distribution using the above mentioned recent advances in landscape development and hydrological processes. Our approach is to create

an analytical 2D (one dimension is elevation, another is the distance from ridge following flow lines) model of soil moisture variation which uses a simple Landscape Development model (Equation 1 below) that includes the principal sediment erosion and transport processes and then incorporates a topographic index (TI) which explains the hydrological processes that determine saturated soil moisture and can explain the plant abundance and distribution on the landscape when combined with plant tolerance curves to soil moisture.

To verify the 2D model, we created 3D synthetic landscapes of different dominant geomorphic processes using a numerical landscape development model—Channel-Hillslope Integrated Landscape Development (CHILD) model (Tucker et al., 2001). Next mapping the TI on three landscapes produced by the model, the frequency distributions of TI for each landscape were computed and compared to the 2D model. To explore the extent to which the abundance and distribution of different plants on the landscapes may be regulated by varying the geomorphic processes, we used tolerance curves of three hypothetical plant groups: xeric, mesic, and hydric plants, to map the performance of these three plant groups on the synthetic landscapes and examined the differences in spatial pattern of dominant plants among the three landscapes.

2. 2D analytical model connecting frequency distribution of soil moisture to geomorphic processes

2.1 Quantify landscape development and connection with soil moisture

We take the simplest form of landscape development that only accounts for the major erosion processes and allows us to obtain an analytical solution (Smith et al., 1997; Perron et al., 2008):

$$\frac{\partial z}{\partial t} = U + D\nabla^2 z - KA^m(\nabla \mathrm{z})^n \qquad (1)$$

where z is elevation (m), U is uplift rate (m/yr), ∇ is the divergence operator, representing the difference in incoming (both upslope and bedrock decay) and outgoing flux per unit length from two spatial dimensions, D is the diffusion coefficient (m^2/yr), K is the advective erosion coefficient (m^{1-2m}/yr), A is upslope contributing area per unit contour length (m^2/m), m and n are constants. The second term on the right-hand side of the equation describes mass movement in forms of linear diffusion. The third term describes both runoff erosion on hillslopes and stream erosion, and is a kinematic wave function. Thus, we refer to mass movement as diffusive erosion and erosion by running water as advective erosion.

Diffusive erosion can be linear or nonlinear. For low to intermediate relief watersheds (gradient < 0.4), the linear diffusion equation may be adequate, but for high relief watersheds non-linear diffusion may be more appropriate (e.g., Martin, 2007; Roering, 2008; Perron et al., 2008). The linear form is presented in Equation 1 for simplification. Also, with non-linear diffusion, erosion rate increases with slope exponentially. But, when erosion rate becomes very high, weathering rate becomes the limiting factor of sediment loss (Martin, 2007). In such a situation, bedrock is exposed. In this study, we are looking at soil mantled watersheds. With low erosion rate, the non-linear diffusion can be approximated by a linear function. The coefficient D is a parameter that gives an overall measure of the coherence of material and the amount of energy involved in removing sediment, both of which are determined by underlying geology, climate, vegetation and animal activity (Carson and Kirkby, 1972; Black and Montgomery, 1991; Roering et al., 1999; Anderson, 2002; Gabet et al., 2003; Furbish et al., 2007; Furbish and Roering, 2013).

Advective erosion refers to the process of flowing surface water detaching and carrying sediment over a hillslope or along a channel. For watersheds with less cohesive material, the

sediment transport rate is the detachment rate and is represented as a power function of shear stress (Istanbulluoglu, 2003; Tucker and Hancock, 2010). Assuming steady, uniform flow, the change in potential energy of the flow is cancelled out by the friction force; thus shear stress is determined by stream power which is a function of discharge per unit width, bed slope, and channel roughness (Tucker and Hancock, 2010). The total discharge at any given location is linked to total contributing area, *A*, using an empirical equation (Leopold and Maddock, 1953; Willgoose et al., 1991; Knighton, 1998). *K* is a scaling coefficient that gives the ratio of amount of sediment transported to shear stress; it incorporates the effect of precipitation, surface roughness and sediment size; *m* and *n* are empirical constants.

For a two-dimensional hillslope, *A* is equivalent to distance to ridge. Thus ∇z is written as dz/dA, the absolute value of which is the local slope *S*. So $\nabla^2 z$ can be written as dS/dA. When the landscape reaches the steady state, elevation at any location no longer changes and the left side of Equation 1 is zero, giving:

$$UA = DS + KA^{m+1}S^{n} \tag{2}$$

Solving Equation 2 for *S* and setting *n*=1, as it is within the range of empirically observed values, to be able to solve the equation analytically gives:

$$S = \frac{UA}{D + KA^{m+1}} \tag{3}$$

Next, in the formula of TI (topographic index), substituting Equation 3 for S gives:

$$TI = \ln\left(\frac{D}{U} + \frac{K}{U}A^{m+1}\right) \tag{4}$$

The contributing area scales at different rates for hillslope, and channels and floodplains (Moglen and Bras, 1995; Perera and Willgoose, 1998); consequently, we write different equations for the contributing area frequency F(A) for hillslopes and channels.

But, first we will define where a channel starts on the landscape and the channel density. Diffusive erosion tends to smooth the surface while advective erosion roughens the surface. A channel starts when advective erosion outcompetes diffusive erosion (Willgoose et al., 1991; Tucker and Bras, 1998; Dietrich et al., 2003). It is worth noticing that channels produced by this mechanism merely represent incisions on a landscape and do not necessarily have consistent flow of water.

There are two approaches to quantify the hillslope to channel transition point. In the first approach, the transition point is defined as the location where diffusive and advective processes transport the same amount of sediment (Willgoose et al., 1991; Tucker and Bras, 1998).

In the second approach, the transition point is defined as the length of hillslope from the ridge where the diffusive erosion rate equals advective erosion rate (Perron et al., 2008; Sweeney et al., 2015). Here we adopt this second approach as the first approach underestimates the contributing area of the transition point (Perron et al., 2008). Thus, the length scale of the transition point is given as:

$$L_C = \left(\frac{D\zeta^{1-n}}{K} \right)^{\frac{1}{2m+2-n}} \tag{5}$$

where L_C is the hillslope length (m) and ζ is the relief of the basin which is obtained by numerically solving the governing equation (Perron et al., 2008).

In the case of n=1, Equation 5 becomes:

$$L_C \approx \left(\frac{D}{K}\right)^{\frac{1}{2m+1}} \tag{6}$$

For a given size basin, the drainage density is the total length of channel divided by total basin area and highly associated with hillsope length. Though the actual mathematical relation is more complicated, the drainage density can be estimated using a simple equation from hillslope length (Horton, 1945):

$$D_d = \frac{1}{2L_C} \tag{7}$$

where D_d is the drainage density (m/m^2) and L_C is the hillslope length (m), which is given by Equation 6. Equation 7 is exact for a rectangular hillslope and approximates hillslopes having other shapes.

Next, we derive the frequency distribution of A for hillslopes and channels. The drainage density and hillslope length will be used to derive the frequency distribution of A for channels. As previously found, the cumulative area scales with contributing area at a different rate for hillslopes and channels (Moglen and Bras, 1995; Perera and Willgoose, 1998); consequently, we have to write different equations of contributing area frequency F(A) for hillslopes and channels.

2.2 The 2D analytical model of frequency distribution of contributing area A

Assuming flow patterns are consistent along the slope (e.g., parallel, converging or diverging at the same rate), the cumulative distribution function of A is:

$$\begin{aligned} CDF(A) &= \int_0^A W_A dA \\ W_A &= W_0 - k_W A \end{aligned} \tag{8}$$

where W_A (m) is the total hillslope width (the length of iso-line) of given A in a basin; W_0 (m) is the hillslope width at the ridge; k_w is a parameter that depends on the flow pattern (0 for parallel flow, positive for convergent flow and negative for divergent flow). The frequency distribution function of A is the derivative of CDF(A); thus, it can be written as:

$$F_h(A) = W_0 - k_W A \tag{9}$$

As for channels, for the sake of simplification we will derive the relation based on the order of the channel instead of for each location in the channel and use that as the approximation for each location belonging to that order channel. The frequency for each order channel in a watershed is given by the total length; the contributing area will be given by averaging over the contributing area of each location of the channel. We assume that the channel network structure is given by Tokunaga's (1978) channel network model. The model has three rules defining channel network structure: 1) converging of two nth order channels produces a $(n+1)$th order channel; 2) the number of nth order channels draining into the side of an $n+1$th order channel is given by a parameter $\boldsymbol{\varepsilon}$; 3) the number of $(n-1)$th order channels draining into the side of an $(n+1)$th order channel is proportional to ε and given by another parameter $\boldsymbol{\kappa}$. These rules give the relation between length and number of different order of channels and the total length of channels in a watershed. Combined with Equation 10, we derived the frequency distribution of the channel as the total length of a given order channel and its average contributing area (see S1 for derivation):

$$F_{C_k}(\overline{A_k} = \frac{3}{16}4^k C^2 L_1^2) = (\frac{2}{3}4^{\lambda-k} + \frac{1}{3})4^{(k-1)/2} L_1 \quad (10a)$$

$$L_1 = \frac{16C^2 \left(D/K\right)^{1/(2m+1)}}{\sqrt{64\left(D/K\right)^{2/(2m+1)} C^2 \frac{1}{A_\lambda} + 9} + 3} \quad (10b)$$

$$\lambda = \frac{1}{2\ln(2)} \ln\left(\frac{1}{64} \frac{\left(\sqrt{64C^2 A_\lambda \left(D/K\right)^{2/(2m+1)} + 9A_\lambda^{\ 2}} + 3A_\lambda\right)^2}{A_\lambda C^2 \left(D/K\right)^{2/(2m+1)}} \right) \quad (10c)$$

where F_{C_K} is the frequency (total length, m) of kth order channel, λ is the order of the watershed, k is the order of channel, ${}_\lambda N_{k_total}$ is the total number of kth order channels in a λth order basin; A_k (m^2) is the average area of kth order sub-watershed, A_λ (m^2) is the area of the watershed, L_1 (m) is the average length of first order channel and C is the shape parameter of the watershed.

2.3 The 2D analytical model of frequency distribution of soil moisture

We can write the frequency distribution function of TI of a watershed from Equation 9 and 10 as (see S2 for derivation):

$$F(TI) = \begin{cases} \frac{W_0}{(m+1)} e^{\frac{TI - TI_{\min}}{m+1}} \left(\frac{D}{K^m}\right)^{\frac{1}{m+1}} & TI_{\min} \le TI \le TI_C \text{ (hillslope)} \quad (11\text{ a}) \\ \frac{L_1}{3}\left(\frac{4^\lambda}{2^k} + 2^k\right), \overline{TI_k} = \ln(\frac{D}{K} + \frac{9}{256} 4^{2k} C^4 L_1^4) - \ln(\frac{U}{K}) \quad (k = 1 \text{ to } \lambda) & TI_C < TI \le TI_{\max} \text{ (channel)} \quad (11\text{ b}) \end{cases}$$

$$TI_{\min} = \ln(1 + \frac{K}{D} A_{\min}^{\ m+1}) + \ln(\frac{D}{U}) \quad (11c)$$

$$TI_C = \ln(2\frac{D}{U}) \quad (11d)$$

$$TI_{\max} = \ln(1 + \frac{K}{D} A_T^{\,m+1}) + \ln(\frac{D}{U}) \qquad (11e)$$

where λ and L_1 are given by Equation 10, TI_{min}, TI_C, and TI_{max} are minimum TI, TI of channel initiation point, and the maximum TI of a basin, A_{min} is the minimum contributing area, the contribution area of the pixels at ridge; A_T is the total contributing area of the basin.

2.4 Results of quantifying the connection of landscape development and soil moisture

The analytical model described by Equation 1 and 11 shows that the relative magnitude of diffusive to advective erosion, the D/K ratio, not only determines the length of first order channel and the basin order, but also determines the shape of the frequency distribution function of TI. On the hillslope (Figure 2.2), the amount of landscape of a given soil moisture increases at an exponential rate (Equation 11a), and the D/K ratio determines that rate (the slope coefficient of the exponential function in Equation 11a). The larger the D/K ratio is, the faster the increasing rate (Figure 2.2).

As for channels (Figure 2.3), the total length of a given channel order decreases with the order of that channel at a power law rate and the mean TI of the channel increases with channel order at a logarithmic rate; together these give the combined power law and logarithmic relation between total length and mean TI of the channel (Equation 11b, Figure 2.3). There are two ratios that impact the mean TI of a given channel, the D/K ratio and U/K ratio (the ratio of uplift rate to advective erosion coefficient) (Equation 11b). The D/K ratio affects the total length of a given order channel through L_1 and λ (Equation 10, Figure 2.4). Increasing D/K ratio increases average TI of a given order channel and decreases the total length of a given order channel. Increasing U/K ratio decreases the mean TI of a given order channel. The two ratios are related. Increasing

D/K ratio can come from increasing D or decreasing K or both. If increasing D/K is from increasing D only, mean TI of channel will increase. If increasing D/K ratio is caused by

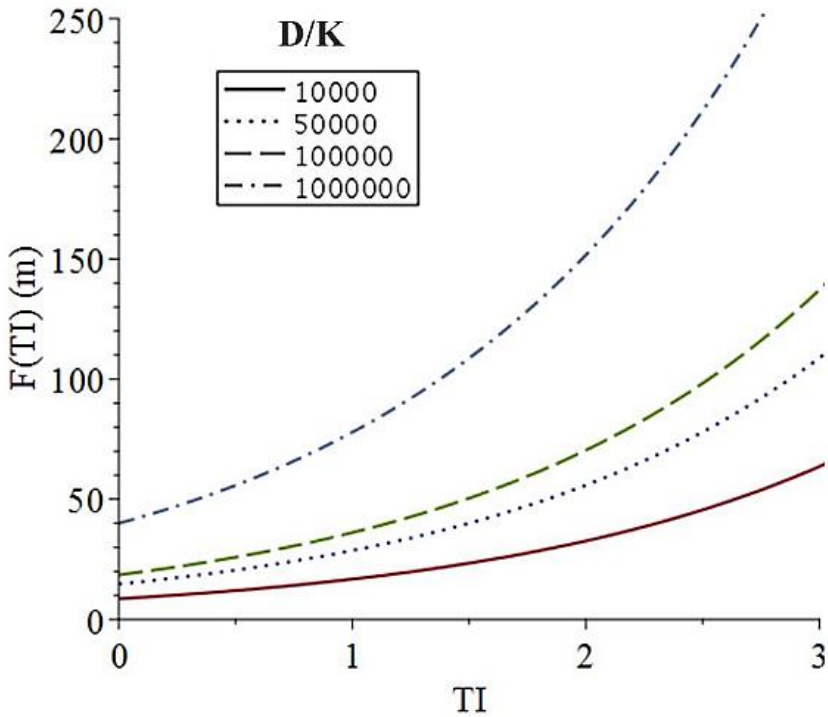

Figure 2.2. Impact of D/K on frequency distribution of TI of hillslope

Increasing D/K ratio increases the slope of the curve and shifts the curve upward.

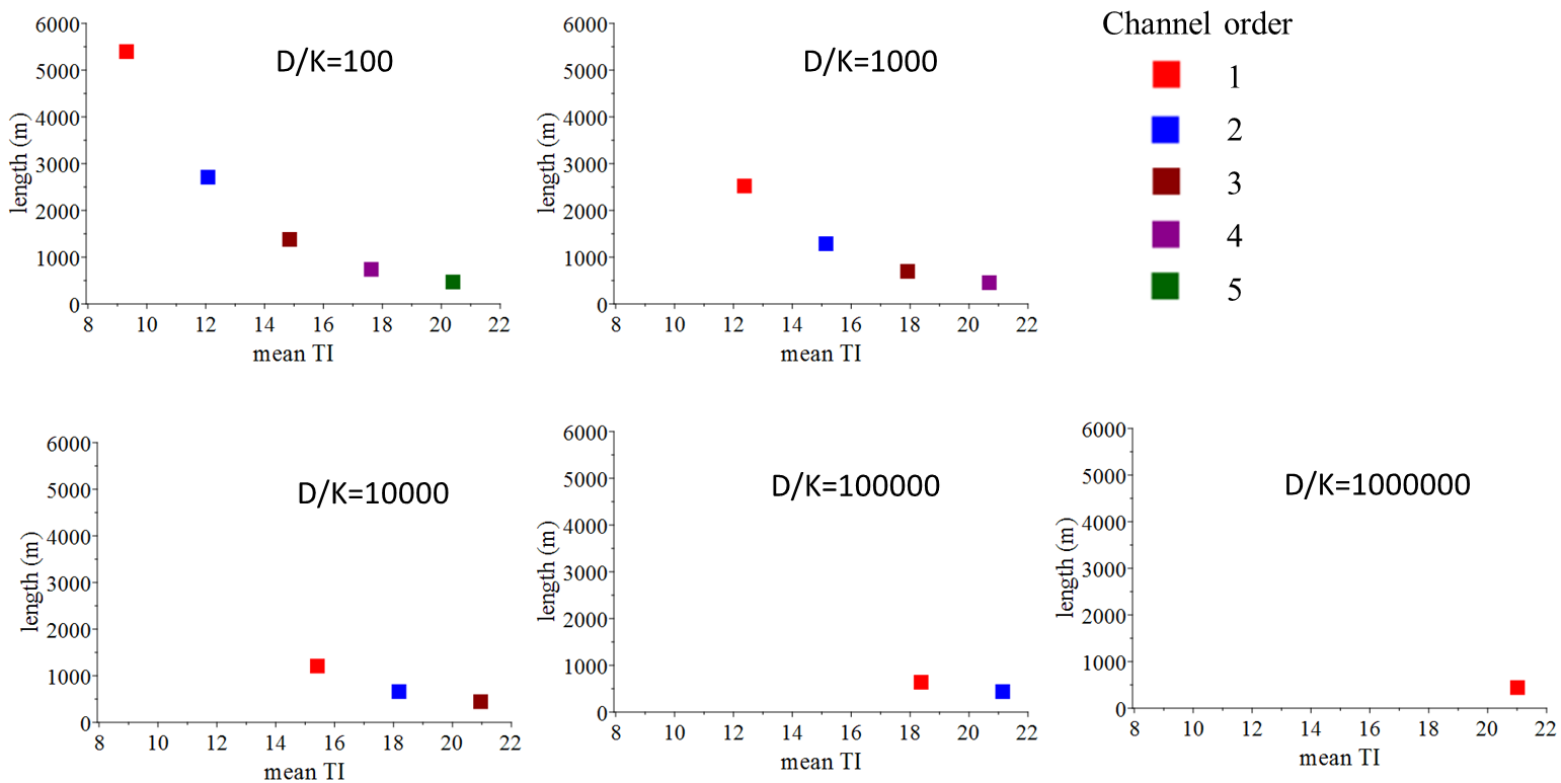

Figure 2.3 Change of the frequency distribution of TI of channel, the order of the basin and the total length of first order channel with D/K ratio.

Graphs showing the change of basin order and total length of each order channel of a given size basin when D/K ratio increases from 100 to 1000000. Each square represents a given order channel indicated by color. The corresponding TI value of that square is the mean TI of that order channel and the length is the total length of that order channel in the basin. The top left graph shows that if the basin has a small D/K ratio (100), it will have five order channels, meaning the basin order is five; the average TI of the first order channel in that basin is around 9 and the total length (the frequency) of the first order channel is 5500 m. The bottom right graph shows the other extreme end: a diffusive erosion dominated basin (D/K =1000000) that has the first order channel, and the basin order is one; the average TI of the first order channel in that basin is about 21 and the total length (the frequency) of the first order channel is 500 m.

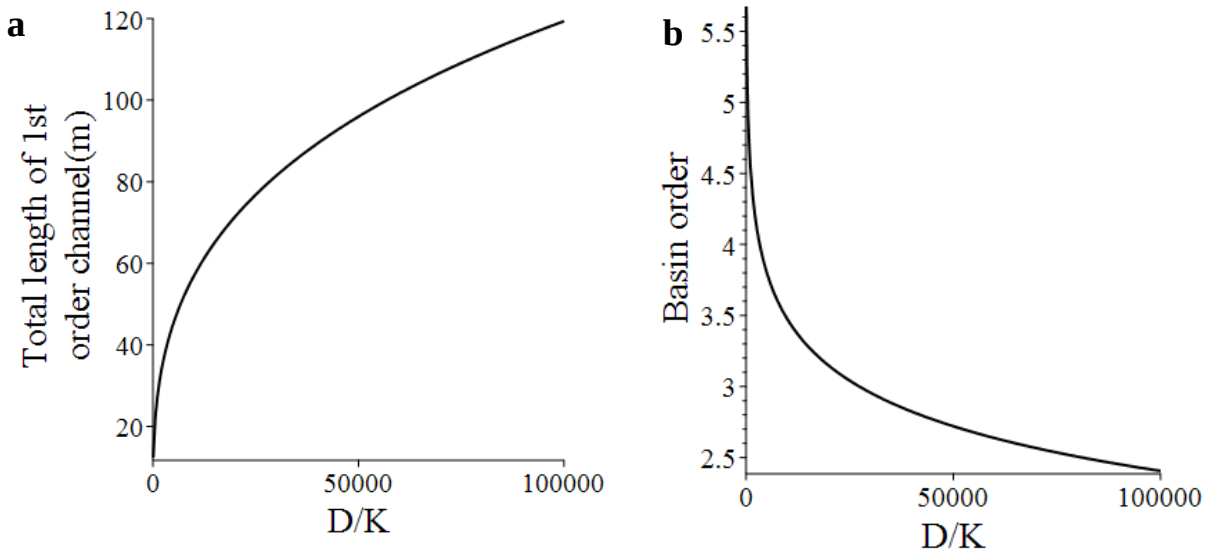

Figure 2.4 Impact of D/K on a) the total length of first order channel and b) basin order.

decreasing K, this also increases U/K ratio which has a negative impact on mean TI, but overall the mean TI of a channel increases with D/K ratio (Figure 2.3). Putting the frequency distribution of TI of hillslope and channel together, the amount of landscape of a given TI first increases with TI on hillslope at an exponential rate and peaks at the hillslope-channel transition point (TI = TIc), then the amount of landscape of given TI decreases with TI by an approximated power law function.

The D/K ratio and D/U ratio impact three important TI values: TI_{min}, TI_C, and TI_{max}. The TI_{min} on a landscape occurs at ridges where contributing area is very small. Thus, the TI_{min} is mainly determined by the D/U ratio. TI_{max} is more sensitive to the change of D/K ratio. If the total area of a basin A_T is much larger than 1, the effect of change in D/K on TI_{max} is exaggerated by A_T. Both TI_{min} and TI_{max} decrease with increasing D/K ratio and increase with increasing D/U ratio. If increasing D/K ratio is associated with increasing D, it may increase TI_{min} but decrease TI_{max}. On the other hand, if increasing D/K is associated with decreasing K, it can result in a slight decrease in TI_{min} and a large decrease in TI_{max}. TI at the hillslope – channel transition area (TI_C) is mainly determined by the relative scale of diffusive erosion to uplifting rate (D/U ratio). Increasing the D/U ratio increases *TIc*. Therefore, increasing the D/K ratio increases the difference between *TIc* and TI_{min} (Equation 12), but decreases the difference between *TIc* and TI_{max} (Equation 13).

$$TI_C - TI_{\min} = \ln(2) - \ln(1 + \frac{K}{D} A_{\min}{}^{m+1}) \qquad (12)$$

$$TI_{\max} - TI_C = \ln(1 + \frac{K}{D} A_T{}^{m+1}) - \ln(2) \qquad (13)$$

In summary, at one extreme the landscape is dominated by advective erosion (hillslope length is less than the size of the basic unit-grid cell of landscape), F(TI) peaks at the low end of the TI gradient and thus the driest place is most abundant on the landscape. At the other extreme when the landscape is dominated by diffusive erosion (e.g., hillslope length is larger than the scale of the landscape of interest), F(TI) peaks at the high end of TI with larger magnitude and thus the wettest place is most abundant on the landscape. When a change occurs from advective erosion dominance to diffusive erosion dominance, the peak of F(TI) moves along the TI gradient from left to right with an increased magnitude, showing more and more of the landscape becoming wetter with increasing relative magnitude of diffusive erosion (Figure 2.5).

We can further infer the 3D topography from the shape of the frequency distribution of TI. A leftward low peak of F(TI) is associated with a landscape of higher channel density and rough topography, which is characteristic of an advective dominated landscape, while a rightward high peak is associated with large areas of hillslopes and few channels.

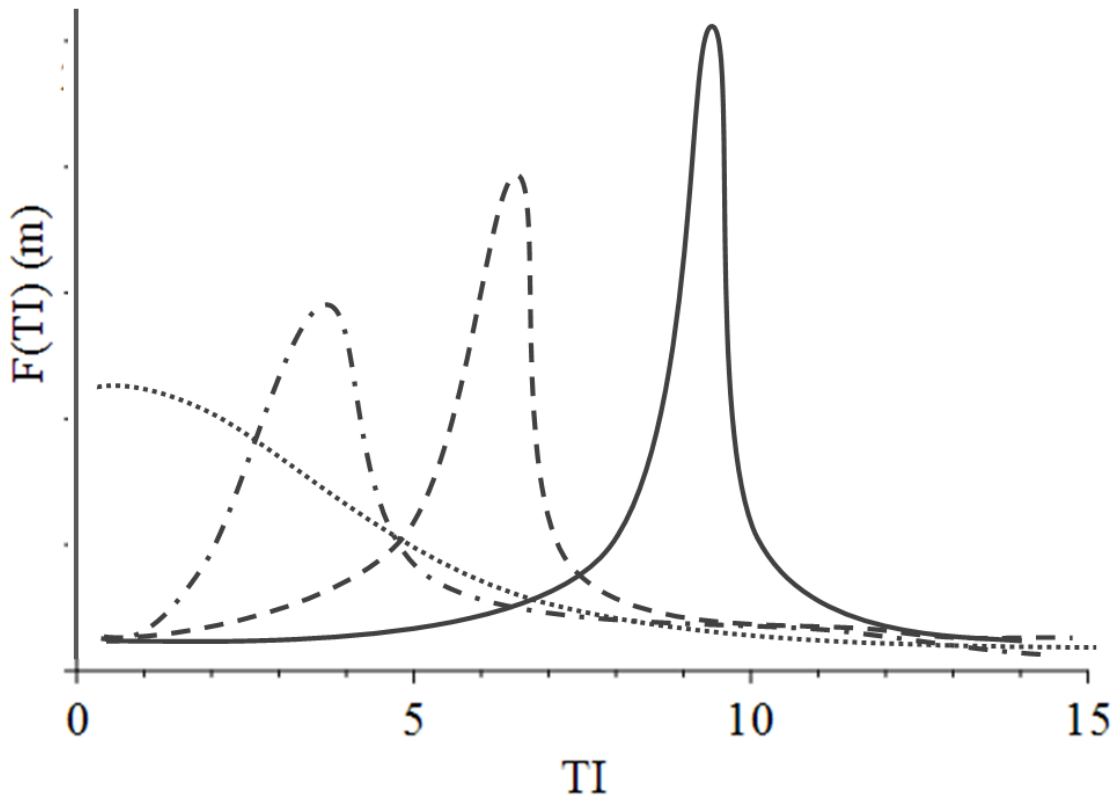

Figure 2.5 Hypothetical change of the shape of frequency distribution of TI of a basin with shifting of the relative magnitude of diffusive erosion to advective erosion.

Two extreme scenarios are shown by: the dot line (advective erosion dominance, e.g D/K=10000), the solid line (strong diffusive erosion dominance, e.g D/K=100000), and two intermediate scenarios, dash-dot line (slight increase in diffusive erosion dominance, e.g D/K=5000) and dash line (more dominance of diffusive erosion, e.g D/K=10000). Shifting from advective erosion dominance to diffusive erosion dominance increases the height of the peak and narrows the shape.

3. Synthetic landscapes

3.1 Model setup

To verify the conceptual TI distribution model (Equations 11), we conducted a numerical experiment using the Landscape Development model (CHILD V10.2, Tucker et al., 2001). We created three simulated (synthetic) landscapes with different D/K ratios: Landscape A has strong diffusive erosion dominance by large D/K (D/K=370). Landscape B has strong advective erosion dominance by small D/K (D/K=50), and Landscape C has an intermediate D/K (D/K=150). The sediment transport is set to be detachment limited, i.e., once the sediments are lifted, they will be carried away and no deposition occurs along the pathway. The linear diffusion function is used. The distance between cells is set to 15 m. Each simulation was run till the landscape reached the steady state. The output of CHILD is an irregular hexagonal mesh. We converted the mesh into 10 m x 10 m regular grids using ArcMap. Then, maps of TI on the three landscapes were created using Tau DEM Version 5 (Tarboton and Mohammed, 2010). The channels on such synthetic landscapes are not specifically distinguished between gully, seasonal stream or annual stream. The low order channels on the advective erosion dominated landscape are most likely to be gullies or swales where plants may grow.

3.2 Results from CHILD model

We next examined the topographic characteristics of three synthetic landscapes (Figure 2.6) produced by numerical landscape development model CHILD and compared the frequency distribution of TIs of the synthetic landscapes to the analytical model (Equation 11). We also examined the impact of D/K on the spatial pattern of TI variation using the synthetic landscapes.

A strong diffusive erosion dominated landscape (larger D/K, Landscape A in Figure 2.6) has fewer channels, is less dissected, and consequently has longer and wider hillslopes, while a strong advective erosion dominance (small D/K, Landscape C in Figure 2.6) results in higher channel density, greater dissection of the landscape and shorter hillslopes. All three synthetic landscapes have low TI at ridges, intermediate TI on hillslopes, and high TI along channels. In general, ridges have low variation of TI compared to channels; landscapes produced by strong diffusive erosion have smaller local variation of TI and a more aggregated spatial pattern of TI (Figure 2.6).

Figure 2.7 shows the frequency distribution of TI of three synthetic landscapes. The frequency distributions of TI of the three synthetic landscapes all have a unimodal, right skewed shape. They have similar extension of the tails but differ in the magnitude of the peaks. The frequency distribution of TI of a strong diffusive erosion dominated landscape (Landscape A) has a higher peak, while decreasing the relative magnitude of diffusive erosion reduces the peak (Landscapes B and C). The difference between TI_{max} and ITc increases with decreasing dominance of diffusive erosion, indicating that the peak of the frequency distribution of TI shifts to the right with increasing advective erosion dominance. The way that the shape of frequency distribution of TI of 3D synthetic landscapes changes with D/K ratios matches the way described by the 2D analytical model, which predicts the slope of the frequency distribution of TI of both hillslopes (Figure 2.2), and channels (Figure 2.3) become steeper with increasing D/K ratio. In summary, a majority of the landscape becomes drier and exhibits reduced soil moisture diversity with increasing dominance of advective erosion. Other studies also found that advective

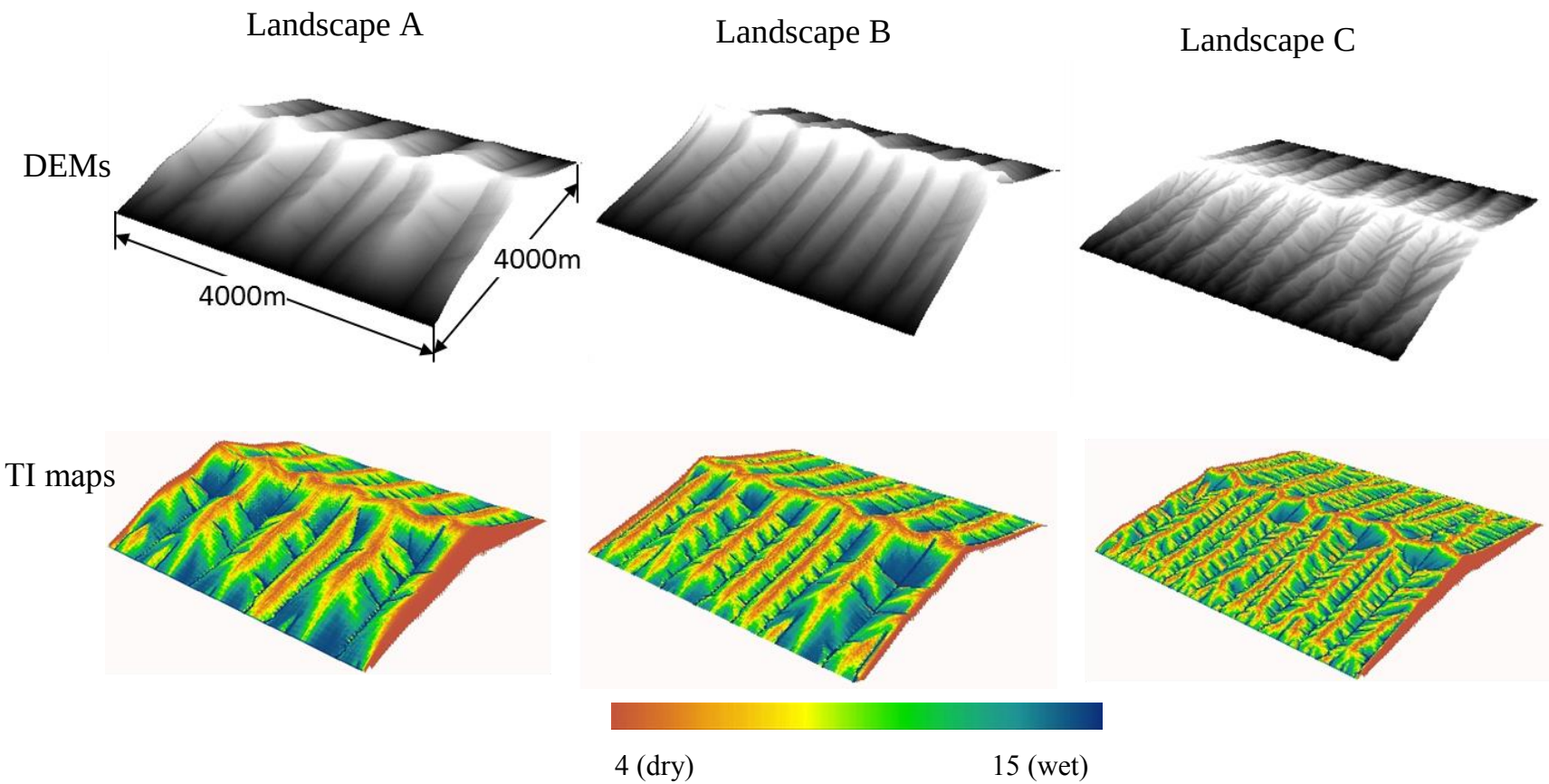

Figure 2.6 Digital elevation model (top) of three synthetic landscapes

landscape A - strong diffusive erosion, Landscape B - intermediate, and Landscape C - strong runoff erosion; as well as TI maps (bottom) of the three landscapes.

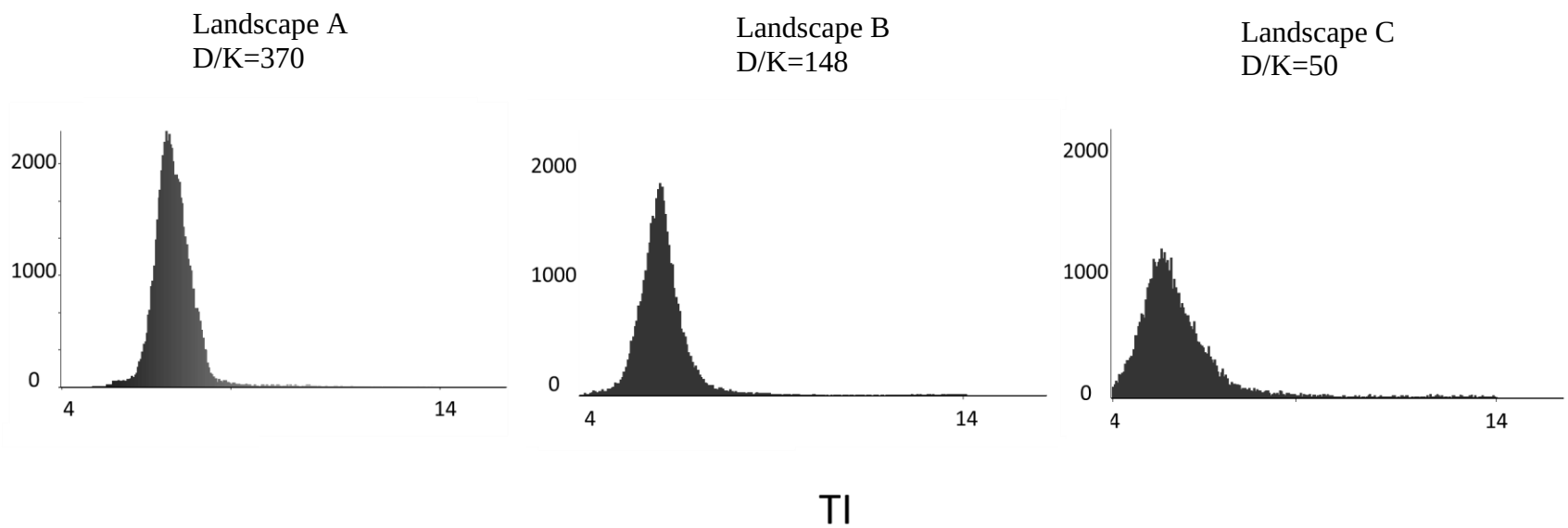

TI_{max}: 14.11
TI_{min}:4.99
Mode($TI=TI_c$): 6.85
$TI_{max} – TI_c$: 7.26
$TI_c – TI_{min}$: 1.86

TI_{max}: 13.8357
TI_{min}:4.5
Mode($TI=TI_c$): 6.27
$TI_{max} – TI_c$: 7.57
$TI_c – TI_{min}$: 1.77

TI_{max}: 14.94
TI_{min}:4.6
Mode($TI=TI_c$): ~6.23
$TI_{max} – TI_c$: 8.71
$TI_c – TI_{min}$: 1.63

Figure 2.7 Frequency distribution of TI of three synthetic landscapes and the values of three critical TI values as well as the range of variation between them. TI_{max} is the maximum TI value, TI_{min} is the minimum TI value and TI_c is the TI value of the peak of the frequency distribution which is the TI value of the theoretical channel initiation point.

erosion dominated hillslopes tend to be drier and diffusive erosion dominated hillslopes tend to be wetter (e.g. Hack and Goodlett, 1960; Yetemen et al., 2010).

In summary, the outcomes of the analytical model and the numerical experiment show that the frequency distribution of TI of landscapes with different D/K ratio all have one mode and a right skewed tail, but they differ in the height of the peak of the mode and the size of the tail. The peak of the TI frequency distribution indicates the end of the hillslope and start of the channel. This is because the rate of TI increase with increasing contributing area decrease and the flow pattern is approximately parallel on the hillslope, therefore the areas that have similar TI increase along the hillslope. The longer the hillslope is, the higher the peak. The flow pattern of the channel is highly convergent. Therefore, in the channel the quantity of a given value of TI decreases with increasing TI value and the mean TI increases with channel order very fast. This gives the frequency distribution of TI a right-skewed tail. However, the landscape with low D/K ratio has a flatter shape than the one with higher D/K ratio. Therefore, all landscapes have a relatively small proportion of area with very high soil moisture, but landscapes with high D/K ratio have very high proportions of intermediate soil moisture while landscapes with low D/K ratio have a relatively even proportion of areas with low and intermediate soil moisture.

Assuming the landscape is homogeneous in climate, soil depth, texture, and nutrients, the results show that the relationship between the landscape properties of hillslope length and width, channel density, and basin order, and the variation of soil moisture is mainly controlled by the relative magnitude of diffusive and advective erosion captured by the D/K ratio. This provides a means to connect plant abundance to geomorphic processes in terms of D/K ratio and the contributing area. To complete the connection, plant tolerance curves are used to link plant abundance to soil moisture and thus to landscape processes.

4. The effect on abundance and spatial distribution of three plant groups

It is a common observation that, on the landscape, some plants prefer relatively dry soil and grow on the area along ridges, some plants prefer intermediate soil moisture and dominate the middle section of hillslopes, and some plants like relatively wet soil and are found along streams. Therefore, plants on a landscape can be grouped into three generic groups: xeric, mesic, and hydric plants. Depending on the actual region, the three groups will be represented by different real plant species occurring in that region. For example, although we will call the plants preferring relatively dry conditions as xeric plants, the xeric plant species in humid regions are not the same as xeric plant species in arid regions. The performance of a given plant is maximized at its ideal environmental condition (in this case, soil moisture), which is genetically determined, and decreases when the environment deviates from the ideal condition (Lynch and Gabriel, 1987). Practically, the performance of plants can be measured by different ways, such as net primary productivity, above ground biomass, and the number of plants observed in a given area. The change of plant performance against an environmental gradient can be described by a Gaussian function, which is called a tolerance curve. We created tolerance curves for three hypothetical plants: xeric, mesic, and hydric plants, in the way that all of them have the same width parameter but differ in the mode (Figure 2.8).

Using these tolerance curves and TI maps, we mapped the performance of three plants on each landscape (Figure 2.9a). From plant performance maps, we produced land cover maps of three landscapes (Figure 2.9b) by assigning every pixel the plant type which had the highest performance associated with the TI value of that pixel among all three plant types. The land

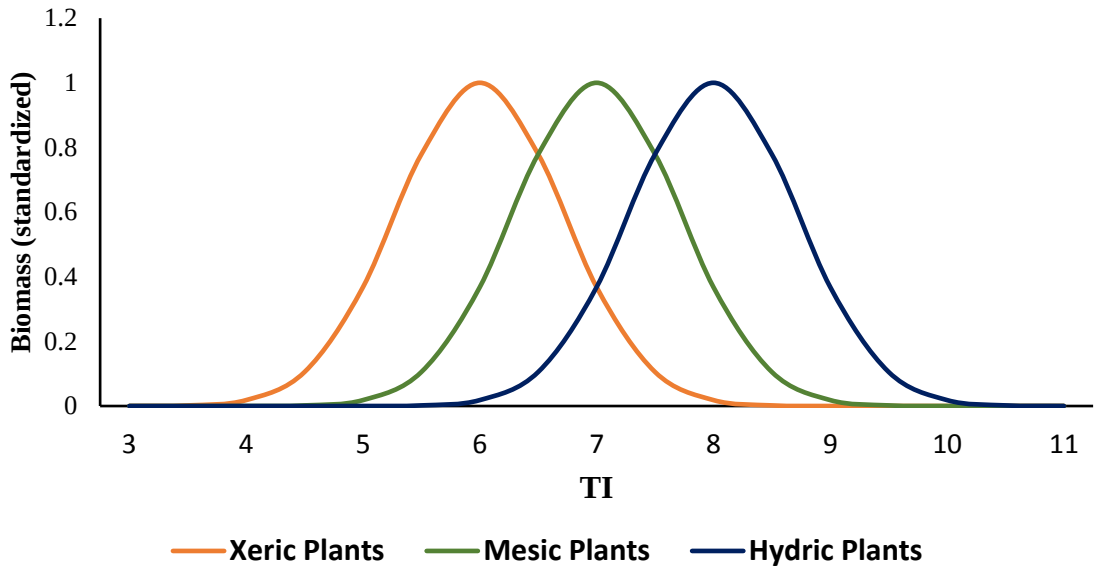

Figure 2.8 Tolerance curves of three hypothetical plants describing changes of performance along a TI gradient generated by Gaussian function.

The performance is between 0 and 1 with 0 meaning poorest performance and 1 representing the best performance. The three tolerance curves have the same shape but are maximized at different TI.

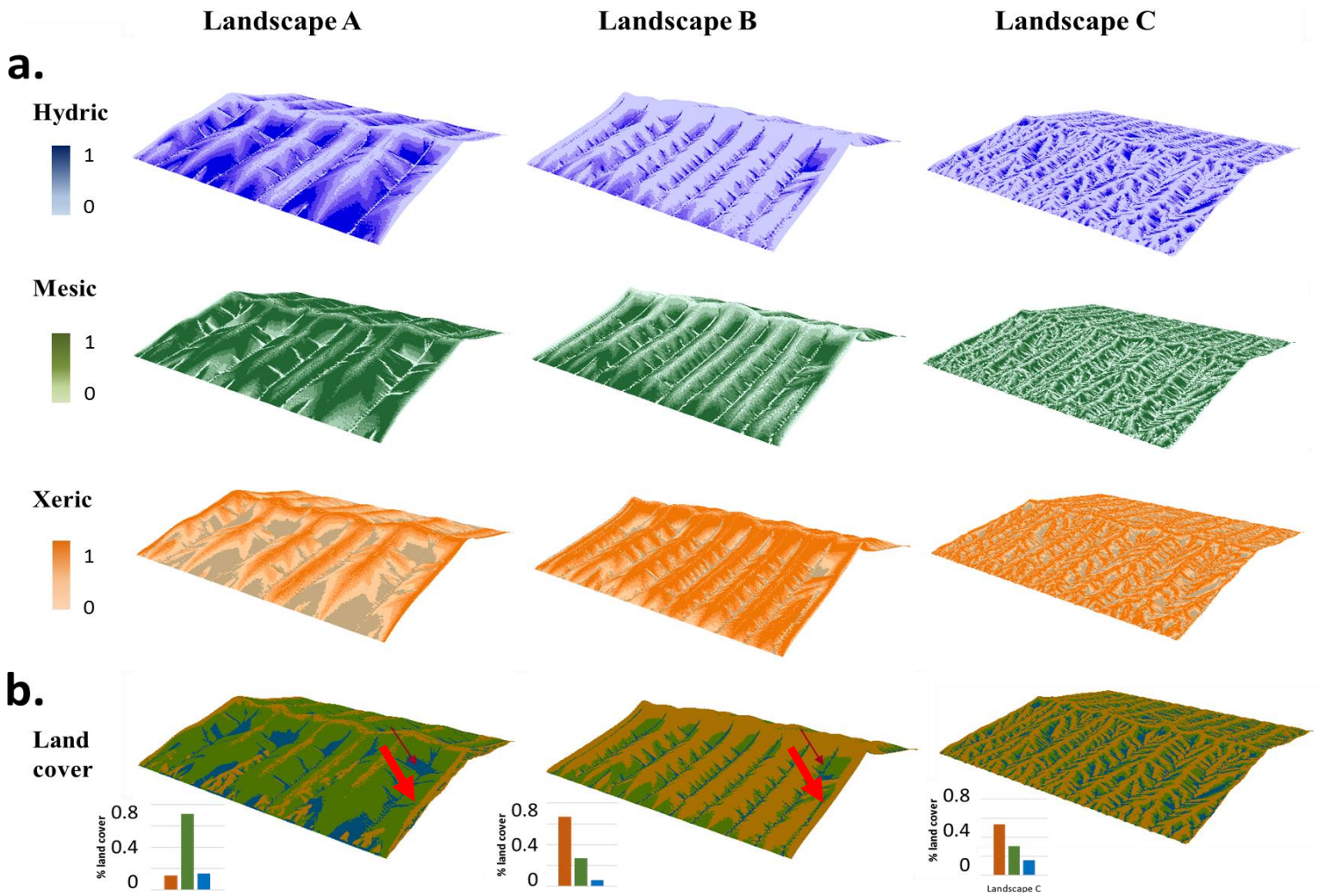

Figure 2.9 Effect of D/K on: a. the distribution of different plants on the landscape; b. spatial variation of the performance of hydric, mesic, and xeric plants on three synthetic landscapes;

land cover maps of the dominant plant on any location of the landscape and the relative abundance of each dominant plant type on three synthetic landscapes shown by bar plots below. The red arrows point to the dominant plant on foot slope: foot slope of Landscape A is dominated by hydric plants but by mesic plants on Landscape B.

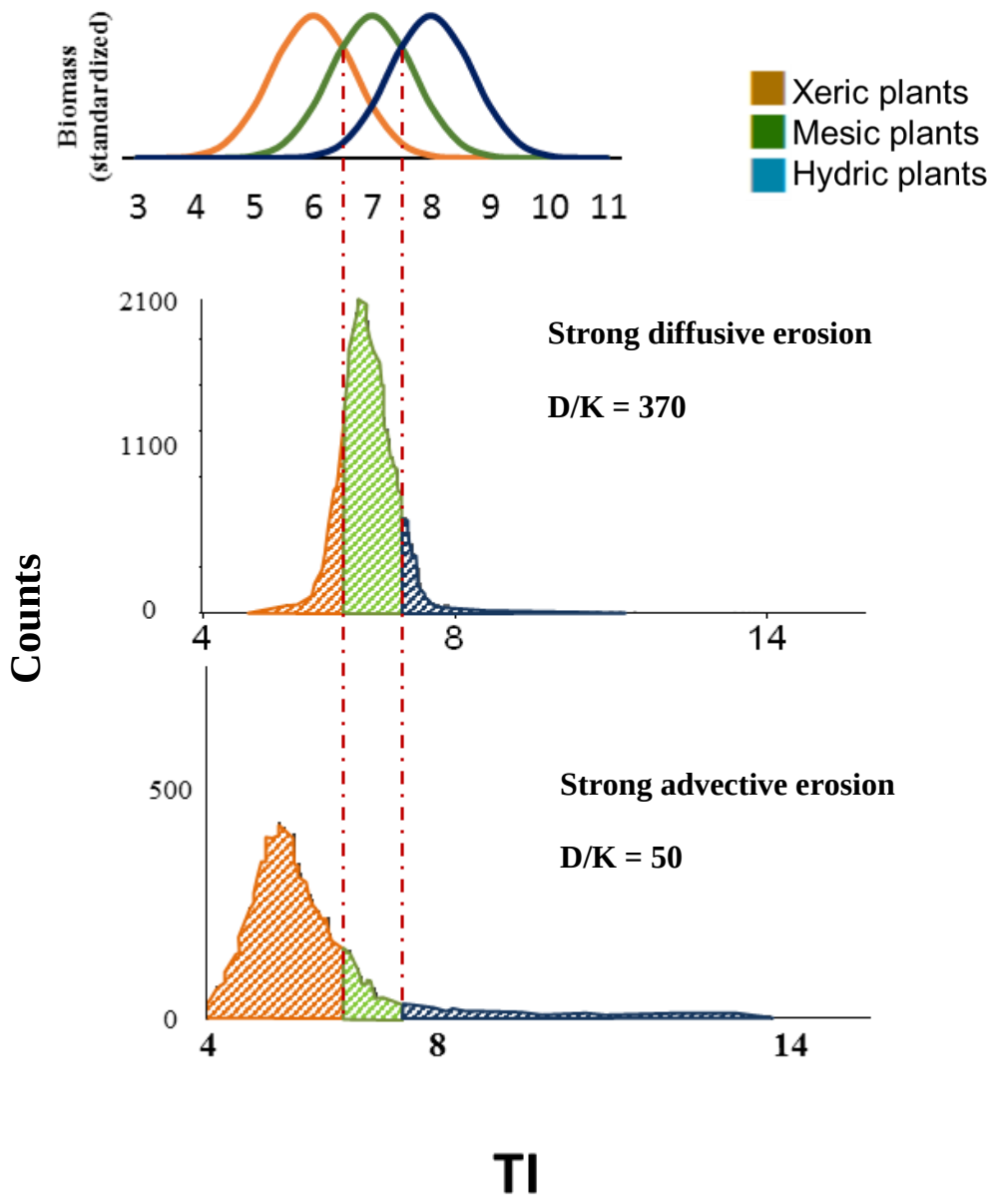

Figure 2.10 The impact of the combined effect of differentiation of moisture preference of plants and the shape of the frequency distributions of TI determined by D/K ratio on the relative proportion of the three plant types on landscapes shown by different colors.

cover maps show where on each landscape a given type of plant performs best and can dominate over the other two.

Hydric plants prefer high moisture conditions (high TI). They have poor or intermediate performance on nose and side slopes where soil moisture is low, and good performance on hollow and foot slopes where soil moisture is high. Mesic plants prefer intermediate moisture conditions (intermediate TI). They perform poorly on nose, foot slope and hollows, but have good performance on side slopes. Xeric plants prefer dry conditions and perform well on nose slopes (Figure 2.9a). A change of relative magnitude of diffusive erosion to advective erosion changes the hillslope length and channel density. This has two effects.

First, varying the hillslope length and channel density changes the proportion of the landscape components that are preferred by different plants (Figure 2.9a). This affects the relative abundance of different plants on the landscape and their spatial distribution (Figure 2.9b). A diffusive erosion dominated landscape (Landscape A) has longer and wider hillslopes and low channel density, thus a large amount of side slopes and small amount of nose and hollows. Therefore, it would have a high abundance of mesic plants and a low abundance of xeric and hydric plants (Figure 2.9b, Landscape A). Increasing the relative magnitude of advective erosion increases the amount of nose and hollows on landscapes and decreases the amount of side slopes and foot slopes through increased channel density. Therefore, xeric plants become more abundant than mesic plants (Figure 2.9b, Landscape B and C). Further, increasing advective erosion changes the relative amount of the landscape that is dominated by each plant type, the mesic plants becomes less abundant whereas the xeric plants become the most abundant one (Figure 2.9b).

Second, a change of relative dominance from diffusive erosion to advective erosion alters the extent of the landscape components. Landscapes created by diffusive erosion (Landscape A) have longer hillslopes and larger zero order basins than those on more advective erosion dominated landscapes (Landscape B and C). The extent of the landscape components (ridge, nose, side slope, foot slope, and hollow) on a diffusive erosion dominated landscape is larger than those on a more advective erosion dominated landscape (Figure 2.6 DEMs). Therefore, plants that prefer different moisture conditions that are associated with these landscape components appear in large patches on diffusive erosion dominated landscapes and in small patches on more advective erosion dominated landscapes (Figure 2.9b).

Third, soil moisture increases with hillslope length, which scales with the D/K ratio. This causes the soil moisture of the same landscape components (e.g., foot slopes) to differ among landscapes created by different D/K ratios. For example, the foot slope of Landscape A is dominated by hydric plants, but the foot slope of Landscape B is dominated by mesic plants (Figure 2.9b). This might explain why the hardwood forest that prefers moist soil was absent from the foot slope and hollows in a small first order valley (valley 1 in Hack and Goodlett, 1960) but dominates those locations in a large valley (valley 3 in Hack and Goodlett, 1960) in the Shenandoah River, Augusta and Rockingham Counties, Virginia, U.S.A.

There is a relationship between topographic properties and the abundance and distribution of plants. High abundance of mesic plants and low abundance of xeric and hydric plants distributed in an aggregated pattern are associated with the landscape properties of longer and convex-upward hillslopes and low channel density, where diffusive erosion such as soil creep is the major erosion process indicated by a large D/K ratio. Relatively even and low abundance of

mesic and hydric plants and slightly higher abundance of xeric plants distributed in a separated pattern is associated with the landscape properties of short and concave hillslope and high channel density, where advective erosion is the major erosion process indicated by a small D/K ratio. The three synthetic landscapes show the change of landscape structure from one extreme (e.g., diffusive erosion dominance) to the other extreme (e.g., advective erosion dominance) and the corresponding change of relative abundance and distribution of the dominant plants on the landscape. Climate change can alter the D/K ratio. Increasing storm intensity can increase total runoff and thus increase the relative magnitude of advective erosion. The landscape structure may slowly change from the one shown by Landscape A to Landscape B. This will result in a decrease in mesic plants and increase in xeric plants and/or disappearance of hydric plants from foot slopes.

It is the combined effect of the plant traits and geomorphic processes (Figure 2.10) that determines the vegetation composition. On the one hand, the topography produced by geomorphic processes regulates soil moisture variation that determines where on the landscape different types of plants dominate. On the other hand, plant traits determine the ideal soil moisture conditions of a given type of plant and how its performance decreases when soil moisture changes. Theoretically, tolerance curves represent the synthesized control of plant physiological, morphological, and biochemical traits on the response of plants to environmental gradients. The traits determine at which moisture level the plant's performance peaks, and the relative magnitude of diffusive erosion to advective erosion determines the soil moisture of the major part of the landscape. Here, we mechanically connected the soil moisture variation to geomorphic processes. However, the tolerance curves are still lacking the physiological

connection that links plant performance to traits. Further studies are needed to make this connection.

Our study has explored the direct control of geomorphic processes on plant abundance and distribution. However, plant ecologists have also long recognized that plants with different functional traits respond to and modify their physical environment differently (Diaz and Cabido, 2001; Garnier, 2004; Kremen, 2005; Grime, 2006; Garnier and Navas, 2012). It has been known that plants (and other organisms) play an important part in geomorphic processes (Murray et al., 2008; Reinhardt et al., 2010; Steiger and Corenblit, 2012; Porder, 2014). Steiger and Corenblit (2012) suggest the long-term effect of the feedback introduces an evolutionary component of landscape organization so that landform and plant community coevolve over time.

Recently, a group of geomorphologists started to incorporate explicitly the effect of vegetation on the geomorphic processes of landscape development models (e.g., Ivanov et al., 2008; Collins and Bras, 2008, 2010; Istanbulluoglu et al., 2008; Yetemen et al., 2010; Zhou et al., 2013). These models are mainly developed for arid or semi-arid regions, and the vegetation dynamic is mainly controlled by the variation of solar radiation induced by slope aspect rather than the topographic regulated lateral flow. In those studies, the landscape development model was coupled with a fully distributed eco-hydrological model that hence required a large input of plant and climatic parameters. This is a disadvantage of those complex models. So far, the interaction between plants and geomorphic processes through topographic regulated groundwater table depth has not been explicitly described in the landscape development model. A recent study showed ground water table depth in mountain regions is highly correlated with topography and regulates the water available to plants (Fan et al., 2017). Through connecting water table depth to erosion rates, the formula we derived provides an easy and simple way to explicitly integrate the

vegetation productivity and landcover types into D and K (e.g., weighted by vegetation productivity and landcover type), and thus provides a simple and direct way to address the feedback between plants and landform.

5. Suggestion on model testing

To test the model, the first step is to select study areas. This model is based on some assumptions. The model is based on the steady state of the landscape; thus, the landform of the study areas should more or less have reached the steady state. While in disequilibrium, the channel network geometry will adjust by either migration of the drainage divide or river capture (Willett et al., 2014). A landscape index χ (Willett et al., 2014) based on the river network geometry can be used to determine whether the channel network is at steady state or not. When the profiles of the rivers on both sides of a drainage divide are the same, the network is at steady state; otherwise, it is not.

Other assumptions of the model (Equation 4 and 11) include: homogeneous soil depth and properties, the bed rock is the parent material, and homogeneous net precipitation. In the real world, these assumptions are not all met. These assumptions might not always hold. To test the generality of the model, one can plot the predicted frequency distribution curve using Equation 11, then compare this to the field observation of average annual soil moisture. If the model prediction is not consistent with the field observation, the assumptions of the model can be relaxed to explicitly express the heterogeneity of former variables.

In case the assumption of steady state is not met, the model can be manipulated to explicitly incorporate the starting surface and time stage for transient landscapes. The initial surface can be described by an equation that expresses the elevation z by location x and y; then

the model can be solved at any time step analytically. In such way, the solution of the landscape evolution model will integrate the starting surface. The equation of the starting surface of the landscape evolution model can be derived from large scale processes such as tectonic and/or glacier erosion. This will need a plate tectonic model or a glacier erosion model or both, which is beyond the scope of this thesis.

6. Conclusions

The diffusive-advective erosion created landscapes have a similar structure across different scales. They are all composed of hillslopes and channels but with different lengths and density, regardless of variations in the drivers and controls including climate and underlying geology (see Rodriguez-Iturbe and Rinaldo, 1997). The relative magnitude of diffusive erosion to advective erosion, the D/K ratio, controls the landscape properties (e.g., hillslope length, drainage density and hillslope shape) that regulate soil moisture variation, one of the critical resources of plants.

In this study, we explored the theoretical relationship between geomorphic processes and the abundance and distribution of plants. The landscape properties determine the hydrological processes that control the soil moisture variation through the contributing area (A) and local slope (S) as given by a Topographic Index.

To connect the Topographic Index to D and K analytically, we simplified the landscape from 3D to 2D (one dimension is the elevation, another dimension is the distance from the ridge equivalence to contributing area). We solved the governing equation of the 2D landscape development (Equation 1) at steady state to produce an analytical equation of the relationship of slope (S) and contributing area (A). We then used this equation to replace slope (S) in the

Topographic Index so that the Topographic Index is expressed in terms of D, K, and A. This gives us the relationship between soil moisture variation and geomorphic processes.

To complete the connection, plant tolerance curves were used to link plant abundance to soil moisture. Using the hypothetical tolerance curves of three plants, we showed that the abundance and distribution of xeric, mesic, and hydric plants on the landscape are regulated by the D/K ratio. As both are controlled by the D/K ratio, properties of topography and the abundance and distribution of plants are associated. The diffusive erosion dominated landscape (large D/K) has high abundance of mesic plants and low abundance of xeric and hydric plants distributed in an aggregated pattern, and the landscape is characterized by longer and convex-upward hillslope and low channel density. Strongly advective erosion dominated landscape (small D/K) has even abundance of different plants with slightly higher abundance of xeric plants distributed in a separated pattern, and the landscape is characterized by short and concave hillslope and high channel density.

7. Acknowledgments

This study was funded by the Natural Sciences and Engineering Research Council of Canada (NSERC). The input file for running CHILD model and the model outcomes are accessible as separate supplementary material. The code of CHILD can be downloaded from http://csdms.colorado.edu/wiki/Model:CHILD.

8. Supporting Material

8.1. Introduction

The supplemental material contains the derivation of the frequency distribution of contributing area A, the frequency distribution of topographic index TI, and the setups of CHILD to produce three synthetic landscapes. The input and output datasets of the CHILD model are uploaded separately.

8.2. Derivations of frequency distribution of contributing area (A) of channel

From rule 2 and 3 of Tokunaga's model (detailed in the paper), the number of a *n*th order channel drains into the side of a (*n*+*i*)th order channel is $\kappa^{i-1}\varepsilon$. From the above rules, Tokunaga (1978) further derived the following relations which we will use to derive our model:

$$ {}_{\lambda}N_k = \frac{Q^{\lambda-k-1} - P^{\lambda-k-1}}{Q-P} Q(2+\varepsilon-P) + P^{\lambda-k-1}(2+\varepsilon) \qquad (S1\text{ a}) $$

$$ A_k = Q^{k-1} A_1 \qquad (S1\text{ b}) $$

$$ L_k = Q^{(k-1)/2} L_1 \qquad (S1\text{ c}) $$

where $P = [2+\varepsilon+\kappa-\sqrt{(2+\varepsilon+\kappa)^2-8\kappa}]/2$, $Q = [2+\varepsilon+\kappa+\sqrt{(2+\varepsilon+\kappa)^2-8\kappa}]/2$, ${}_{\lambda}N_k$ is the total number of *k*th order channels in a λth order basin; A_1 (m^2) is the average area of 1st order basin, A_k (m^2) is the average area of *k*th order basin, L_k (m) is the average length of *k*th order channel and L_1 (m) is the average length of first order channel. Here we are using the typical values of two parameters by Tokunaga (1978): ε =1 and κ =2, then P=1, Q=4. This gives the relationship of channel length between different order channels as well as the channel length and basin area of a given order basin.

The total length of kth order channels in a λth order basin is the total number of kth order channels in a λth order basin (${}_{\lambda}N_k$) multiplied by the average length of kth order channel (L_k), which are given by Equation S1a and S1c:

$$ {}_{\lambda}L_{k_total} = {}_{\lambda}N_k \bullet L_k \tag{S2} $$

Substituting ${}_{\lambda}N_k$ by Equation 4a, L_k by Equation 4c, and Q by 4, Equation A2 can be written as:

$$ {}_{\lambda}L_{k_total} = (\frac{2}{3}4^{\lambda-k} + \frac{1}{3})L_1 4^{(k-1)/2} \tag{S3} $$

For a kth order channel, if assuming the channels with same order drain directly into its side is evenly spaced, we can write the average contributing area per unit channel width of kth order channel as:

$$ \begin{aligned} \overline{A_k} &= \frac{2A_{k-1} + A_k}{2} \\ &= \frac{3}{16}4^k C^2 L_1^2 \end{aligned} \tag{S4} $$

Now, both the total length of kth order channel and the average contributing area are expressed by L_1 and basin order λ. Next, using the relation between drainage density and hillslope length, we connect L_1 and λ to the parameter of the governing equation of landscape development (Equation 1).

Then the total length of channels of a basin of order λ is:

$$ L_{total} = \sum_{k=1}^{\lambda} {}_{\lambda}L_{k_total} \tag{S5} $$

Substituting ${}_{\lambda}L_{k_total}$ by Equation S5:

$$L_{total} = \sum_{k=1}^{\lambda} (\frac{2}{3} 4^{\lambda-k} + \frac{1}{3}) L_1 4^{(k-1)/2}$$
$$= \frac{1}{3} L_1 \left(4^{\lambda} + 2^{\lambda} - 1\right) \quad \text{(S6)}$$

Drainage density of a basin is the total channel length divided by basin area, which gives:

$$D_d = \frac{L_{total}}{A_\lambda} = \frac{L_1 \left(4^{\lambda} + 2^{\lambda} - 1\right)}{3A_\lambda} \quad \text{(S7)}$$

Equating Equation S7 to Equation 7, we get:

$$\frac{L_1 \left(4^{\lambda} + 2^{\lambda} - 1\right)}{3A_\lambda} = \frac{1}{2L_C} \quad \text{(S8)}$$

Equation S8 connects the length of first order channel to hillslope length for a given basin.

The main stream length of a given order basin, L_k, often shows a power law relation with its total area, A_k (Smart and Surkan, 1967; Eagleson, 1970):

$$L_k \sim A_k^h \quad \text{(S9)}$$

where h is the coefficient of the exponent. Following the assumption of Tokunaga (1978), h is 0.5 and the relation for the first order basin can be expressed as:

$$L_1 = CA_1^{0.5} \quad \text{(S10)}$$

Using Equation S1b, A_1 can be written as:

$$A_1 = \frac{A_\lambda}{Q^{\lambda-1}} \quad \text{(S11)}$$

Substituting A_1 in Equation S11 by Equation S10 and Q by 4, we get:

$$L_1 = \frac{2CA_\lambda^{0.5}}{2^{\lambda}} \quad \text{(S12)}$$

Solving Equation S8 and S12 together, we get the length of first order channel, L_1, and the order of the basin, λ:

$$L_1 = \frac{16C^2 A_\lambda L_C}{\sqrt{64 L_0{}^2 C^2 A_\lambda + 9A_\lambda{}^2} + 3A_\lambda}$$

$$\lambda = \frac{1}{2\ln(2)} \ln\left(\frac{1}{64} \frac{\left(\sqrt{64 L_C{}^2 C^2 A_\lambda + 9A_\lambda{}^2} + 3A_\lambda\right)^2}{A_\lambda L_C{}^2 C^2} \right) \tag{S13}$$

Substituting L_0 in Equation S13 by Equation 6, and putting Equation S6 and S13 together, we get the frequency distribution of TI of the channel:

$$F_{C_k}(\overline{A_k} = \frac{3}{16} 4^k C^2 L_1^2) = {}_\lambda L_{k_total} = (\frac{2}{3} 4^{\lambda - k} + \frac{1}{3}) 4^{(k-1)/2} L_1 \tag{S14a}$$

$$L_1 = \frac{16C^2 \left(D/K\right)^{1/(2m+1)}}{\sqrt{64\left(D/K\right)^{2/(2m+1)} C^2 \frac{1}{A_\lambda} + 9} + 3} \tag{S14b}$$

$$\lambda = \frac{1}{2\ln(2)} \ln\left(\frac{1}{64} \frac{\left(\sqrt{64C^2 A_\lambda \left(D/K\right)^{2/(2m+1)} + 9A_\lambda{}^2} + 3A_\lambda\right)^2}{A_\lambda C^2 \left(D/K\right)^{2/(2m+1)}} \right) \tag{S14c}$$

8.3. Derivations of frequency distribution of TI

For a hillslope, we use the equation of transformation of a continuous random variable to derive the probability density function of TI:

$$f\left(y\right)=f\left(x\left(y\right)\right)\left|\frac{dx}{dy}\right| \tag{S15}$$

In our case, in Equation S15, y is TI and x is *A*.

Rearranging Equation 4, we can write *A* as a function of TI and the derivation as:

$$\begin{aligned} A &= \left(\frac{Ue^{TI}-D}{K}\right)^{\frac{1}{m+1}} \\ \frac{dA}{dTI} &= \frac{Ue^{TI}}{(m+1)(UKe^{TI}-KD)^{\frac{m}{m+1}}} \end{aligned} \tag{S16}$$

Using Equation S15, the frequency distribution of TI of the hillslope is:

$$\begin{aligned} F_h(TI) &= (W_0-k_W A)\frac{Ue^{TI}}{(m+1)(UKe^{TI}-KD)^{\frac{m}{m+1}}} \\ &= (W_0-k_W\left(\frac{Ue^{TI}-D}{K}\right)^{\frac{1}{m+1}})\frac{Ue^{TI}}{(m+1)(UKe^{TI}-KD)^{\frac{m}{m+1}}} \end{aligned} \tag{S17}$$

Assuming the flow pattern of the hillslope is parallel, Equation S17 is reduced to:

$$\begin{aligned} F_h(TI) &= \frac{W_0Ue^{TI}}{(m+1)(UKe^{TI}-KD)^{\frac{m}{m+1}}} \\ &= \frac{W_0\frac{U}{KD^{\frac{m}{m+1}}}e^{TI}}{(m+1)(\frac{U}{D}e^{TI}-1)^{\frac{m}{m+1}}} \end{aligned} \tag{S18}$$

The minimum TI estimated from Equation 4 for A equals 10 m^2 m^{-1} is around 4; if the ratio of uplifting to diffusive erosion is not very small, Equation S4 can be approximated as:

$$F_h(TI) = \frac{W_0 \frac{U}{KD^{\frac{m}{m+1}}} e^{TI}}{(m+1)(\frac{U}{D} e^{TI})^{\frac{m}{m+1}}} = \frac{W_0 U^{\frac{1}{m+1}} K^{-\frac{m}{m+1}} e^{\frac{TI}{m+1}}}{(m+1)} \tag{S19}$$

For the channel, we use the transformation equation of a discrete random variable given y=w(x):

$$F_Y(y) = \sum_{x:w(x)=y} F_X(x) \tag{S20}$$

From Equation S14, we can write the probability density function of TI of kth order channel (with Q=4):

$$\begin{aligned} p_{C_k}(\overline{TI}_k) &= p_{C_k}(\overline{A}_k) = \frac{f_{C_k}(\overline{A}_k)}{A_\lambda} \\ &= \frac{1}{A_\lambda}(\frac{2}{3}4^{\lambda-k} + \frac{2}{3})4^{(k-1)/2} \frac{4}{C2^k}\sqrt{\frac{\overline{A}_k}{3}} \qquad (k = 1 \text{ to } \lambda) \\ \overline{TI}_k &= \ln(\frac{D + K\overline{A}_k^{\,2}}{U}) \\ \overline{A}_k &= \frac{2Q^{k-2} + Q^{k-1}}{2} C^2 L_1^2 = \frac{3}{16} 4^k C^2 L_1^2 \end{aligned} \tag{S21}$$

8.4. Description of the Setting of CHILD

CHILD allows the user to choose different situations. In our scenarios, we use the linear diffusive equation. The advective erosion is modelled as purely detachment limited erosion without a threshold, there is no change of channel geometry, and runoff is generated as infiltration exceeding surface runoff.

$$q_m = -D\nabla z \tag{S22}$$

$$q_m = \frac{D\nabla z}{1-(\frac{\nabla z}{S_c})^2} \tag{S23}$$

where D is the diffusion coefficient and S_c is the critical local hillslope. The coefficient D is a parameter that gives an overall measure of the coherence of material, the amount of energy involved in removing sediment (Carson and Kirkby, 1972; Black and Montgomery, 1991; Roering et al., 1999; Gabet, 2000; Anderson, 2002; Furbish et al., 2007; Furbish and Roering, 2013). S_c represents the point of mechanical failure and equals the effective friction coefficient of the sediment. There is evidence that at low to intermediate relief watersheds (gradient < 0.4), the linear diffusion equation is sufficient while at high relief watersheds the non-linear diffusion is more appropriate (Martin, 2007; Roering, 2008; Perron, Dietrich, and Kirchner, 2008). We use the linear diffusion function here.

The sediment transport rate is the detachment rate which is represented as the power function of excess shear stress, the difference between the shear stress that flowing water exerts on the particle and the shear strength (as threshold shear stress) that holds particles together (Istanbulluoglu, 2003; Tucker and Hancock, 2010):

$$\nabla q_f = \begin{cases} k_b(\tau - \tau_c)^{P_b} & \tau > \tau_c \\ 0 & \tau \leq \tau_c \end{cases} \tag{S24}$$

where τ is bed shear stress of an open uniform channel, τ_c is the shear strength or threshold shear stress, k_r is the regolith erodibility coefficient (m yr^{-1}), and P_b is a dimensionless constant giving how sediment entrainment rate scales with shear stress. If threshold shear stress τ_c is zero, Equation S24 becomes:

$$\nabla q_f = k_r \tau^{P_b} \tag{S25}$$

In CHILD shear stress is calculated as:

$$\tau = k_t q^{Mb} S^{Nb} \quad \text{(S26)}$$

$$q = \frac{Q}{w}$$

$$Q = (P - I)A$$

$$w = k_w Q^{1/2}$$

where k_t is a coefficient, Mb and Nb are constants, q (m^2 yr^{-1}) is discharge per unit width, S is the bed slope, Q (m^3 yr^{-1}) is the total discharge of a cross-section of stream, and w (m) is the width of the stream, P (m yr^{-1}) is the rate of precipitation, I (m yr^{-1}) is the infiltration rate, and A is the upslope contributing area. Combining Equation S23 and S24, the advective erosion rate is:

$$\nabla q_f = k_r {k_t}^{P_b} {k_w}^{-MbP_b} (P - I)^{MbP_b/2} A^{MbP_b/2} S^{NbP_b} \quad \text{(S27)}$$

Equation S25 has exactly the same form as the third term on the right side of Equation 1, where

$$K = k_r k_t^{P_b} k_w^{(-MbP_b)} (P - I)^{(MbP_b/2)}$$
$$m = MbP_b / 2$$
$$n = NbP_b$$

Table 1 Detailed setting of each parameter of three scenarios

Parameters	Scenario A (Large	Scenario B	Scenario C (small

	D/K)	(Intermediate)	D/K)
D	0.04	0.008	0.0199
Kr	0.000004	0.000004	0.000004
Kt	800	1200	1200
kw	10	10	10
P	6.8	16.22	6.5
I	3	2.2	4
P_b	1	1	1
Mb	0.375	0.375	0.375
Nb	0.81	0.81	0.81

9. References

Anderson, R. S. 2002. “Modeling the Tor-Dotted Crests, Bedrock Edges, and Parabolic Profiles of High Alpine Surfaces of the Wind River Range, Wyoming.” *Geomorphology* 46(1-2): 35–58.

Barling, R. D., I. D. Moore, and R. B. Grayson. 1994. “A Quasi-Dynamic Wetness Index for Characterizing the Spatial Distribution of Zones of Surface Saturation and Soil Water Content.” *Water Resource Research* 30(4): 1029–44. https//doi.org/10.1029/93WR03346

Beven, K. J., and M. J. Kirkby. 1979. “A Physically Based, Variable Contributing Area Model of Basin Hydrology / Un Modèle À Base Physique de Zone D’appel Variable de L'hydrologie Du Bassin Versant.” *Hydrological Sciences Bulletin* 24(1): 43–69.

Black, T. A, and D. R. Montgomery. 1991. “Sediment Transport by Burrowing Mammals, Marin County, California.” *Earth Surface Processes and Landforms* 16: 163–72.

Bridge, S. R. J., and E. A. Johnson. 2000. “Geomorphic Principles of Terrain Organization and Vegetation Gradients.” *Journal of Vegetation Science* 11: 57–70.

Brolsma, R. J., and M. F. P. Bierkens. 2007. “Groundwater-Soil Water-Vegetation Dynamics in a Temperate Forest Ecosystem along a Slope.” *Water Resources Research* 43(1): 1–10. https//doi.org/10.1029/2005WR004696

Carson, M. A., and M. J. Kirkby. 1972. *Hillslope Form and Process*. Cambridge University Press. New York.

Collins, D. B. G., and R. L. Bras. 2008. “Climatic Control of Sediment Yield in Dry Lands Following Climate and Land Cover Change.” Water Resources Research 44(10). http://doi.wiley.com/10.1029/2007WR006474.

———. 2010. “Climatic and Ecological Controls of Equilibrium Drainage Density, Relief, and Channel Concavity in Dry Lands.” Water Resources Research 46(4): W04508. http://www.agu.org/pubs/crossref/2010/2009WR008615.shtml.

Curtis, J. T. 1959. *The Vegetation of Wisconsin: An Ordination of Plant Communities*. Madison: Univ. Wisconsin Press.

Diaz, S., and M. Cabido. 2001. “Vive La Difference: Plant Functional Diversity Matters to Ecosystem Processes.” Trends in Ecology and Evolution 16(11): 646–55.

Dietrich, W. E., D. G. Bellugi, L. S. Sklar, and J. D. Stock. 2003. “Geomorphic Transport Laws for Predicting Landscape Form and Dynamics.” *Geophysical Monograph* 135(D24): 1–30.

Dirnbock, T., R. J. Hobbs, R. J. Lambeck, and P. A. Caccetta. 2002. “Vegetation Distribution in Relation to Topographically Driven Processes in Southwestern Australia.” *Applied Vegetation Science* 5: 147–58.

Dymond, C. C., and E. A. Johnson. 2002. “Mapping Vegetation Spatial Patterns from Modeled Water, Temperature and Solar Radiation Gradients.” *ISPRS Journal of Photogrammetry and Remote Sensing* 57(1-2): 69–85.

Eagleson, P. S. 1970. *Dynamic Hydrology*. New York: McGraw-Hill Book Company.

Fan, Y, et al. 2017. “Hydrologic Regulation of Plant Rooting Depth.” *Proceedings of the National Academy of Sciences* 114(40): 201712381. http://www.pnas.org/lookup/doi/10.1073/pnas.1712381114.

Furbish, D. J., K. K. Hamner, M. Schmeeckle, M. N. Borosund, and S. M. Mudd. 2007. “Rain Splash of Dry Sand Revealed by High-Speed Imaging and Sticky Paper Splash Targets.” *Journal of Geophysical Research: Earth Surface* 112(1): 1–19. http://dx.doi.org/10.1029/2006JF000498

Furbish, D. J., and J. J. Roering. 2013. “Sediment Disentrainment and the Concept of Local versus Nonlocal Transport on Hillslopes.” *Journal of Geophysical Research: Earth Surface* 118(2): 937–52. https//doi.org/10.1002/jgrf.20071

Gabet, E. J., O. J. Reichman, and E. W. Seabloom. 2003. “The Effects of Bioturbation on Soil Processes and Sediment Transport.” *Annual Review of Earth and Planetary Sciences* 31(1): 249–73.

Garnier, E., et al. 2004. “Plant Functional Markers Capture Ecosystem Properties during Secondary Successsion.” *Ecology* 85(9): 2630–37.

Garnier, E., and M-L. Navas. 2012. A Trait-Based Approach to Comparative Functional Plant Ecology: Concepts, Methods and Applications for Agroecology. A Review. *Agronomy for Sustainable Development* 32*:365–399*

Grime, J. P. 2006. “Trait Convergence and Trait Divergence in Herbaceous Plant Communities: Mechanisms and Consequences.” *Journal of Vegetation Science* 17: 255–60. http://dx.doi.org/10.1111/j.1654-1103.2006.tb02444

Hack, J. T., and J. C. Goodlett. 1960. *Geomorphology and Forest Ecology of a Mountain Region in the Central Appalachians*. *USGS Geological Survey Professional Paper 347*

Hancock, G., and G. Willgoose. 2001. "Use of a Landscape Simulator in the Validation of the SIBERIA Catchment Evolution Model: Declining Equilibrium Landforms." *Water Resources Research* 37(7): 1981–92. http://dx.doi.org/10.1029/2001WR900002

Horton, R. E. 1945. "Erosional Development of Streams and Their Drainage Basins; Hydrophysical Approach to Quantitative Morphology." *Geological Society Of America Bulletin* 56(1): 151–80.

Howard, A. D. 1990. "Theoretical Model of Optimal Drainage Networks." *Water Resources Research* 26(9): 2107–17. http://dx.doi.org/10.1029/WR026i009p02107

Howard, A. D. 1994. "A Detachment-Limited Model of Drainage Basin Evolution." *Water Resources Research* 30: 2261–85. http://dx.doi.org/10.1029/94WR00757

Iorgulescu, I. Ã., and A. Musy. 1997. "Generalization of TOPMODEL for a Power Law Transmissivity Profile." *Hydrological Processes* 11(February): 1353–55.

Istanbulluoglu, E. 2003. "A Sediment Transport Model for Incision of Gullies on Steep Topography." *Water Resources Research* 39(4). http://dx.doi.org/10.1029/2002WR001467

Istanbulluoglu, E., et al. 2008. "Eco-Geomorphic Implications of Hillslope Aspect: Inferences from Analysis of Landscape Morphology in Central New Mexico." *Geophysical Research Letters* 35*(14): 1–6*.

Ivanov, V. Y., R. L. Bras, and E, R. Vivoni. 2008. “Vegetation-Hydrology Dynamics in Complex Terrain of Semiarid Areas: 2. Energy-Water Controls of Vegetation Spatiotemporal Dynamics and Topographic Niches of Favorability.” *Water Resources Research 44(3)*: http://doi.wiley.com/10.1029/2006WR005595

Kirkby, M. J. 1971. “Hillslope Process-Response Models Based on the Continuity Equation.” *Institute of British Geographers Special Publication* 3: 15–30.

Knighton, D. 1998. *Fluvial Forms and Processes: A New Perspective*. 2nd ed. Abingdon, UK: Routledge.

Kremen, C. 2005. “Managing Ecosystem Services: What Do We Need to Know about Their Ecology?” *Ecology Letters* 8(5): 468–79.

Leopold, L. B., and T. Maddock. 1953. “The Hydraulic Geometry of Stream Channels and Some Physiographic Implications.” *Geological Survey Professional Paper 252*: 57.

Lynch, M., and W. Gabriel. 1987. “Environmental Tolerance.” *The American Naturalist* 129(1): 283-303.

Martin, Y., and M. Church. 1997. “Diffusion in Landscape Development Models: On The Nature of Basic Transport Relations.” *Earth Surface Processes and Landforms* 22(3): 273–79.

Martin, Y. 2007. “Wildfire Disturbance and Shallow Landsliding in Coastal British Columbia over Millennial Time Scales: A Numerical Modelling Study.” *Catena* 69(3): 206–19.

Moglen, G. E., and R. L. Bras. 1995. “The Importance of Spatially Heterogeneous Erosivity and the Cumulative Area Distribution within a Basin Evolution Model.” *Geomorphology* 12(3): 173–85.

Murray, A. B., M. A. F. Knaapen, M. Tal, and M. L. Kirwan. 2008. “Biomorphodynamics: Physical-Biological Feedbacks That Shape Landscapes.” *Water Resources Research* 44(11): http://doi.wiley.com/10.1029/2007WR006410

O’Loughlin, E. M. 1986. “Prediction of Surface Saturation Zones in Natural Catchments by Topographic Analysis.” *Water Resources Research* 22(5): 794–804. http://dx.doi.org/10.1029/WR022i005p00794

Oddershede, A., J.-C. Svenning, and C. Damgaard. 2015. “Topographically Determined Water Availability Shapes Functional Patterns of Plant Communities Within and Across Habitat Types.” *Plant Ecology* 216: 1231–42.

Perera, H., and G. Willgoose. 1998. “Aphysical Explanation of the Cumulative Area Distribution Curve.” *Water Resources Research* 34(5): 1335–43. http://dx.doi.org/

Perron, J. T., W. E. Dietrich, and J. W. Kirchner. 2008. “Controls on the Spacing of First-Order Valleys.” *Journal of Geophysical Research* 113(F4): F04016. http://dx.doi.org/10.1029/2007JF000977

Porder, S. 2014. “Coevolution of Life and Landscapes.” *Proceedings of the National Academy of Sciences of the United States of America* 111(9): 3207–8.

Reinhardt, L., et al. 2010. “State of Science Dynamic Interactions of Life and Its Landscape : Feedbacks at the Interface of Geomorphology.” *Earth Surface Processes and Landforms* 101: 78–101.

Rodriguez-Iturbe, I., and A. Rinaldo. 1997. *Fractal River Basins: Chance and Self-Organization*. Cambridge, UK: Cambridge University Press.

Roering, J. J., J. W. Kirchner, and W. E. Dietrich. 1999. “Evidence for Nonlinear, Diffusive Sediment Transport on Hillslopes and Implications for Landscape Morphology.” *Water Resources Research* 35(3): 853–70. http://dx.doi.org/10.1029/1998WR900090

Roering, J. J. 2008. “How Well Can Hillslope Evolution Models ‘Explain’ Topography? Simulating Soil Transport and Production with High-Resolution Topographic Data.” *Geological Society of America Bulletin* 120(9-10): 1248–62.

Smith, T. R., and F. P. Bretherton. 1972. “Stability and the Conservation of Mass in Drainage Basin Evolution.” *Water Resources Research* 8(6): 1506. http://dx.doi.org/10.1029/WR008i006p01506

Sørensen, R., U. Zinko, and J. Seibert. 2006. “On the Calculation of the Topographic Wetness Index : Evaluation of Different Methods Based on Field Observations.” *Hydrology and Earth System Science* 10(1): 101–12.

Steiger, J., and D. Corenblit. 2012. “The Emergence of an ‘Evolutionary Geomorphology’?” *Central European Journal of Geosciences* 4(3): 376–82.

Sweeney, K. E, J. J. Roering, and C. Ellis. 2015. “Experimental Evidence for Hillslope Control of Landscape Scale.” *Science* 349(6243): 51–53.

Tarboton, D. G., and I. N. Mohammed. 2013. *Taudem 5.1 Quick Start Guide to Using the TauDEM ArcGIS Toolbox, Utah State University, Logan, Utah.* [Available at http://hydrology.usu.edu/taudem/taudem5/index.html.]

Tokunaga, E. 1978. “Consideration on the Composition of Drainage Networks and Their Evolution.” *Geographical Reports of Tokyo Metropolitan University* 13.

Tucker, G. E., and R. L. Bras. 1998. “Hillslope Processes, Drainage Density, and Landscape Morphology.” *Water Resources Research* 34(10): 2751–64. http://dx.doi.org/10.1029/98WR01474

Tucker, G. E., S. T. Lancaster, N. M. Gasparini, and R. L. Bras. 2001. “The Channel-Hillslope Integrated Landscape Development Model (CHILD).” In *Landscape Erosion and Evolution Modeling*, New York: Kluwer Academic. pp. 349–88.[available at: http://csdms.colorado.edu/wiki/Model:CHILD]

Tucker, G. E., and G. R. Hancock. 2010. “Modelling Landscape Evolution.” *Earth Surface Processes and Landform* 50: 28–50.

Western, A. W., R. B. Grayson, G. Blöschl, G. R. Willgoose, and T. A. McMahon. 1999. “Observed Spatial Organization of Soil Moisture and Its Relation to Terrain Indices.” *Water Resources Research* 35(3): 797–810. http://dx.doi.org/10.1029/1998WR900065

Whittaker, R. H. 1956. “Vegetation of the Great Smoky Mountains.” *Ecological Monograph* 26: 1–80.

Yetemen, O., E. Istanbulluoglu, and E. R. Vivoni. 2010. “The Implications of Geology, Soils, and Vegetation on Landscape Morphology: Inferences from Semi-Arid Basins with Complex Vegetation Patterns in Central New Mexico, USA.” *Geomorphology* 116(3-4): 246–63.

Zhou, X., E. Istanbulluoglu, and E. R. Vivoni. 2013. “Modeling the Ecohydrological Role of Aspect-Controlled Radiation on Tree-Grass-Shrub Coexistence in a Semiarid Climate.” *Water Resources Research* 49(5): 2872–95.

Willett, S. D., et al. 2014. “Dynamic Reorganization of River Basins.” *Science* 343(6175): 1248765. http://www.ncbi.nlm.nih.gov/pubmed/24604204.

Willgoose, G., R. L. Bras, and I. Rodriguez-ITurbe. 1991. “A Coupled Channel Network Growth and Hillslope Evolution Model 1.” *Water Resources Research* 27(7): 1671–84. http://dx.doi.org/10.1029/91WR00935

Willgoose, G. 1994. “A Physical Explanation for an Observed Relationship for Catchments with Declining Relief.” *Water Resources Research* 30(2): 151–59. http://dx.doi.org/10.1029/93WR01810

Yetemen, O., E. Istanbulluoglu, and E. R. Vivoni. 2010. “The Implications of Geology, Soils, and Vegetation on Landscape Morphology: Inferences from Semi-Arid Basins with Complex Vegetation Patterns in Central New Mexico, USA.” *Geomorphology* 116(3-4): 246–63.

Zinko, U., J. Seibert, M. Dynesius, and C. Nilsson. 2005. “Plant Species Numbers Predicted by a Topography-Based Groundwater Flow Index.” *Ecosystems* 8(4): 430–41. http://dx.doi.org/10.1002/wrcr.20259

Chapter 3: A Constrained Maximization Model for Optimization of Stoma and Leaf Size in Relation to Water Potential: A Theory

1. Introduction

Leaves are the fundamental energy production units of plants, which utilize carbon dioxide as their main fuel source. Due to the importance of leaves, natural selection processes drive plants to maximize their net leaf carbon gain (Chabot and Hicks, 1982; Williams et al., 1989; Westoby et al., 2002; Blonder et al., 2011) which ultimately affects plant fitness (Kikuzawa, 1995; Wright et al., 2004; Shipley et al., 2006). To maintain the overall health and function of plant leaves, the water status of a leaf is critical. When the water potential of the leaf vein conduit reaches a critical low value, cavitation occurs. Cavitation in minor vein conduits blocks their ability to fill with water and causes the loss of cell turgor pressure. Loss of cell turgor pressure negatively affects the biochemical processes of photosynthesis by reducing the maximum carboxylation rate, damaging ATP, and increasing mesophyll resistance for CO_2 diffusion (Grassi and Magnani 2005; Niinemets et al., 2005; Lawlor and Tezara, 2009).

To avoid the negative impacts of cavitation, the leaf will increase its stomatal resistance to reduce transpiration rate. However, this adjustment comes at the cost of reduced carbon fixing rate since increasing stomatal resistance slows the carbon intake rate. Recently, many studies have used stomatal optimization models to investigate this process (e.g. Katul et al., 2010; Casson, 2014; Medrano et al., 2015). These studies suggest that optimally stomata would operate at the safety-efficiency margin to maximize the carbon assimilation rate with respect to water loss. Furthermore, leaf surface area, even within the same species, can vary many fold and has

been found to be positively associated with soil moisture levels (e.g. Xu et al., 2009; Wright et al., 2017). It is suggested that adjustment of leaf area to soil moisture through the cell division enhance growth rate over time can influence the stomatal resistance in response to temporal fluctuating temperature and vapor pressure (Maseda and Fernández, 2006).

Leaf shape, a genetically determined trait, is found to be associated with habitat types and one of the traits defining plant water use strategies. Leaf width was found to increase with increasing precipitation and/or soil moisture (Givnish, 1987; McDonald et al., 2003). Some general patterns of plant distribution have been observed on hillslopes: dry ridge tops are dominated by narrow leaf species, the moist riparian areas are dominated by broadleaf species, and the middle mesic hillslopes are occupied by mixtures of species having a wider range of leaf shapes.

Evidence suggests that leaf shape may regulate venation network structure. In order to provide structural support of a leaf, the major vein must extend from the petiole to the end of the leaf and second order major veins must extend from the major vein to the boundary of the leaf (Roth-Nebelsick et al., 2001; Cochard et al., 2004). Therefore, assuming the venation has a dendritic structure following the metabolic scaling theory (Price and Enquist, 2007), the width to length ratio of a leaf regulates the vein network parameter Υ (the ratio of the length of $n+1$th order vein to nth order vein). In addition, research has shown that the optimal average distance between two adjacent smallest minor veins approximates the distance from minor vein to the leaf surface, which is approximately half of the leaf thickness (Noblin et al., 2008). These two parameters determine the rate of total leaf xylem resistance scaled with leaf area (see West, 1999). In addition, leaf venation network has been connected to net carbon assimilation rate, life

span, leaf mass per area and nitrogen content to explain the leaf economic spectrum (Blonder et al., 2011).

These studies suggest that venation structure, leaf area, leaf shape and stomatal resistance are all related and affect the leaf carbon budget regarding soil moisture. However, they haven't been formally connected to give a physical explanation on how plants can maximize their net leaf primary productivity based on these traits with respect to soil moisture variation.

Here, we present a leaf model that connects vein structure to leaf shape, which is further integrated into the coupling of transpiration and carbon assimilation processes to investigate: 1) how a plant can maximize its net leaf carbon productivity through co-adjustment of both stomatal resistance and leaf area regarding average soil moisture conditions over the life span of a leaf, and 2) how leaf shape impacts the way by which leaf optima change with soil moisture through regulating vein structure. When combined with metabolic scaling theory, this model provides a means to connect plant performance, e.g., net primary productivity, or total biomass, to soil moisture.

2. The leaf optimization model

The vein network of our leaf model has a dendritic structure as described by Price and Enquist (2007). Water flows through the xylem conduits contained by veins. The xylem conduits branch where veins branch. So, the length ratio of two consecutive orders of veins and that of the two consecutive orders of conduits are the same, which we denoted as γ. In our model, the branching ratio of xylem conduit which we denoted as m, and the vein branching ratio, which we denoted as n, are not the same. The ratio of two consecutive conduits is denoted as β. Assuming the conservation of total conduit cross-sectional area, xylem conduit branching ratio, m, equals $1/\beta^2$.

Based on previous studies as discussed above, we make two connections between vein structure and leaf shape. First, the length ratio of two consecutive veins, γ, is proportional to half of the width to length ratio of the leaf. Second, the distance between two adjacent terminal minor veins is half of the leaf thickness (Figure 3.1). Note, when we mention xylem water potential, we refer to the water potential of xylem conduits.

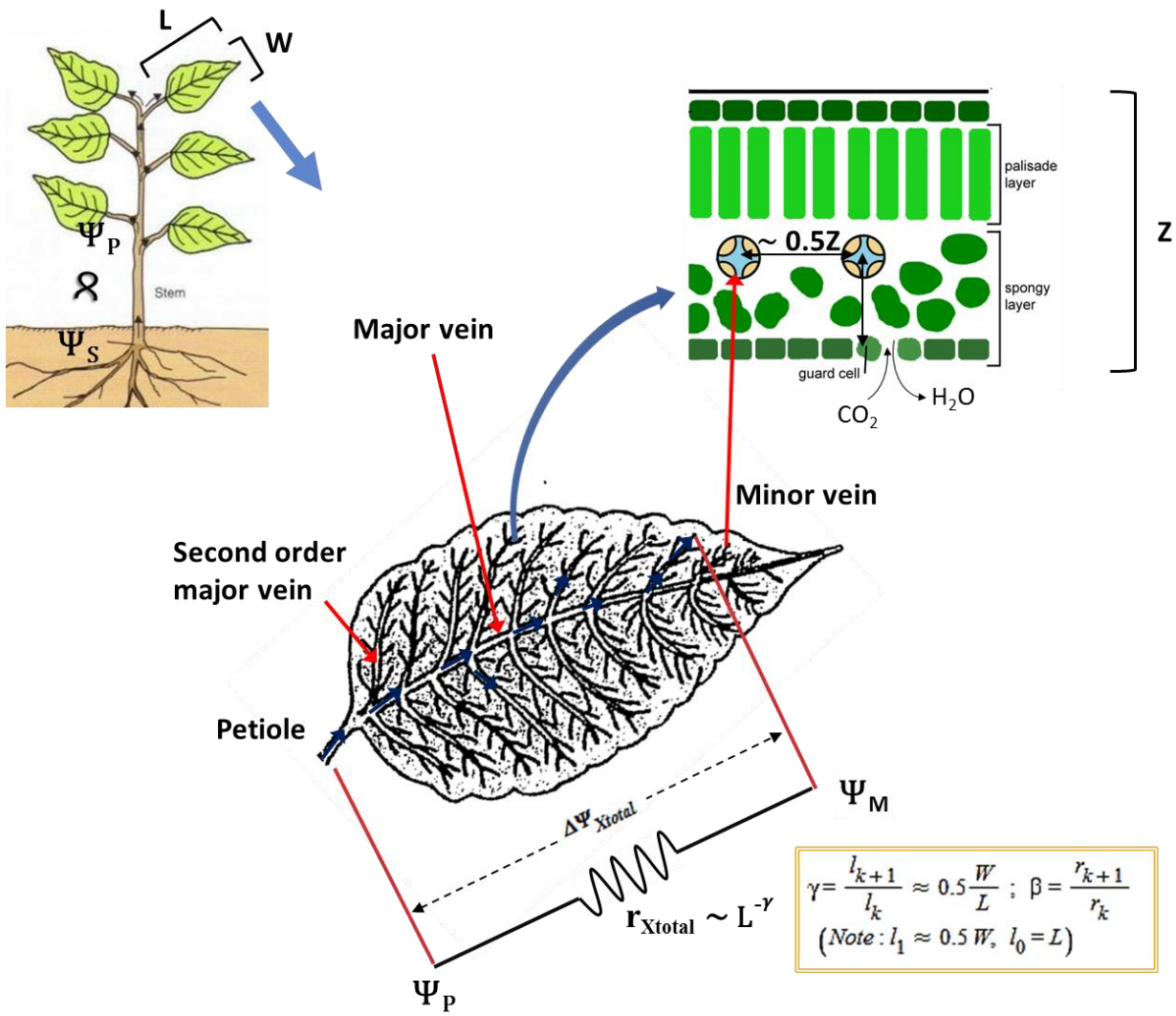

Figure 3.1 Schematic leaf model

.

Though soil moisture holds ultimate control over a plant's leaf water status, its impact on leaf water status is indirect and is confounded by many other traits of the plant, including plant stem size, stem hydraulic properties, and root depth and density. These traits are all subject to environmental adaptation. Thus, the petiole xylem water potential on one hand directly affects the water status of the leaf, but on the other hand is related to soil moisture. When focus is on the leaf, control of soil moisture on leaf water status is best reflected by the petiole xylem water potential. In our model, the water entering the leaf through the petiole then flows all the way along the xylem network and reaches the terminal minor veins where it diffuses through mesophyll into the inner space of the leaf and then through the stomata to air. The xylem water potential also decreases along the flow path due to viscosity resistance and reaches its lowest value at the terminal minor vein.

If the water potential of the xylem conduits of terminal minor veins becomes lower than a threshold (Ψ_C), cavitation will occur and thus leaf cell turgor pressure will no longer be maintained. The threshold xylem water potential is a functional hydraulic trait determined by the vulnerability curve (Pammenter and Willigen, 1998; Markesteijn et al., 2011). Therefore, the difference between the actual petiole xylem water potential and the critical water potential determines how much water potential is lost through the flow pathway.

The total loss of water potential along the flow path of the xylem of the vein network is proportional to the product of velocity and total xylem resistance. The velocity is determined by transpiration rate which is regulated by stomatal resistance; the total xylem resistance increases with leaf size. Both decreasing stomatal resistance and increasing leaf area will increase net leaf primary productivity but also increase the total loss of water potential. The rate at which total xylem resistance of a leaf scales with leaf area is determined by the vein network structure.

The net leaf primary productivity is described here as the balance between the leaf carbon assimilation rate (first term of the right side of Equation 1) and the rate of total carbon loss from respiration and construction over its life span (the second term of the right side of Equation 1). The model maximizes net leaf primary productivity, defined as an objective function f() (Equation 1) over the total loss of xylem water potential constrained by the difference between the petiole xylem water potential and the critical xylem water potential, defined as a constraint function g() (Equation 2, see Appendix S1 for derivation):

$$f(r_{es}, LA) : NPP_{leaf} = \frac{p1}{p2 \cdot r_{es} + p3} \cdot LA - (R_C + R_R) \cdot LA \tag{1}$$

Over

$$g(r_{es}, LA) : \Delta\Psi_{Xtotal} = p4 \cdot \frac{e_{sat} - e_a}{r_{em} + \frac{r_{es}}{Cons2}} \cdot r_{Xtotal} \tag{2}$$

constrained by

$$\Psi_P - \Psi_C \tag{3}$$

With

$$p1 = a_1 \cdot C_a$$
$$p2 = Cons1 \cdot Cons3 \cdot a_1$$
$$p3 = (a_2 + S \cdot C_a)$$

$$p4 = \frac{Z \cdot l_T}{2 \cdot \pi \cdot r_T^2}$$

$$r_{em} = \frac{\left(\frac{Z}{2}\right) e_{sat}}{D_m w_0}$$

$$r_{Xtotal} = \frac{8\mu\left(\left(\frac{l_T}{L}\right)^{\frac{\ln(\beta^2)}{\ln(\gamma)}-1}\beta^2-\gamma\right)}{g r_T^2(\gamma-\beta^2)\cdot l_T}$$

where NPP_{leaf} (μmol s^{-1}) is the net primary productivity of a mature leaf. GPP (μmol m^{-2} s^{-1}) is the gross primary productivity rate or net carbon fixation rate per unit leaf area. The formula of GPP used here is adapted from the linear model of Katul et al. (2010) at equilibrium. R_C (μmol m^{-2} s^{-1}) is the life span standardized construction cost (e.g., the total mass of the leaf divided by its lifespan); R_R (μmol m^{-2} s^{-1}) is the respiration loss; LA (m^2) is the leaf area; L (m) is the length of the leaf as measured by the distance from the leaf collar to the tip. a_1 (μmol m^{-2} s^{-1}) is the maximum carboxylation capacity, a_2 (510 μmol mol^{-1}) is a biophysical constant. C_a (0.0004 mol mol^{-1}) is the CO_2 concentration of air. r_{es} is the stomatal resistance of water vapor. Cons1 (1.42) is the ratio of stomatal resistance of CO_2 to water vapor. Cons3 (1 kg m^{-3} x 5.55 x 10^{-5} mol kg^{-1}) is a constant for volume to mass conversion of water. r_{es} (s m^{-1}) is the stomatal resistance of vapor. *S* is the ratio of leaf CO_2 concentration to CO_2 concentration of air, which is considered as a constant with value around 0.6 (Katul et al., 2010). $\Delta\Psi_{Xtotal}$ (Pa) is the total loss of xylem water potential from petiole to terminal minor vein; e_{sat} is the saturated vapor pressure; e_a is the atmospheric vapor pressure; r_{em} (s m^{-1}) is the mesophyll resistance, the formula of r_{em} is taken from Noblin et al. (2008); *Cons2* is a physical constant (7.27 x 10^6 s^2 m^{-2}); r_{Xtotal} (s m^{-1}) is the total xylem resistance of a leaf vein; E (kg s^{-1}) is the transpiration rate; Ψ_P (Pa) is the petiole xylem water potential; Ψ_C (Pa) is the critical vein water potential at which the percentage of the vein that forms cavitation will cause a detrimental effect on biochemical processes (Ψ_{50}). D_m (m^2 s^{-1}) is the mesophyll diffusivity given by Noblin et al. (2008). w_0 (mol m^{-3}) is the saturated water

concentration of mesophyll; l_T: (m) is the length of minor vein; r_T (m) is the radius of minor vein conduit.

The net leaf primary productivity is maximized when it is equally limited by the loss of xylem water potential from stomatal resistance and from leaf area induced total xylem resistance. These are obtained by solving the Lagrangian function of the model:

$$\mathcal{L}(r_{es}, LA) = f(r_{es}, LA) - \lambda g(r_{es}, LA) \tag{4a}$$

As

$$\begin{cases} \lambda = \dfrac{f_{r_{es}}}{g_{r_{es}}} = \dfrac{f_{LA}}{g_{LA}} & (4b) \\ \Delta\Psi_{Xitotal} - (\Psi_P - \Psi_C) = 0 & (4c) \end{cases}$$

for NPP_{leaf}, LA, r_{es}, and λ where λ is the Lagrange multiplier

The solution expresses the maximum net leaf primary productivity, optimal leaf area and stomatal resistance and Lagrange multiplier by the set of biophysical and environment variables (see Appendix S2 for the full formula):

$$NPP_{leaf}\max = h_1(p1, p2, \ldots \boldsymbol{\Psi_P}, \boldsymbol{W/L}) \tag{5a}$$
$$LA^* = h_2(p1, p2, \ldots \boldsymbol{\Psi_P}, \boldsymbol{W/L}) \tag{5b}$$
$$r_{es}^* = h_3(p1, p2, \ldots \boldsymbol{\Psi_P}, \boldsymbol{W/L}) \tag{5c}$$
$$\lambda^* = h_3(p1, p2, \ldots \boldsymbol{\Psi_P}, \boldsymbol{W/L}) \tag{5d}$$

Aside from the petiole xylem water potential and the leaf width and length which are treated as variables, the parameters of the leaf model are set using the middle value of the realistic range across different species for biological parameters and the annual average values for the environmental parameters (Appendix S3).

3. Optimal leaf size, stomatal resistance, and maximum net leaf primary productivity

Maximum net leaf primary productivities (NPP_{leaf}) of leaves with different W/L ratio all increase with petiole xylem water potential (Ψ_p) at slightly decreasing rates. The maximum NPP_{leaf} of a narrow leaf (small W/L) is overall lower than that of a broad leaf (large W/L); it also increases with Ψ_p at a much slower rate than that of a broad leaf (Equation 5a, Figure 3.2). Optimal leaf sizes of narrow and broad leaves increase with increasing Ψ_p but the optimal leaf size of a narrow leaf increases with Ψ_p more slowly than that of a broad leaf; also, the optimal leaf size of a narrow leaf is overall smaller than that of a leaf with large W/L (Equation 5b, Figure 3.2). Optimal stomatal resistances of leaves with different W/L ratios all decrease with increasing Ψ_p; the optimal stomatal resistance of narrow leaves is higher than that of broad leaves at any petiole xylem water potential (Equation 5c, Figure 3.3). The λ^* of leaves with different W/L all decrease with increasing Ψ_p; the λ^* of a narrow leaf is overall smaller than that of a broad leaf (Equation 5d, Figure 3.4). The result of the optimization shows that both the maximum net leaf primary productivity and the leaf area increase with petiole xylem water potential while stomatal resistance decreases, each at different rates. The marginal increasing of maximum net leaf primary productivity of a narrow leaf is smaller than that of a broad leaf (the meaning of the λ^*).

When the net leaf primary productivity is equally limited by loss of xylem water potential from the stomatal resistance and by leaf size, the condition for maximum net leaf primary productivity is where the rate of substitution of stomatal resistance to leaf size in regards to the total loss of vein water potential equals the rate of substitution of stomatal resistance to leaf size

in net carbon gain, where the isoline of the constraint function touches the isoline of the objective function f(). This is given by the formula of λ (Equation 4b). This means that the optima and the maxima of NPP_{leaf} are determined by the locations of the isolines of the objective and the constraint functions.

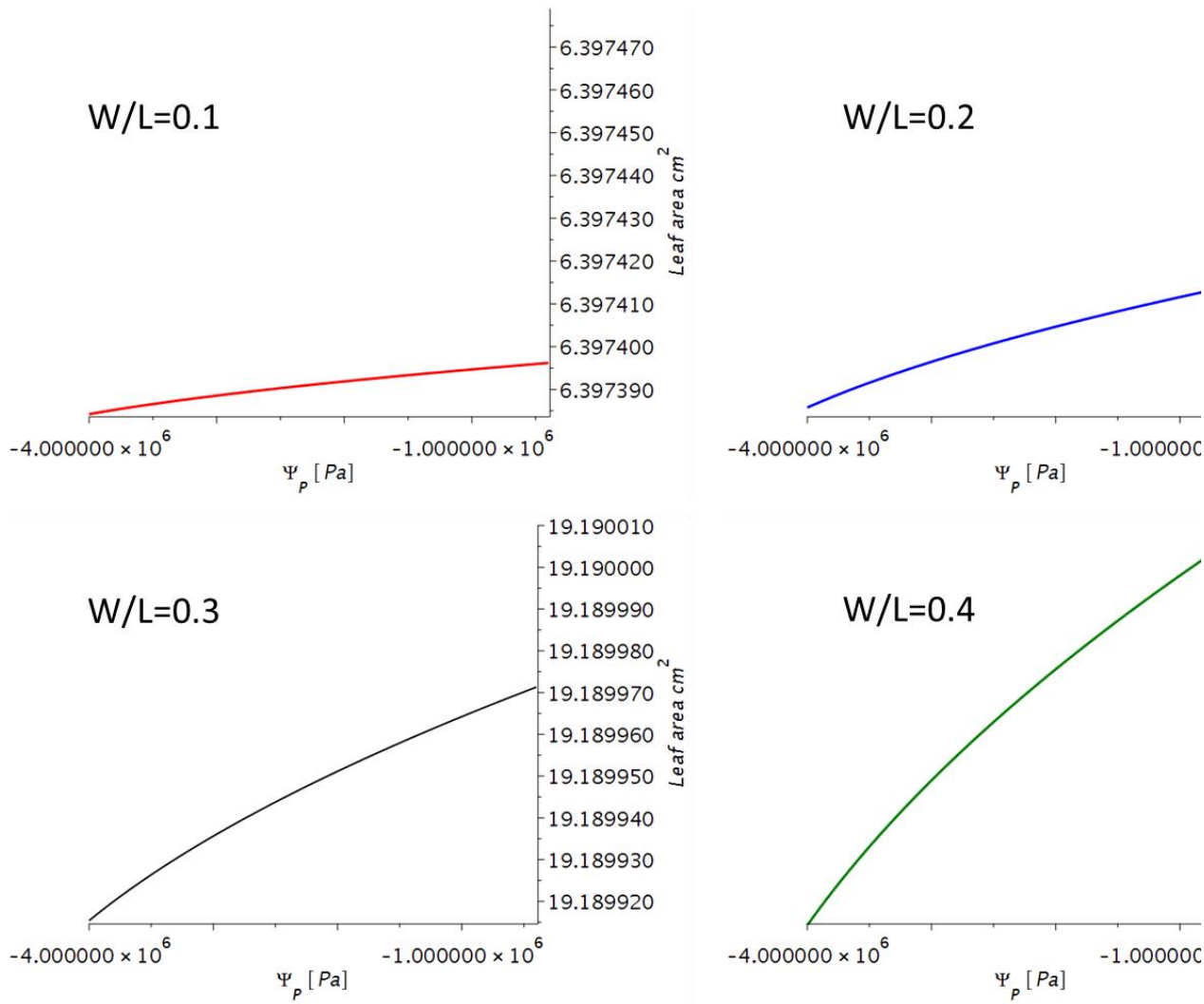

Figure 3.2 Change of maximum net leaf primary productivity with petiole xylem water potential of leaves with different width to length (W/L) ratio

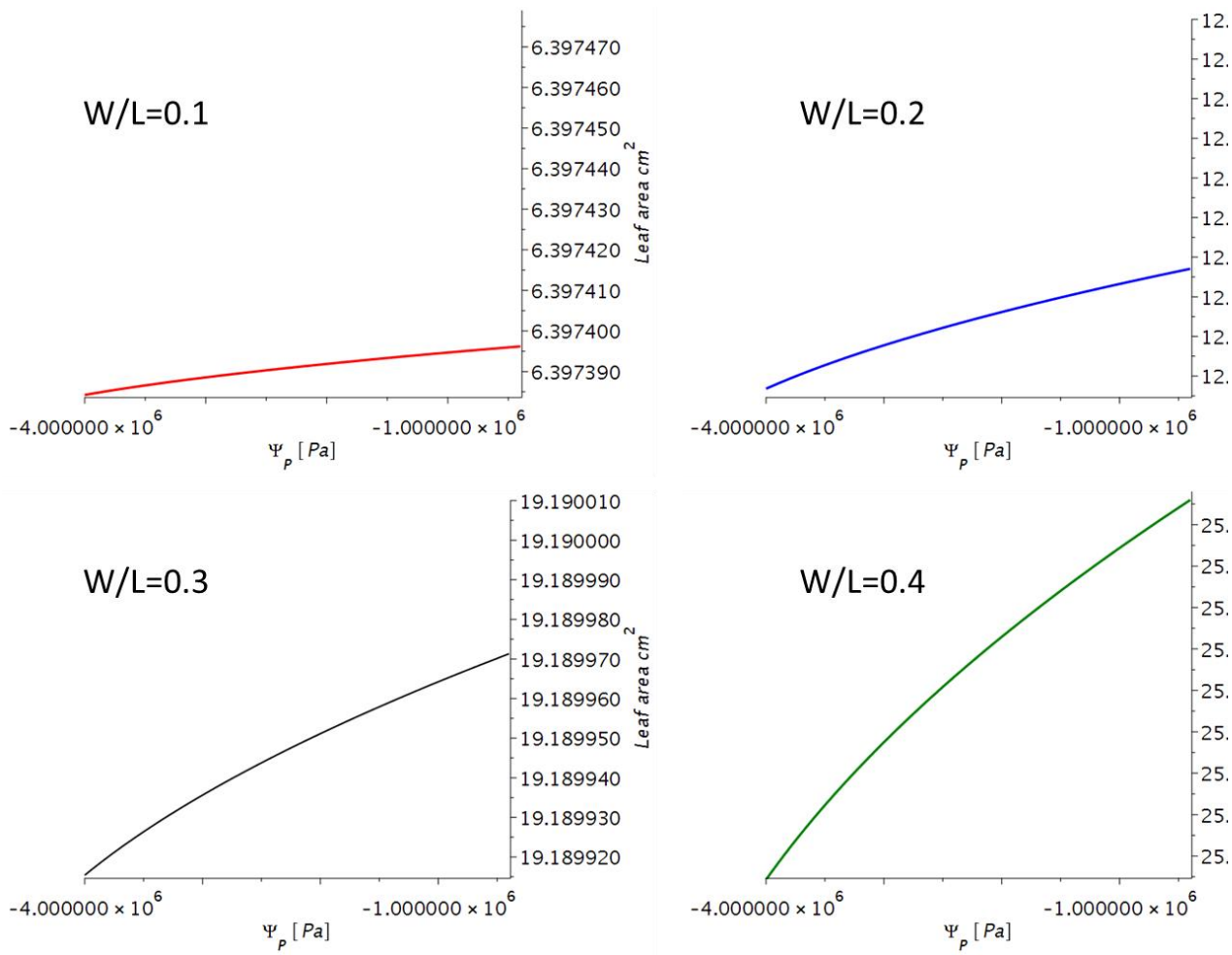

Figure 3.3 Impact of leaf shape on the relation between of optimal leaf size and xylem water potential at the petiole.

With the same petiole xylem water potential, a narrow leaf (smaller width to length ratio) has smaller total optimal leaf area than a broad leaf (large width to length ratio); optimal leaf size of a narrow leaf increases with increasing petiole xylem water potential at a slower rate than a broad leaf.

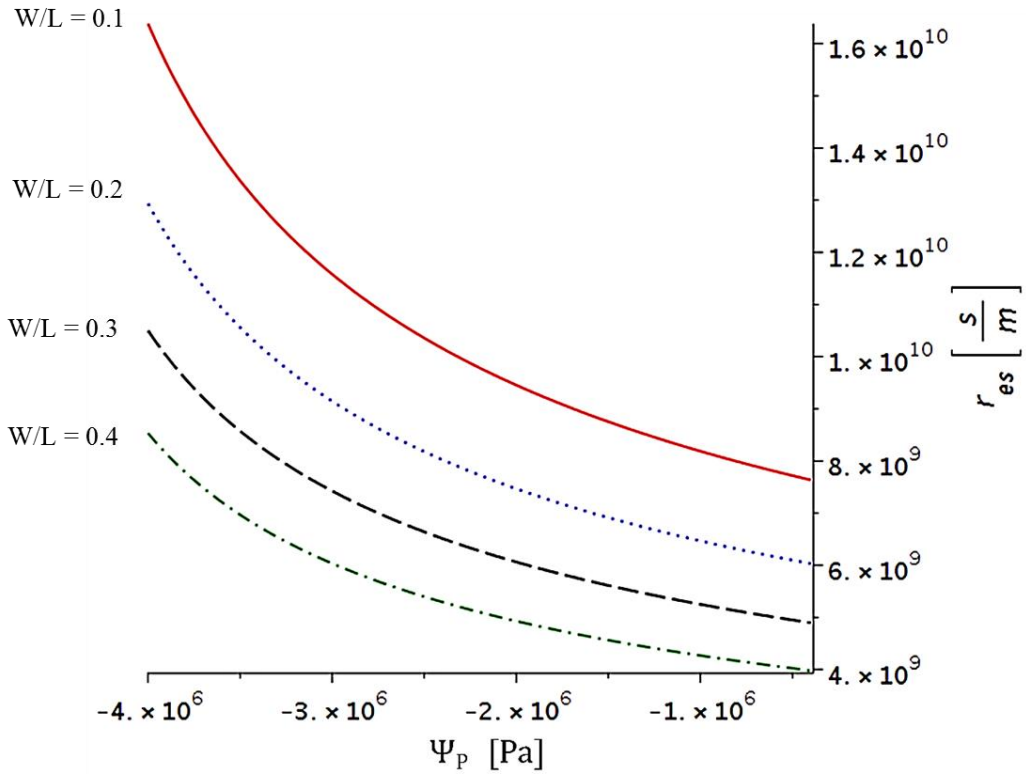

Figure 3.4 Impact of leaf shape on the relation between optimal stomatal resistance and petiole xylem water potential.

Optimal stomatal resistance of leaves with different width to length ratio all decreases with increasing petiole xylem water potential at a decreasing rate. The optimal stomatal resistance of a narrow leaf is higher than of a broad leaf at any petiole xylem water potential.

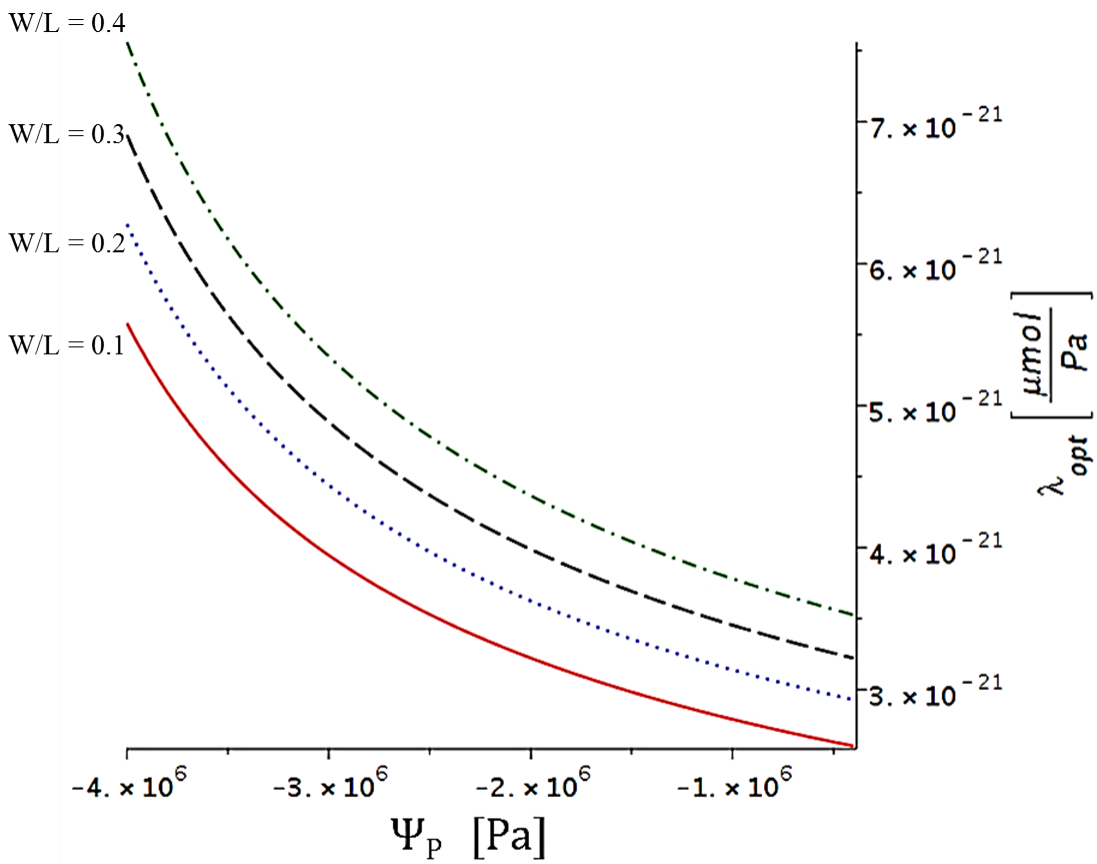

Figure 3.5 Impact of leaf width to length ratio (W/L) on the optimal marginal increase of net leaf primary productivity to petiole total xylem water potential ratio (λopt) at different petiole xylem water potential (Ψ_P).

By rearranging the constraint function (Equation 2), we can write the equation of the isoline of function g() as:

$$\frac{\left(r_{em} + \frac{r_{es}}{Cons2}\right)}{r_{Xtotal}} = \frac{p4 \cdot \left(e_{sat} - e_a\right)}{\left(\Psi_P - \Psi_C\right)} \qquad (6)$$

Thus Equation 6 shows that the stomatal resistance and total xylem resistance of the vein has a linear relationship on the isoline of the constraint function. Therefore, for a given value of Ψ_P , assuming Ψ_C is the same for both narrow leaf and broad leaf, the stomatal resistance must be

proportional to total xylem resistance, which means inefficiency in transporting water also means inefficiency in carbon assimilation (Figure 3.6a). When plotting the isoline of the constraint function in the form as stomatal resistance against leaf area, leaves differing in W/L have different lines; for the same level of g(), the isoline of a narrow leaf is steeper than that of a broad leaf (Figure 3.6b). This causes the narrow leaf to have smaller optimal leaf area but higher optimal stomatal resistance than those of a broad leaf and consequently lower maximum net leaf primary productivity. This is because, with the same leaf area, the total xylem resistance of a narrow leaf is higher than that of a broad leaf and also increases faster with increasing leaf area, and, consequently, the stomatal resistance of a narrow leaf is higher than that of a broad leaf.

The reason that the rate of total xylem resistance of a narrow leaf scales faster with leaf area is that it has smaller γ. The relationship between the total xylem resistance and leaf area is determined by the two leaf xylem structure parameters γ and β (formula of r_{Xtotal} in Equation 3). Both theoretical and empirical evidence show that β does not vary very much across plant species (Petit et al., 2008). Therefore, the difference in the scaling rate is mainly determined by the parameter γ, thus the W/L ratio: the higher the W/L ratio, the more slowly the total xylem resistance increases with leaf size (Figure 3.8).

a

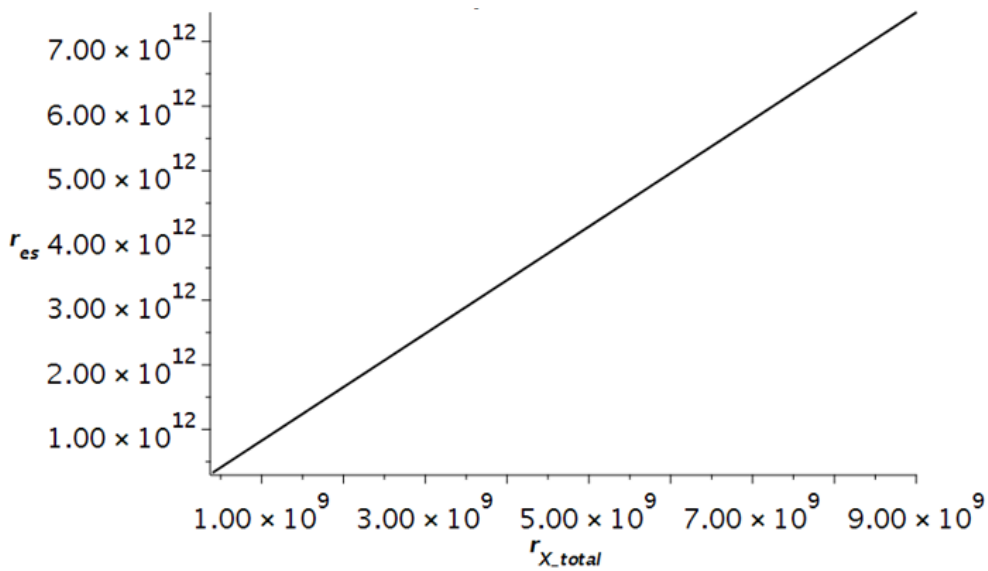

b

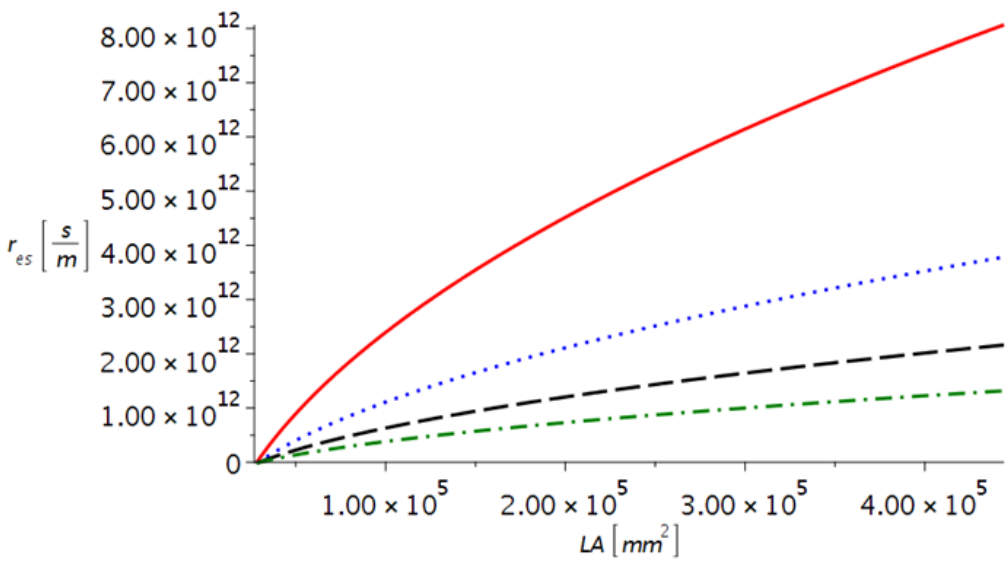

Figure 3.6. Isoline of the constraint function g() at -10^6 Pa with a) r_{es} vs. r_{Xtotal}, b) r_{es} vs. LA

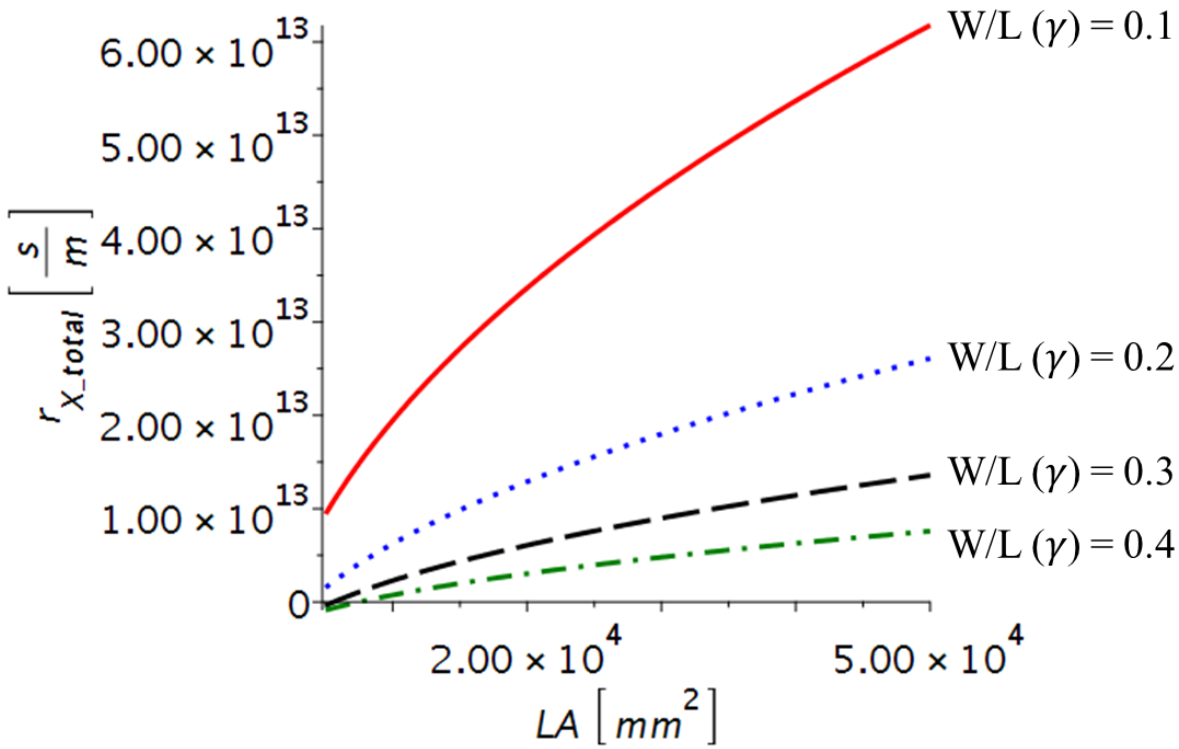

Figure 3.7 Change of total xylem resistance with leaf area

Through Υ, leaf shape affects vein structure properties: the total numbers of vein orders, the radius and the arrangement of lower order veins (e.g., second order major veins and third order veins). The total number of xylem conduits of the major vein (zero order vein) is:

$$M_0 = \frac{M_T}{m^T} \tag{7}$$

where T is the total vein order given by (see Appendix S1 for derivation):

$$T = \frac{\ln\left(\dfrac{l_T}{\left(\dfrac{LA}{k_{SP}}\right)^{0.5}}\right)}{\ln\left(\dfrac{1}{2}k_{SP}\right)} \tag{8}$$

Expanding Equation 18, T can be expressed as:

$$T = \frac{-2\ln(l_T) - \ln(k_{SP}) + \ln(LA)}{2\ln(2) - 2\ln(k_{SP})} \tag{9}$$

where k_{SP} = W/L, LA is the total leaf area (m^2). Both numerator and denominator of Equation 9 decrease with increasing W/L but the numerator decreases at a faster rate than the denominator. Therefore, T increases with increasing W/L ratio. M_T is determined by the leaf size, minor vein length, the distance between minor veins and the number of conduits contained by a single minor vein. Assuming the minor vein is invariant (e.g., similar in length and the number of conduits contained) and minor vein distance is determined by leaf thickness, the number of minor veins is the total length of minor vein divided by minor vein length. Total length of minor veins is the

leaf area divided by minor vein distance. Thus, with the same *LA*, M_T is the same for leaves differing in W/L ratios if they have the same thickness. With larger *T*, the number of xylem conduits of the major vein of a broad leaf is less than that of a narrow leaf (Equation 9). With the conservation of the total area of xylem conduit of a cross section, the radius of xylem conduit of the major vein r_0 of a leaf having larger W/L is larger than of a leaf having smaller W/L. Therefore, leaves having small W/L ratio will have less numbers of vein orders and a larger number of smaller size conduits of the major vein compared to a leaf with large W/L. Empirical evidence supports this prediction. In cycads, conifers, Ginkgo and several other extinct seed plant lineages, a single order of veins leads straight, parallel courses to a distal margin. Angiosperms, however, exhibit many hierarchical orders of reticulate, internally directed veins (Boyce et al., 2009; Nicotra et al., 2011). As from the model prediction, narrow leaf has no advantage. However, on a whole plant perspective, narrow leaf plants can have advantage by having smaller conduit at petiole, which will be discussed in later section 4.2.

In this study, we propose that plants will optimize leaf *NPP* over water potential loss rather than water loss. So that our study looks at the carbon assimilation over the loss of water potential—a measure of the loss of energy rather than of water. This is the major difference between this study and the previous ones. Previously, water use efficiency (WUE), the measure of plant productivity over water loss, has been used as the standard measure related to plant strategy either in empirical and experimental studies (e.g., French and Schultz, 1984; Sivamani et al., 2000; Condon et al., 2002, 2004; Blum, 2009) or in optimization theories (e.g., Parkhurst and Loucks, 1972; Landsberg and Fowkes, 1978; Katul et al., 2010; Manzoni et al., 2013). Water use efficiency might be a good measure for crop production and for arid and semiarid areas where surface recharge is the major source of water. However, WUE can't explain the effect of soil

moisture on the plant carbon budget in mountainous regions and in humid and semi humid areas. A recent study shows that where a groundwater table exists, the majority of plant roots are distributed above the groundwater table and the plant water supply is from the capillary fringe of the groundwater table (Fan et al., 2017). In mountainous regions, the entire upland will contribute to the water supply for the plants growing on a hillslope. Thus, no matter how much water of the capillary fringe the plant uptakes, it can always be recharged from groundwater at the saturated zone. Since roots usually do not grow in the saturated zone, when there is a water table, the highest water potential of the root zone will be the water potential of the capillary fringe. The maximum average soil water potential of the root zone will be the water potential of field capacity. In addition, the average soil water potential of the root zone decreases with water table depth. Fan et al. (2017) found that the soil moisture profile has three zones: the surface layer is wet due to infiltration, the low layer also has high soil moisture maintained by the water table, and in between is the zone where soil moisture is low. Thus, the lower the water table, the larger the low moisture zone, resulting in low average soil water potential across the root zone. Also, the soil water potential limits the transpiration rate, because the higher the rate, the quicker the loss of xylem water potential along the flow path. For humid areas, water may not be the limiting factor, but water potential is, because no matter how much precipitation a humid area can receive, the maximum soil water potential cannot exceed the saturated water potential (0 Pa).

4. From Stoma to Plant to Landscape – Ways to upscale through plant vascular system

4.1 Implication on whole plant performance and impact on plant distribution along hillslope

Empirical studies have shown that leaves having smaller conduits are more resistant to cavitation (Blackman et al., 2010; Brodribb et al., 2016; Scoffoni et al., 2016). A narrow leaf has

small γ and small xylem conduits, thus will be more resistant to cavitation, but it has higher total xylem resistance compared to a broad leaf with the same leaf area which also increases with leaf area faster. In addition, following the scaling relationship, small conduits at the petiole will result in smaller conduits all along their network. Thus, plants with narrow leaves will have smaller xylem conduits and be more resistant to cavitation, thus have an advantage when soil moisture is low which can be detrimental to plants having broad leaves with larger xylem conduits that are less resistant to cavitation. But due to their small conduits, narrow leaf plants are less efficient in transporting water. This represents the trade-off between efficiency and safety—plants whose vascular system is more resistant to cavitation but inefficient at water transport (McElrone et al., 2004; Hacke et al., 2006; Markesteijn et al., 2011; Manzoni et al., 2013). Since as we have shown above that inefficiency in water transport also means inefficiency in carbon fixation, a narrow leaf plant will have an advantage when soil moisture is low, but gradually lose that advantage with increasing soil moisture. So, the net primary productivities of narrow leaf plants increase with soil moisture slower than those of broad leaf plants. Consequently, with their size increasing more slowly with increasing soil moisture, narrow leaf plants will gradually lose their advantage to broad leaf plants.

Soil moisture is regulated by topography (Beven and Kirkby, 1979; O'Loughlin, 1986; Barling et al., 1994; Iorgulescu and Musy, 1997). Soil moisture is lowest at the ridge top and increases along the flow path moving down the hillslope towards the channel. Thus, along the hillslope, narrow leaf plants will dominate the ridge area where soil moisture is low. Moving down along the hillslope, the soil becomes wetter and broad leaf plants become more dominant (Figure 3.8).

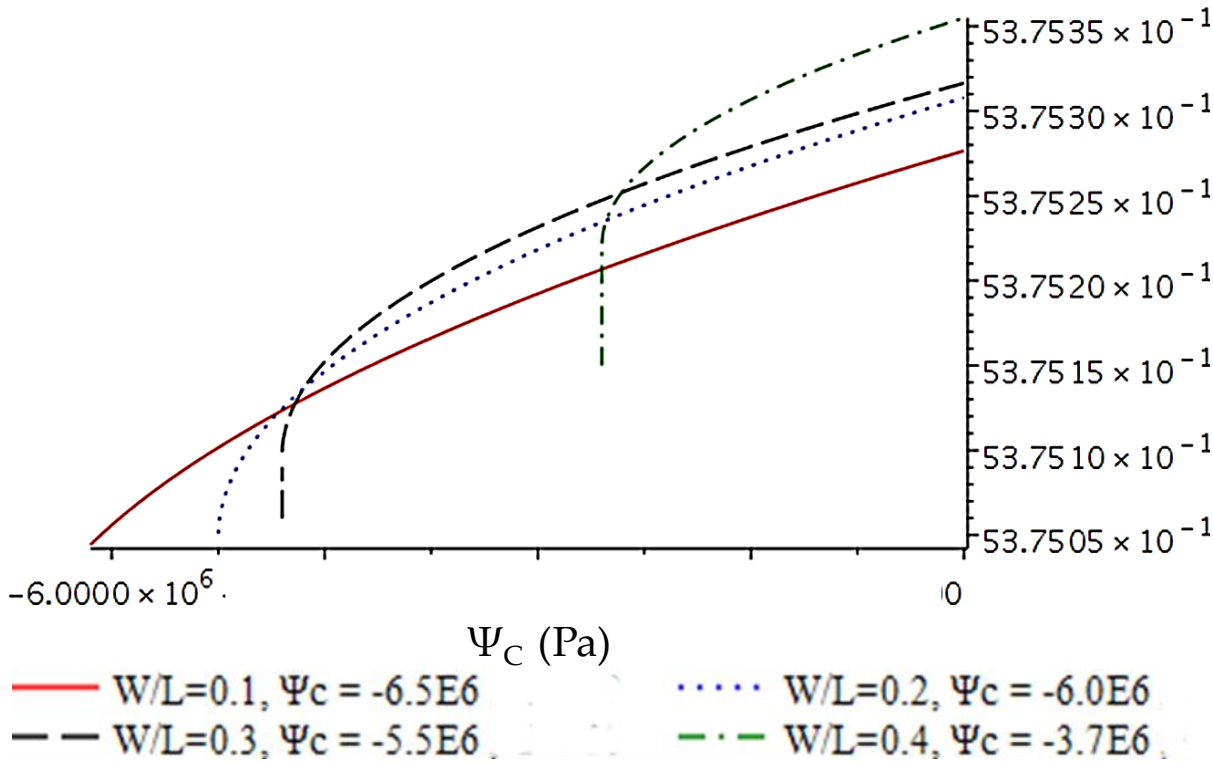

Figure 18 Modelled the relation between total leaf NPP and average petiole xylem potential

Modelled the relation between total leaf NPP and average petiole xylem potential of plants differ in leaf width to length ratio with different Ψ_C (Ψ_C is set to increase with leaf W/L), assuming all the plants will have same number of leaves.

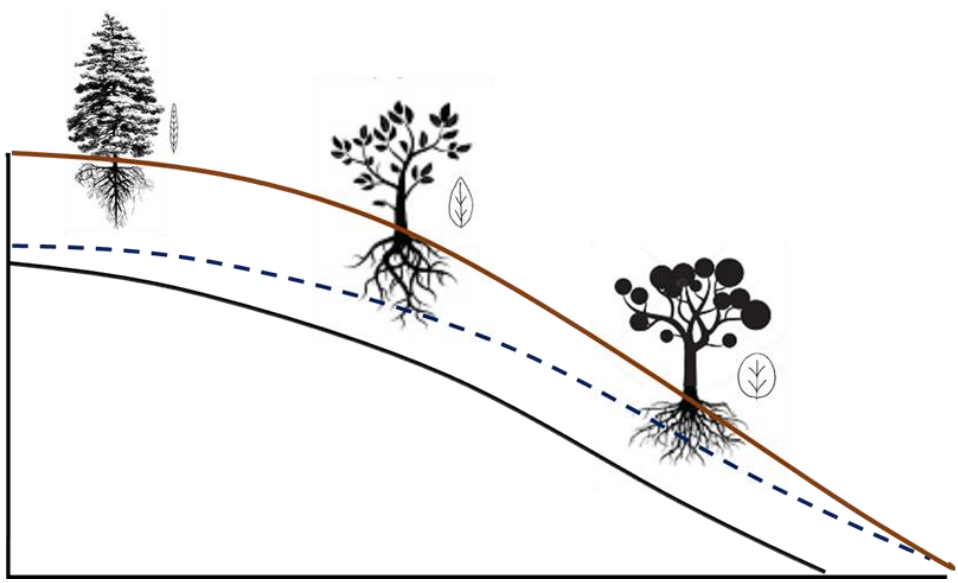

Figure 3.9 Schematic change of plants along hillslope as a result of safety-efficiency trade-off (top-right) of plant hydraulic system and topographically induced soil moisture gradient

4.2 Connecting plant hydraulic system properties with other traits by the leaf shape

In this study, we made the connection between vein structure and leaf shape, which is further incorporated into the coupling of transpiration and photosynthesis processes. This provided us a way to upscale biophysical processes occurring at the stoma scale to whole plants and further to the landscape through the plant hydraulic system using leaf shape. Leaf shape can also affect leaf temperature and light distribution. A narrow leaf has a thinner boundary layer which also increases with leaf size slower than a broad leaf, thus requiring less transpiration to cool the leaf. The impact of temperature can be integrated in the model through parameter a_1 and R_R in Equation 1. a_1, the maximum carboxylation, is expressed as the function of maximum carboxylation at 25 degrees ($V_{m,25}$) and leaf temperature (T_l) as:

$$a_1 = V_{m,\,25} \cdot \frac{2.0^{0.1 \cdot \left(T_l - 298.15\right)}}{1 + e^{\left(1.3 \cdot \left(T_l - 328.15\right)\right)}}. \qquad (10)$$

Michaletz et al. (2015) derived a leaf thermal regulation model (Equation II in Michaletz et al., 2015) to express leaf temperature by leaf shape, size, and other traits. This equation can be used to replace leaf temperature T_l in the expression of a_1. Using this parameter, we can couple the leaf thermal regulation model with our model.

Leaf shape also affects the light distribution of the canopy. This further affects the architecture of the crown to maximize light utility which is achieved by regulating the stem branching network structure. Through this mechanism, our model can be coupled with the light utility and crown architecture models (Johnson et al., 2005; Niinemets and Anten, 2009) to scale from leaf to the whole plant.

Recently, the recognition of the interaction between plants and earth surface processes led to a new interdisciplinary study in co-evolution of plants and their physical environment. People are still seeking an appropriate means to explicitly integrate the plants in the feedback mechanism between plants and earth surface processes. The leaf model can further facilitate these studies. Ding et al. (in revision) developed a formula that can be used to directly connect soil moisture to two erosion processes on low order basins. Once being scaled to the whole plant and integrated into that formula, we can predict the abundance and distribution of a given plant on the landscape using the two erosion coefficients and the leaf shape.

5. Future Study

5.1 Testing the assumptions of the model

Here we link the vein structure to width to length ratio of leaf. As for the simplification, we assume that the vein angles of all the leaves and of different order veins are all the same. However, this does not consistent with reality in which the vein structure is more complicated. The vein angle of different plants can vary in over a wide range and may not be the same for different order vein even for the same species. The variation of these traits can alter the relation between vein structure and leaf shape described in our model. It need to be tested whether the variation of vein angles will affect the relations predicted by this simple leaf model, and to which degree. Future study would be conducted to explore how the variation of these traits can affect the slope coefficient and the exponent of the power law relation of totally xylem resistance and leaf size.

Second, as for the xylem network structure, the leaf model follows the assumptions of metabolic scaling theory: the space filling (as for leaf, the surface filling) self-similar fractal network, with area conservation. The main assumptions underline metabolic theory certainly affects the validity of the leaf. The metabolic scaling theory WBE has been extended to leaf, though there is still argument whether it is appropriate to be applied for leaf or not. How well the WBE is for leaf will need further verification. One way to deal with this problem is to use the channel numbering rule used by geomorphologists to describe channel network structure, such Horton-Strahler system (Horton 1945), or a more complicated one, Tokanagan system (Tokunaga 1978). Vein network is more like drainage network on landscape. The vein order can be ranked by diameter. The terminal minor vein will have lowest order. The lower order vein can

inject into any higher order vein, rather than the one right above it. Such way to characterize vein network structure can produce more realistic scaling relationship.

Third, in the leaf model, the variation of the leaf thickness and mesophyll thickness are not addressed as the mainly focus of the model is to link vein structure to leaf shape. Our model treats them the same for different leaves. The leaf thickness and mesophyll properties can complicate the prediction of our model. Our model however, incorporates these two traits thus can be used to examine the effect of these two traits on leaf economic in relation with vein structure, leaf shape and many other traits.

Thought, our leaf model is based on many simplifications, it provides a basis for further investigate the combined effect of different leaf functional traits.

5.2 Empirical verification

There are some empirical evidences support the prediction of the relation between leaf size and properties of vascular system. Schreiber et al. (2016) found that large leaf size is correlated with wider vessel and more vulnerable xylem. Brocious and Hacke, (2016) found that stomatal conductance (reverse of stomatal resistance) scales with vessel size at petiole of hybrid poplar leaves. Their finding supports the prediction of our model. Our model predicts that plant with high total plant xylem resistance will have low NPP. A study on Chaparral shrub species along the south-western coast of North America found that fast growth species of non-sprouters had the greatest hydraulic conductance per unit leaf and sapwood area at the whole seedling level than slow growth species (Pratt et al. 2010). Our model predicts that low soil water availability will results in higher stomatal resistance and smaller vessel size of the plants. This relation has been observed by empirical studies (Lovisolo and Schubert 1998). Brodribb et al. (2012) found that

the leaf stomatal conductance form linear relation with total leaf xylem conductance for the species of angiosperm, conifer, and tropic ferns in dry forest in the northwest of Costa Rica, Santa Rosa National Park, and in southern Chile. Their finding confers the model prediction.

Though there are some empirical evidences support the prediction of our leaf model. It has not been strictly tested in field experiment. In addition, in our model, the safety – efficiency tradeoff is expressed as the consequence of the conduit size. The safety strategy comes with an inevitable cost of efficiency. But, plants can develop different safety strategies which may not reduce the efficiency (Gleason et al. 2015). Whether small conduit size is the major safety strategy can affect the model prediction. Next step of future study is to test this leaf model in the field across climate and geological regimes. This will help us to identify under which condition(s), the model is valid.

6. Conclusion

We connected leaf vein structure to leaf shape which gave the scaling relation of total xylem resistance of vein with leaf area. This relation is incorporated into the coupling of transpiration and leaf carbon budget of a leaf model to investigate the impact of leaf shape on how plants co-adjust stomatal resistance and leaf area to maximize net leaf primary productivity. We discovered that both maximum net leaf primary productivity (NPP_{leaf}) and leaf area increase with soil moisture while stomatal resistance decreases, each at different rates. A narrow leaf has overall lower maximum NPP_{leaf} and leaf area, but higher stomatal resistance compared to a broad leaf because a broad leaf has a larger vein length ratio γ as suggested by our model. At the same size, a broad leaf will have average larger conduits, and consequently more efficient transportation of water and less resistance to cavitation than a narrow leaf. By incorporating the impact of vein structure on the vulnerability curve, we are able to show that there is a trade-off

between higher marginal leaf carbon fixing rate with respect to xylem water potential and the ability of the leaf to resist cavitation. This explains how plants adapted to dry conditions will gradually lose their advantage with increasing soil moisture. Using the link between vein structure and leaf shape, we can further connect plant hydraulic traits to other traits affecting the strategies of leaf thermal regulation and canopy light utility, thereby providing a way to upscale from stoma to whole plants and the ecosystem.

6. **Supplemental Material**

6.1. Derivation of Equation 2 and 8

Following the metabolic scaling theory (), it is assumed the conduits contained by vein branch with vein, but the branching ratio are different, the length of kth order conduit is the same as the length of kth order vein. Based on these assumptions, we define:

$$n = \frac{N_{k+1}}{N_k}, m = \frac{M_{k+1}}{M_k}, \beta = \frac{r_{k+1}}{r_k}, \gamma = \frac{l_{k+1}}{l_k}$$

where n is branching ratio of vein, m is the branching ratio of xylem conduit, β is the ratio of the radius of the conduits of two consecutive vein, γ is the ratio of the length of the conduits of two consecutive vein.

Given $l_T = \gamma^T \cdot l_0$ (S1)

Since 0th order vein is the major vein. l_0=L, and LA=L*W, and W=(W/L)*L, thus LA=L^2*(W/L)

assigning L/W=K_{sp}, L can be written as $\left(\frac{LA}{k_{SP}}\right)^{0.5}$, substituting L by this formula and rearranging the Equation S1 , we get:

$$T = \frac{\ln\left(\frac{l_T}{\left(\frac{LA}{k_{SP}}\right)^{0.5}}\right)}{\ln\left(\frac{1}{2}k_{SP}\right)} \quad \text{(S2)}$$

The xylem resistance of kth order vein is:

$$r_{Xk} = \frac{8 \cdot \mu}{r_k^2 \rho_w} \cdot l_k \qquad \text{(S3)}$$

The total xylem resistance of the vein of a single flow path is:

$$\begin{aligned} r_{Xtotal} &= \sum_{k=0}^{T} \frac{8 \cdot \mu}{r_k^2 \rho_w} \cdot l_k = \frac{8 \cdot \mu}{\rho_w} \cdot \left(\frac{l_0}{r_0^2} + \frac{l_1}{r_1^2} + \cdots + \frac{l_T}{r_T^2} \right) \\ &= \frac{8 \cdot \mu}{\rho_w} \cdot \left(\frac{l_0}{r_0^2} + \frac{\gamma \cdot l_0}{(\beta \cdot r_0)^2} + \cdots + \frac{\gamma^T \cdot l_0}{(\beta^T \cdot r_0)^2} \right) \\ &= \frac{8 \cdot \mu}{\rho_w} \cdot \frac{l_0}{r_0^2} \cdot \left(1 + \cdots + \frac{\gamma^T}{\beta^{2 \cdot T}} \right) \\ &= \frac{8 \cdot \mu}{\rho_w} \cdot \frac{l_0}{r_0^2} \frac{1 - \left(\frac{\gamma}{\beta^2} \right)^{T+1}}{1 - \frac{\gamma}{\beta^2}} \end{aligned} \qquad \text{(S4)}$$

Substituting r_0 by $rT*\beta^{-T}$, l_0 by $L*\gamma^{-T}$, and T by Equation S2, total xylem resistance can be written as:

$$r_{Xtotal} = \frac{8 \cdot \mu \cdot \left(\gamma - \left(\frac{l_T}{L} \right)^{\frac{\ln(\beta^2)}{\ln(\gamma)} - 1} \cdot \beta^2 \right)}{g \cdot r_T^2 \cdot (\gamma - \beta^2) \cdot l_T} \qquad \text{(S5)}$$

The total drop of the xylem water potential along the single flow pathway from petiole to terminal minor vein is:

$$\Delta\Psi = J \cdot r_{Xtotal} \qquad \text{(S6)}$$

where J is the average flow velocity (given the energy conservation assumption, J is constant). At equilibrium, the total water movement through the total cross-section of each level of vein

equals total transpiration rate of the leaf, which is the transpiration rate per unit leaf area multiplied by leaf surface area. μ is dynamic viscosity of water (kg m-1 s-1), g is the acceleration of gravity (9.8 m s^{-2}). This gives:

$$\rho_w \cdot J \cdot \pi \cdot r_T^2 \cdot N_T = E \cdot W \cdot L \qquad \text{(S7)}$$

The vein network is space filling, thus:

$$d_{k+1} \cdot l_{k+1} \cdot N_{k+1} = d_k \cdot l_k \cdot N_k = WL \qquad \text{(S8)}$$

where dk is the distance between two adjacent veins of order k, lk is the length of kth order vein and Nk is the number of kth order vein. As for minor veins:

$$d_T \cdot l_T \cdot N_T = W \cdot L \qquad \text{(S9)}$$

This gives the number of minor veins as:

$$N_T = \frac{W \cdot L}{d_T \cdot l_T} \qquad \text{(S10)}$$

The density of minor veins, the length of minor per unit leaf area is:

$$\frac{l_T \cdot N_T}{WL} = \frac{2}{Z \cdot} \qquad \text{(S11)}$$

Since the distance between two adjacent minor veins is half of the leaf thickness (Noblin et al., 2008), substituting dT by Z/2, we get:

$$N_T = \frac{W \cdot L}{\frac{Z}{2} \cdot l_T} \qquad \text{(S12)}$$

Substituting N_T in Equation by Equation S11 and rearranging the Equation S7, we get:

$$J = \frac{E \cdot W \cdot L}{\rho_w \cdot \pi \cdot r_T^2 \cdot \frac{2\,WL}{Z\,l_T}} = \frac{E \cdot Z \cdot l_T}{2 \cdot \pi \cdot r_T^2 \cdot \rho_w} \qquad \text{(S13)}$$

Substituting J in Equation S6 by Equation S13, the total drop of xylem water potential is:

$$\Delta\Psi = \frac{E \cdot Z \cdot l_T}{2 \cdot \pi \cdot r_T^2 \cdot \rho_w} \cdot r_{Xtotal} \qquad \text{(S14)}$$

The diffusion rate of water vapor from inner leaf space to atmosphere is:

$$E = \frac{0.622\,\rho}{p} \cdot \frac{e_l - e_a}{r_{es}} \qquad \text{(S15)}$$

where p is average air pressure at sea level (101.325 kPa) and ρ is air density (at 25°C), both of which are constants. Thus, we define a new constant Cons2 = 0.622 ρ/p = 7.27 x 10^{-6}*s^2 m^{-2}.

The formula of Em is given by Noblin (2008):

$$E_m = D_m \cdot (w_0 - w_l) \cdot L_T^* \qquad \text{(S16)}$$

where D_m (m^2 s^{-1}) is the mesophyll diffusivity given by Noblin et al. (2008). w_0 (mol m^{-3}) is the water concentration of mesophyll surface touching the minor vein surface, w_l (mol m^{-3}) is the water concentration at evaporative mesophyll surface, L_T^* is minor vein density given by Equation S11. The relation between w_l and w_0 (Randau and Doyle, 2005; Noblin et al., 2008) is given as:

$$w_l = \frac{e_l}{e_{sat}} \cdot w_0 \qquad \text{(S17)}$$

Substituting w_l in Equation S16 by Equation S17, E_m becomes:

$$E_m = D_m \cdot w_0 \cdot \left(1 - \frac{e_l}{e_{sat}}\right) \cdot L_T^* \qquad \text{(S18)}$$

At equilibrium, the rate water diffuses from inner leaf space to the atmosphere (E) as vapor equals the water diffusing from a minor vein into inner leaf space per unit leaf area E_m,: $E=E_m$. Now we have two equations (Equation S15 and S18) and two variables: E and e_l. Solving Equation S15 and S18 for E, we get:

$$E = \frac{e_{sat} - e_a}{\frac{\left(\frac{Z}{2}\right) e_{sat}}{D_m w_0} + \frac{r_{es}}{Cons2}} \qquad \text{(S19)}$$

The first term of the denominator on the right side of Equation S19 is equivalent to the mesophyll resistance, so we write:

$$E = \frac{e_{sat} - e_a}{r_{em} + \frac{r_{es}}{Cons2}} \qquad \text{(S20)}$$

with $r_{em} = \frac{\left(\frac{Z}{2}\right) e_{sat}}{D_m w_0}$

Now, we can substitute Equation S20 for E in Equation S14, giving:

$$\Delta\Psi = \frac{Z \cdot l_T}{2 \cdot \pi \cdot r_T^2 \cdot \rho_w} \cdot \frac{e_{sat} - e_a}{r_{em} + \frac{r_{es}}{Cons2}} \cdot r_{Xtotal} \qquad \text{(S21)}$$

6.2. Solution of optimization model

$$LA^{*} = \left(\frac{W}{L}\right)\left(\frac{\left(-4\,p_R p_c + p_a\right)\left(\Psi_P - \Psi_C\right)}{4\cdot p_R p_b\, prx2\, Pstr1} + \left(\frac{Lmn}{l_T}\, prx2 - prx1\right)\right.$$
$$- \frac{1}{4\, p_R p_b\, prx2\, Pstr1}\left(\left(-8\, p_a\left(\left(-p_c p_R - \frac{1}{8}\, p_a\right)\left(\Psi_P - \Psi_C\right)\right.\right.\right.$$
$$\left.\left.\left.\left. + p_R p_b\, Pstr1\left(\frac{Lmn}{l_T}\cdot prx2 - prx1\right)\right)\left(\Psi_P - \Psi_C\right)\right)^{1/2}\right)\right) \qquad \text{(S22)}$$

$$r_{es}^{*} = \frac{\left(-4\,p_R p_c + p_a\right)}{4 p_R p_b} -$$
$$\frac{1}{4 p_R p_b\left(\Psi_P - \Psi_C\right)}\left(\left(-8\, p_a\left(\left(-p_c p_R - \frac{1}{8}\, p_a\right)\left(\Psi_P - \Psi_C\right)\right.\right.\right.$$
$$\left.\left.\left. + p_R p_b\, Pstr1\left(\frac{Lmn}{l_T}\cdot prx2 - prx1\right)\right)\left(\Psi_P - \Psi_C\right)\right)^{1/2}\right) \qquad \text{(S23)}$$

with

$$prx1 = \frac{\left(\gamma - \left(\frac{l_T}{Lmn}\right)^{\frac{\ln(\beta^2)}{\ln(\gamma)} - 1}\cdot\beta^2\right)}{\left(\gamma - \beta^2\right)\cdot l_T}$$

$$prx1 = \frac{\left(\frac{l_T}{Lmn}\right)^{\frac{\ln(\beta^2)}{\ln(\gamma)} - 1}\left(\frac{\ln(\beta^2)}{\ln(\gamma)} - 1\right)\beta^2}{\overline{L}\left(\gamma - \beta^2\right)\cdot l_T}$$

With Equation S22 and S23, the maximum NPP_{leaf} can be obtained by Equation 1 and 4b.

Table 2 Parameters of the leaf model

Symbol	Description	Units	Value	Source
a_1	plant biochemical parameter, in case of Rubisco limited photosynthesis, it is the maximum carboxylation capacity (Vc,max or Vm)	μmol m^{-2} s^{-1}	60	Katul et al., 2010
a_2	biochemical constant	μmol mol^{-1}	510	Katul et al., 2010
Ca	CO_2 concentration of air (ambient CO2 concentration)	mol mol^{-1}	0.0004	Buckley and Schymanski, 2014
Cons1	the ratio of resistance of CO2 to H2O		1.4	
Cons2	reverse of the specific gas constant of water vapor R_wT	s^2 m^{-2}	$7.27x10^{-6}$	
Cons3	mass per volume of liquid water	mol m^{-3}	$5.55x10^{-5}$	
D_e	water vapor diffusivity in air	m^2 s^{-1}	24 x 10^{-6}	
D_m	diffusivity of water in mesophyll	m^2 s^{-1}	8.5 x 10^{-10}	Noblin et al., 2008
e_a	partial pressure water vapor of air at 25 °C	Pa	1584.5	calculated from relative humidity of 50% at 25 degree
e_{sat}	saturated water vapor pressure at 25°C	Pa	3169	
k_S	slope of xylem vulnerability curve	Pa^{-1}	15 x 10^{-6}	Markesteijn et al., 2011; Hack, 1995; Scoffoni et al, 2017; Pammenter, 1998
LA_{mn}	mean leaf area	m^2	0.0006	
r_{es_min}	minimum stoma resistance of water vapor	s m^{-1}	300	Jones, 2013
r_T	radius of xylem conduit of terminal vein	μm	3	Blackman, Brodribb, and Jordan, 2010;

				Dunbar-co, Sporck, and Sack, 2009
w_0	saturated water concentration in mesophyll	mol m^{-3}	40	Noblin et al., 2008
Z	thickness of leaf	m	293×10^{-6}	Niinemets, 1999; Noblin et al., 2008;
Ψ_C	critical xylem water potential	Pa	-5×10^{6}	Scoffoni et al., 2017

7. References

Barling, R. D., I. D. Moore, and R. B. Grayson. 1994. "A Quasi-Dynamic Wetness Index for Characterizing the Spatial Distribution of Zones of Surface Saturation and Soil Water Content." *Water Resource Research* 30(4): 1029–44.

Beven, K. J., and M. J. Kirkby. 1979. "A Physically Based, Variable Contributing Area Model of Basin Hydrology / Un Modèle À Base Physique de Zone D'appel Variable de L'hydrologie Du Bassin Versant." *Hydrological Sciences Bulletin* 24(1): 43–69.

Blackman, C. J., T. J. Brodribb, and G. J. Jordan. 2010. "Leaf Hydraulic Vulnerability Is Related to Conduit Dimensions and Drought Resistance across a Diverse Range of Woody Angiosperms." *New Phytologist* 188(4): 1113–23.

Blonder, B., C. Violle, L. P. Bentley, and B. J. Enquist. 2011. "Venation Networks and the Origin of the Leaf Economics Spectrum." *Ecology Letters* 14(2): 91–100.

Blum, A. 2009. "Effective Use of Water (EUW) and Not Water-Use Efficiency (WUE) Is the Target of Crop Yield Improvement under Drought Stress." *Field Crops Research* 112(2): 119–23.

Boyce, C. K., T. J. Brodribb, T. S. Feild, and M. A. Zwieniecki. 2009. "Angiosperm Leaf Vein Evolution Was Physiologically and Environmentally Transformative." *Proceedings of the Royal Society B: Biological Sciences* 276(1663): 1771–76. http://rspb.royalsocietypublishing.org/cgi/doi/10.1098/rspb.2008.1919.

Brocious, Caroline A., and Uwe G. Hacke. 2016. “Stomatal Conductance Scales with Petiole Xylem Traits in Populus Genotypes.” *Functional Plant Biology* 43(6): 553–62.

Brodribb, T. J., D. Bienaimé, and P. Marmottant. 2016. “Revealing Catastrophic Failure of Leaf Networks under Stress.” *Proceedings of the National Academy of Sciences* 113(17): 201522569. http://www.pnas.org/content/early/2016/04/06/1522569113\nhttp://www.ncbi.nlm.nih.gov/pubmed/27071104\nhttp://www.pnas.org/content/early/2016/04/06/1522569113.full\nhttp://www.pnas.org/content/early/2016/04/06/1522569113.full.pdf.

Cochard, H., A. Nardini, and L. Coll. 2004. “Hydraulic Architecture of Leaf Blades: Where Is the Main Resistance?” *Plant, Cell and Environment* 27(10): 1257–67.

Condon, A. G., R. A. Richards, G. J. Rebetzke, and G. D. Farquhar. 2002. “Improving Intrinsic Water-Use Efficiency and Crop Yield.” *Crop Sci. 42, 122–131.* doi: 10.2135/cropsci2002.1220.

———. 2004. “Breeding for High Water-Use Efficiency.” *Journal of Experimental Botany* 55(407): 2447–60.

Ding, Junyan, E. A. Johnson, and Y. E. Martin. 2018. "Linking soil moisture variation and abundance of plants to geomorphic processes: a generalized model for erosional-uplifting landscapes". *Journal of Geophysical Research: Biogeoscience*

Fan, Y. et al. 2017. “Hydrologic Regulation of Plant Rooting Depth.” *Proceedings of the National Academy of Sciences* 114(40): 201712381. http://www.pnas.org/lookup/doi/10.1073/pnas.1712381114.

Franks, P. J., and S. Casson. 2014. “Connecting Stomatal Development and Physiology.” *New Phytologist* 201(4): 1079–82.

French, R. J., and J. E. Schultz. 1984. “Use Efficiency of Wheat in a Mediterranean-Type Environment. I. The Relation between Yield, Water Use and Climate.” *Australian Journal of Agricultural Research,* 35(6): 743–64.

Givnish, T. J. 1987. “Comparative Studies of Leaf Form: Assessing the Relative Roles of Selective Pressures and Phylogenetic Constraints.” *New Phytologist* 106: 131–60.

Gleason, Sean M et al. 2015. “Weak Tradeoff between Xylem Safety and Xylem- Specific Hydraulic Efficiency across the World ’ S Woody Plant Species .” *New Phytologist* 209(1): 123–36.

Grassi, G., and F. Magnani. 2005. “Stomatal, Mesophyll Conductance and Biochemical Limitations to Photosynthesis as Affected by Drought and Leaf Ontogeny in Ash and Oak Trees.” *Plant, Cell and Environment* 28(7): 834–49.

Hacke, U. G., J. S. Sperry, J. K. Wheeler, and L. Castro. 2006. “Scaling of Angiosperm Xylem Structure with Safety and Efficiency.” *Tree Physiology* 26(6): 689–701. https://academic.oup.com/treephys/article-lookup/doi/10.1093/treephys/26.6.689.

Horton, Robert E. 1945. “Geological Society of America Bulletin.” *Geological Society Of America Bulletin* 56(1): 151–80.

Iorgulescu, I. Ã., and A. Musy. 1997. “Generalization of TOPMODEL for a Power Law Transmissivity Profile.” *Hydrological Processes* 11(February): 1353–55.

Johnson, D. M., W. K. Smith, T. C. Vogelmann, and C. R. Brodersen. 2005. “Leaf Architecture and Direction of Incident Light Influence Mesophyll Fluorescence Profiles.” *American Journal of Botany* 92(9): 1425–31.

Katul, G., S. Manzoni, S. Palmroth, and R. Oren. 2010. “A Stomatal Optimization Theory to Describe the Effects of Atmospheric CO_2 on Leaf Photosynthesis and Transpiration.” *Annals of Botany* 105(3): 431–42.

Kikuzawa, K.. 1995. “The Basis for Variation in Leaf Longevity of Plants.” *Vegetatio* 121(1-2): 89–100.

Landsberg, J. J., and N. D. Fowkes. 1978. “Water Movement Through Plant Roots.” *Annals of Botany* 42(1969): 493–508.

Lawlor, D. W., and W. Tezara. 2009. “Causes of Decreased Photosynthetic Rate and Metabolic Capacity in Water-Deficient Leaf Cells: A Critical Evaluation of Mechanisms and Integration of Processes.” *Annals of Botany* 103(4): 561–79.

Lovisolo, C., and A. Schubert. 1998. “Effects of Water Stress on Vessel Size and Xylem Hydraulic Conductivity in Vitis Vinifera.” *L. Journal of experimental botany* 49(321): 693–700.

Ma, J., G. Lin, J. Chen, and L. Yang. “An Improved Topographic Wetness Index Considering Topographic Position.” *Geoinformatics, 18th International Conference on. IEEE, 2010*.

Manzoni, S., et al. 2013. “Hydraulic Limits on Maximum Plant Transpiration and the Emergence of the Safety-Efficiency Trade-Off.” *New Phytologist* 198(1): 169–78.

Markesteijn, L., et al. 2011. “Ecological Differentiation in Xylem Cavitation Resistance Is Associated with Stem and Leaf Structural Traits.” *Plant, Cell and Environment* 34(1): 137–48.

Maseda, P. H., and R. J. Fernández. 2006. “Stay Wet or Else: Three Ways in Which Plants Can Adjust Hydraulically to Their Environment.” *Journal of Experimental Botany* 57(15): 3963–77.

McDonald, P. G., C. R. Fonseca, J. McC Overton, and M. Westoby. 2003. “Leaf-Size Divergence along Rainfall and Soil-Nutrient Gradients: Is the Method of Size Reduction Common among Clades?” *Functional Ecology* 17(1): 50–57.

McElrone, A. J., W. T. Pockman, J. Martínez-Vilalta, and R. B. Jackson. 2004. “Variation in Xylem Structure and Function in Stems and Roots of Trees to 20 m Depth.” *New Phytologist* 163(3): 507–17.

Medrano, H., et al. 2015. “From Leaf to Whole-Plant Water Use Efficiency (WUE) in Complex Canopies: Limitations of Leaf WUE as a Selection Target.” *Crop Journal* 3(3): 220–28. http://dx.doi.org/10.1016/j.cj.2015.04.002.

Michaletz, S. T., et al. 2015. “Plant Thermoregulation: Energetics, Trait-Environment Interactions, and Carbon Economics.” *Trends in Ecology and Evolution* 30(12): 714–24. http://dx.doi.org/10.1016/j.tree.2015.09.006.

Nicotra, A. B., et al. 2011. “The Evolution and Functional Significance of Leaf Shape in the Angiosperms.” *Functional Plant Biology* 38: 535–52.

Niinemets, Ü., and N. P. Anten. 2009. “Packing the Photosynthetic Machinery: From Leaf to Canopy.” In *Photosynthesis in Silico*, Springer Netherlands, 363–99.

Niinemets, Ülo et al. 2007. “Do We Underestimate the Importance of Leaf Size in Plant Economics? Disproportional Scaling of Support Costs within the Spectrum of Leaf Physiognomy.” *Annals of Botany* 100(2): 283–303.

Niinemets, Ü., A. Cescatti, M. Rodeghiero, and T. Tosens. 2005. “Leaf Internal Diffusion Conductance Limits Photosynthesis More Strongly in Older Leaves of Mediterranean Evergreen Broad-Leaved Species.” *Plant, Cell and Environment* 28(12): 1552–66.

Noblin, X., et al. 2008. “Optimal Vein Density in Artificial and Real Leaves.” *Proceedings of the National Academy of Sciences of the United States of America* 105(27): 9140–44. http://www.pnas.org/content/105/27/9140.short.

O’Loughlin, E. M. 1986. “Prediction of Surface Saturation Zones in Natural Catchments by Topographic Analysis.” *Water Resources Research* 22(5): 794–804.

Pammenter, N. W., and C. V. Willigen. 1998. “A Mathematical and Statistical Analysis of the Curves Illustrating Vulnerability of Xylem to Cavitation.” *Tree Physiology* 18(Equation 1): 589–93. http://treephys.oxfordjournals.org/content/18/8-9/589.short\npapers3://publication/uuid/A3003D0D-DA97-4326-9DB3-5F916B741EC4.

Parkhurst, D. F., and O. L. Loucks. 1972. “Optimal Leaf Size in Relation to Environment.” *Journal of Ecology* 60(2): 505–37.

Petit, G., T. Anfodillo, and M. Mencuccini. 2008. “Tapering of Xylem Conduits and Hydraulic Limitations in Sycamore (*Acer Pseudoplatanus*) Trees.” *New Phytologist* 177(3): 653–64.

Pratt, Robert B. et al. 2010. “Xylem Root and Shoot Hydraulics Is Linked to Life History Type in Chaparral Seedlings.” *Functional Ecology* 24(1): 70–81.

Price, C. A., and B. J. Enquist. 2007. “Scaling Mass and Morphology in Leaves: An Extension of the WBE Model.” *Ecology* 88(5): 1132–41.

Roth-Nebelsick, A., D. Uhl, V. Mosbrugger, and H. Kerp. 2001. “Evolution and Function of Leaf Venation Architecture: A Review.” *Annals of Botany* 87(5): 553–66. http://aob.oxfordjournals.org/content/87/5/553.abstract.

Schreiber, Stefan G. et al. 2016. “Leaf Size Serves as a Proxy for Xylem Vulnerability to Cavitation in Plantation Trees.” *Plant Cell and Environment* 39(2): 272–81.

Scoffoni, C., et al. 2016. “Leaf Vein Xylem Conduit Diameter Influences Susceptibility to Embolism and Hydraulic Decline.” *New Phytologist* 213(3): 1076–92.

Shipley, B., M. J. Lechowicz, I. Wright, and P. B. Reich. 2006. “Fundamental Trade-Offs Generating the Worldwide Leaf Economics Spectrum.” *Ecology* 87(3): 535–41.

Sivamani, E., et al. 2000. “Improved Biomass Productivity and Water Use Efficiency under Water Deficit Conditions in Transgenic Wheat Constitutively Expressing the Barley HVA1 Gene.” *Plant Science*, 155(1): 1–9.

Tokunaga, E. 1978. “Consideration on the Composition of Drainage Networks and Their Evolution.” *Geographical Reports of Tokyo Metropolitan University* 13.

West, G. B. 1999. “The Fourth Dimension of Life: Fractal Geometry and Allometric Scaling of Organisms.” *Science* 284(5420): 1677–79. http://www.sciencemag.org/cgi/doi/10.1126/science.284.5420.1677 (July 21, 2014).

Westoby, M., et al. 2002. “Plant Ecological Strategies: Some Leading Dimensions of Variation between Species.” *Annual Review of Ecology and Systematics* 33(1): 125–59.

Williams, K., C. Field, and H. A. Mooney. 1989. “Relationships among Leaf Construction Cost, Leaf Longevity, and Light Environment in Rain-Forest Plants of the Genus Piper.” *American Naturalist* 133: 198–211.

Wright, I. J., et al. 2004. “The Worldwide Leaf Economics Spectrum.” *Nature* 428(6985): 821–27.

Wright, I. J., et al. 2017. “Global Climatic Drivers of Leaf Size.” *Science* 357(6354): 917–21. http://www.sciencemag.org/lookup/doi/10.1126/science.aal4760.

Xu, F., et al. 2009. “Leaf Morphology Correlates with Water and Light Availability: What Consequences for Simple and Compound Leaves.” *Progress in Natural Science* 19(12): 1789–98. http://dx.doi.org/10.1016/j.pnsc.2009.10.001.

Chapter 4 Knowledge Gaps and Direction for Future Study

1. Introduction

There are a number of knowledge gaps we will have to fill in before we can close the plants-landscape feedback circle. The major knowledge gaps are: 1) scaling from leaf NPP to whole plant NPP, 2) impact of plant biomass and traits on weathering and erosion, and 3) impact of disturbance and population dynamics.

2. Knowledge gaps and future study

On the biological side, the knowledge gap is to upscale from leaf NPP to whole plant NPP. In my search for optimal leaf traits, I left out the root system, using petiole water potential to approximate soil water potential, while it is the plant roots that connect the soil hydrology to the leaves. In my second paper, I suggested the ways to upscale from leaf to the above ground component of the whole plants. But, in order to do so, we need to make a connection between the aboveground part of the plant and the root system. The connection can be made through the two functions carried out by the root system: absorbing nutrients and providing structural anchor for the whole plant; thus, roots also fall into two functional categories: fine fibrous roots that absorb water/nutrients from the soil (akin to leaves that absorb light and CO_2), and coarse woody roots that provide structural anchor and water/nutrient transport from absorbing roots to stems (akin to aboveground stems). With resource-limits (e.g., carbon allocation to root growth) and space (e.g., soil depth), a plant having more fine roots will have less coarse roots. The more fine roots, the more efficient absorption of water and nutrients, but this will result in less woody roots and mechanical strength. Therefore, there is a tradeoff between the two root functions. Plants must adjust their root structure to balance the two functions. The ideal distribution and structural

properties of a root system are determined by the groundwater-root interaction. The root zone depth is constrained by water table depth and water-absorbing rate depends on soil water.

On the geomorphic side, the challenge is to explicitly integrate the effects of above- and below-ground plant traits on weathering and erosion and their joint effect on landform. The root system also plays an important role from a geomorphic perspective. The variations in plant root structure across the landscape will impose a spatially varying biological force on the physical landscape. Plants can affect their physical habitat in many ways, but roots are the critical biophysical link between plants and the land. Roots stabilize soil (Bardgett, Mommer, and De Vries, 2014). Roots inject atmospheric CO_2 into deep sediments through root respiration, increasing soil-groundwater acidity and chemical weathering rates (Bardgett, Mommer, and De Vries, 2014; Pawlik, Phillips, and Šamonil, 2016). Roots are the base of the soil food web, further enhancing physical and biogeochemical weathering (Pawlik, Phillips, and Šamonil, 2016). The two biological functional groups of roots also differ in their importance in physical and chemical weathering. Woody roots are more efficient in physical weathering (e.g., by prying open rock fractures), and fine roots are more efficient in chemical weathering (e.g., by growing into small pore spaces increasing rock-fluid contact surface). Such root functions will vary across landscapes because the varying hydrology demands varying plant rooting strategies, hence varying weathering/erosion.

Understanding the groundwater-root interaction can provide the solution to closing the feedback cycle. Future study should address the following questions: What are the optimal root structures, such as coarse vs. fine root proportions at different soil depths and along the hydrologic gradient from xeric to hydric habitats? Can we explain the observed patterns of

rooting structures across the landscape? How will including root traits constrain the optimal leaf traits without roots, and how will the whole-plant approach alter what we know about the linked evolution of aboveground and belowground plant hydraulic traits, which have been studied in isolation so far?

Fan et al. (2017) found that the maximum rooting depth, a key root trait, is strongly linked to soil hydrology. On hilltops, roots terminate at rain infiltration depths, but on lower slopes, roots can be pulled deeper to tap the groundwater or pushed shallower by waterlogging. To answer the two questions above, a root architecture model can be created by expanding Fan et al.'s rooting depth model to test two hypotheses: (a) besides rooting depths, other root traits, such as the allocation of fine vs. coarse roots at different soil depths and root lateral spread, will also vary significantly with hydrology, and (b) by integrating optimal leaves with optimal roots we will gain new insights on how whole-plant traits adapt to and evolve in their environment. The root architecture model can be tested by comparing the predictions of leaf and root traits with the global plant trait database TRY(Kattge et al., 2011).

The next step will be to build into the landscape evolution model a mechanistic dependence of weathering and erosion rates on root structure across the landscape. Specifically, rates of bedrock lowering and mineral dissolution/nutrient release, diffusive (e.g., creep, landslide) and advective (e.g., channel incision) erosion of soil/sediments will depend on plant rooting profile and tensile strength (coarse woody roots and fine fiber roots will have different roles). Then, a set of carefully designed model experiments will need to be conducted to isolate the importance of each of the processes or links outlined above and shown in Figure 1.1 in shaping the evolution of plants and change of their habitats.

3. Additional Notions

Once the plant-landscape feedback cycle is closed, we need to further integrate other biological/ecological processes, e.g., population dynamics and disturbance which are major ecological processes regulating the landscape distribution of different plant groups. Before, organisms were always thought to respond to the physical environment while nowthe evolution is toward the feedback processes between organisms and their environment. Previous studies all focused on the biological interactions that can affect evolution. This thesis aims to fill in this gap. However, it is extremely important for us to remember that an environment of an organism includes both biotic and abiotic components. Thus, in order to fully understand how the feedback between plants and their physical environment is shaping the plant community and landscape, we must integrate the biological drivers into the biotic-abiotic feedbacks so that the feedback cycle includes both biotic and biotic-abiotic interactions.

4. References

Bardgett, R. D., L. Mommer, and F. T. De Vries. 2014. “Going Underground: Root Traits as Drivers of Ecosystem Processes.” *Trends in Ecology and Evolution* 29(12): 692–99. http://dx.doi.org/10.1016/j.tree.2014.10.006.

Fan, Y., et al. 2017. “Hydrologic Regulation of Plant Rooting Depth.” *Proceedings of the National Academy of Sciences* 114(40): 201712381. http://www.pnas.org/lookup/doi/10.1073/pnas.1712381114.

Kattge, J., et al. 2011. “TRY–a Global Database of Plant Traits.” *Global Change Biology* 17(9): 2905–35.

Pawlik, Ł., J. D. Phillips, and P. Šamonil. 2016. “Roots, Rock, and Regolith: Biomechanical and Biochemical Weathering by Trees and Its Impact on Hillslopes—A Critical Literature Review.” *Earth-Science Reviews* 159: 142–59.

Chapter 5: Conclusion

This thesis provides a theoretical approach that can be used to explain the interaction between plants and their physical environment which can drive and be driven by the evolution of plants using first order principles—the physical laws. In the feedback cycle, the groundwater-plant hydraulic system interaction plays the key role in linking the biological, hydrological and geomorphic processes. Using this interaction, I show the physical connection between geomorphic processes and soil moisture variation, as well as plant productivity and soil moisture mediated by functional traits. I further identified the critical knowledge gap: the groundwater-root interaction, the critical component of the feedback cycle. To close the cycle, future study will be focused on understanding how the groundwater-root interaction affects root properties under different climatic and tectonic regimes.

In this thesis, I tackled a very significant and complex research question and undertook theoretical and modeling analysis that investigates mechanistic relations between topography, soil moisture and plant distribution. The thesis makes contribution to interdisciplinary, biogeoscience research questions.